THE JOURNAL OF PHYSICAL CHEMISTRY Letters

Letter

pubs.acs.org/JPCL

Coupled Cluster Method with Single and Double Excitations Tailored by Matrix Product State Wave Functions

Libor Veis,[*,†,⊥] Andrej Antalík,[†,⊥] Jiří Brabec,[†] Frank Neese,[‡] Örs Legeza,[*,§] and Jiří Pittner[*,†]

[†]J. Heyrovský Institute of Physical Chemistry, Academy of Sciences of the Czech Republic, v.v.i., Dolejškova 3, 18223 Prague 8, Czech Republic

[‡]Max Planck Institut für Chemische Energiekonversion, Stiftstrasse 34-36, D-45470 Mülheim an der Ruhr, Germany

[§]Strongly Correlated Systems "Lendület" Research Group, Wigner Research Centre for Physics, H-1525 Budapest, Hungary

Supporting Information

ABSTRACT: In the past decade, the quantum chemical version of the density matrix renormalization group (DMRG) method has established itself as the method of choice for calculations of strongly correlated molecular systems. Despite its favorable scaling, it is in practice not suitable for computations of dynamic correlation. We present a novel method for accurate "post-DMRG" treatment of dynamic correlation based on the tailored coupled cluster (CC) theory in which the DMRG method is responsible for the proper description of nondynamic correlation, whereas dynamic correlation is incorporated through the framework of the CC theory. We illustrate the potential of this method on prominent multireference systems, in particular, N_2 and Cr_2 molecules and also oxo-Mn(Salen), for which we have performed the first post-DMRG computations in order to shed light on the energy ordering of the lowest spin states.

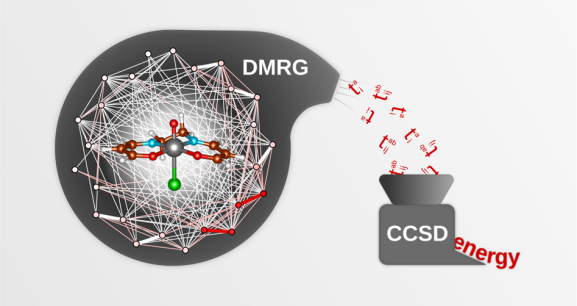

The coupled cluster (CC) approach, introduced to quantum chemistry (QC) by Čížek,[1] is one of the most accurate ab initio methods for the treatment of dynamic electron correlation. The advantages of this scheme include a compact description of the wave function, size-extensivity, invariance to orbital rotations, together with a systematic hierarchy of approximations converging toward the full configuration interaction (FCI) limit.[2] Despite the great success of QC and, in particular, the CC methodology[3] in standard (single-reference) cases, the situation is dramatically different for strongly correlated (multireference) systems,[4] where the usual single-reference approaches become inaccurate or even completely break down. One category of methods designed for the treatment of such systems are multireference coupled cluster (MRCC) approaches, which generalize the CC exponential parametrization of the wave function.[5−7] Out of many formulations of MRCC theories, the class of methods relevant to this work are externally corrected CC, which extract information about the most important higher excitations or active space single and double excitations from an "external" calculation performed by a different method like complete active space self-consistent field (CASSCF) or multireference configuration interaction (MRCI).[8−19] In this Letter, we present a further development in this field concerning the tailored CC (TCC) method, where the information for external correction is obtained from a density matrix renormalization group (DMRG) calculation.

DMRG is a very powerful approach suitable for treatment of strongly correlated systems originally developed in solid-state physics.[20−22] The success of DMRG in this field motivated its application to QC problems[23−31] where it has proven the potential to outperform traditional QC methods for systems that require very large active spaces, like molecules containing several transition metal atoms.[32,33] Despite the favorable scaling of the DMRG method, it is computationally prohibitive to treat the dynamic correlation by including all virtual orbitals into the active space. Because the dynamic correlation has in general a very significant chemical impact, development of "post-DMRG" methods, which aim to describe this effect, is of high importance. During the past few years, several such methods have been developed, for example, DMRG-CASPT2,[34] DMRG-icMRCI,[35] canonical transformation (CT),[36] or matrix product state (MPS)-based formulation of a multireference perturbation theory.[37]

The general TCC wave function employs the following split-amplitude ansatz[15]

$$|\Psi_{\mathrm{TCC}}\rangle = e^{T}|\Phi_0\rangle = e^{T_{\mathrm{ext}}+T_{\mathrm{CAS}}}|\Phi_0\rangle = e^{T_{\mathrm{ext}}}e^{T_{\mathrm{CAS}}}|\Phi_0\rangle \quad (1)$$

where T_{CAS} represents the amplitudes obtained from the CI coefficients of the precomputed complete active space

Received: August 23, 2016
Accepted: September 28, 2016
Published: September 28, 2016

DOI: 10.1021/acs.jpclett.6b01908
J. Phys. Chem. Lett. 2016, 7, 4072−4078

configuration interaction (CASCI) wave function and T_{ext} is the rest of the cluster operator. Because $|\Phi_0\rangle$ is a single-determinant reference wave function, T_{ext} and T_{CAS} mutually commute, which keeps the method very simple. At the level of truncation to single and double excitations (TCCSD), the wave function reads

$$|\Psi_{TCCSD}\rangle = e^{(T_{ext}^{(1)}+T_{ext}^{(2)})}e^{(T_{CAS}^{(1)}+T_{CAS}^{(2)})}|\Phi_0\rangle \quad (2)$$

where the superscript denotes the excitation rank of a cluster operator. $T_{CAS}^{(1)}$ and $T_{CAS}^{(2)}$ are calculated from the CASCI expansion coefficients according to the well-know relationship between the CC and CI expansions

$$T_{CAS}^{(1)} = C^{(1)} \quad (3a)$$

$$T_{CAS}^{(2)} = C^{(2)} - \frac{1}{2}[C^{(1)}]^2 \quad (3b)$$

$T_{CAS}^{(1)}$ and $T_{CAS}^{(2)}$ are expected to properly describe the nondynamic correlation[38] and are kept constant during the CC procedure. They thus "tailor" the external amplitudes corresponding to the $T_{ext}^{(1)}$ and $T_{ext}^{(2)}$ operators, which are, on the other hand, supposed to be responsible for the main part of the dynamic correlation and that are calculated from the usual projective CCSD amplitude equations analogous to the single-reference CC method

$$\langle\Phi_i^a|He^{T_{ext}}e^{T_{CAS}}|\Phi_0\rangle_c = 0 \qquad \{i, a\} \not\subset \text{CAS} \quad (4a)$$

$$\langle\Phi_{ij}^{ab}|He^{T_{ext}}e^{T_{CAS}}|\Phi_0\rangle_c = 0 \qquad \{i, j, a, b\} \not\subset \text{CAS} \quad (4b)$$

The TCC approach has been successfully applied[16,19] and generally performs well, although a large active space and CASSCF orbitals might be required for good accuracy.[15] TCC also features the desirable property of being rigorously size-extensive.[15]

In order to circumvent the prohibitive scaling of the CASCI method, when large active spaces are used, we propose to use MPS wave functions generated by the DMRG method to acquire active space amplitudes that correctly describe the nondynamic correlation in the subsequent CCSD calculations.

The DMRG method[39] is a variational procedure that optimizes the wave function in the form of MPS.[40] It is a nonlinear wave function ansatz made from the product of variational objects (matrices) corresponding to each site of a one-dimensional lattice that in QC represents a chain of molecular orbitals. Therefore, MPS refers to the wave function ansatz, whereas DMRG refers to the efficient self-consistent optimization algorithm that provides it. In the QC version of DMRG (QC-DMRG),[26−31] correlations between individual molecular orbitals are taken into account by means of an iterative procedure that variationally minimizes the energy of the electronic Hamiltonian. The method eventually converges to the FCI solution in a given orbital space, that is, to CASCI.

The practical version of DMRG is the two-site algorithm, which, in contrast to the one-site approach, is less prone to get stuck in a local minimum.[39] It provides the wave function in the two-site MPS form[40]

$$|\Psi_{MPS}\rangle = \sum_{\{\alpha\}} \mathbf{A}^{\alpha_1}\mathbf{A}^{\alpha_2}\cdots\mathbf{W}^{\alpha_i\alpha_{i+1}}\cdots\mathbf{A}^{\alpha_n}|\alpha_1\alpha_2\cdots\alpha_n\rangle \quad (5)$$

where $\alpha_i \in \{|0\rangle, |\downarrow\rangle, |\uparrow\rangle, |\downarrow\uparrow\rangle\}$ and for a given pair of adjacent indices $[i, (i+1)]$, $\mathbf{W}$ is a four-index tensor, which corresponds to the eigenfunction of the electronic Hamiltonian expanded in the tensor product space of four tensor spaces defined on an ordered orbital chain, the so-called *left block* (M_l-dimensional tensor space), *left site* (four-dimensional tensor space of the ith orbital), *right site* (four-dimensional tensor space of the $(i+1)$th orbital), and *right block* (M_r-dimensional tensor space). The MPS matrices $\mathbf{A}$ are obtained by successive application of the singular value decomposition (SVD) with truncation on $\mathbf{W}$'s and iterative optimization by going through the ordered orbital chain from *left* to *right* and then sweeping back and forth.

The maximum dimension of MPS matrices that is required for a given accuracy, the so-called bond dimension [$M_{max} = \max(M_l, M_r)$], can be regarded as a function of the level of entanglement in the studied system.[41] Among others, M_{max} strongly depends on the order of orbitals along the one-dimensional chain[25,42] as well as their type.[43−45]

The two crucial correlation measures, which play an important role in tuning the performance of DMRG (e.g., employed in orbital ordering optimization), are single-orbital entanglement entropy (s_i) and mutual information (I_{ij}).[41,46−48] s_i quantifies the importance of orbital i in the wave function expansion and can be computed as $-\mathrm{Tr}\,\rho_i \ln \rho_i$, where ρ_i represents the reduced density matrix of orbital i.[41,49−51] Similarly, when substituting a single orbital with a pair of orbitals (i, j), the two-orbital entanglement entropy, s_{ij}, can be obtained. The mutual information then reads $I_{ij} = s_{ij} - s_i - s_j$, and it describes how orbitals i and j are correlated with each other as they are embedded in the whole system.[47,48]

When employing the two-site MPS wave function (eq 5) for the purposes of the TCCSD method, the CI expansion coefficients c_i^a and c_{ij}^{ab} for $a,b,i,j \in$ CAS can be efficiently calculated by contractions of MPS matrices.[52,53] We would like to note that using the two-site DMRG approach in practice means using the wave function calculated at different sites and it can only be employed together with the dynamical block state selection (DBSS) procedure[25] assuring the same accuracy along the sweep. Alternatively, one can use the one-site approach in the last sweep.[54]

Regarding the computational scaling of the DMRG-TCCSD method, it is indeed an interplay of contributions from both parent methods. The formal computational scaling of DMRG is $O(M^3n^3) + O(M^2n^4)$,[23] where M denotes the bond dimension and n the number of orbitals in the DMRG space.[55] The scaling of CCSD[2] is $O(N_{occ}{}^2N_{virt}{}^4) \approx O(N^6)$, where to distinguish between DMRG and CC orbital spaces N refers to the size of the full (CC) orbital space and $n < N$. Which contribution is in practice the rate-limiting step depends on the size of the DMRG active space, the underlying entanglement, as well as the size of the system. Computation of the CI expansion coefficient itself is negligible compared to the cost of DMRG.[56]

Looking upon at eq 2 and taking into account that the action of $(\exp(T_{CAS}^{(1)}) + \exp(T_{CAS}^{(2)}))$ (with the exact amplitudes) on the reference function $|\Phi_0\rangle$ approximates the MPS wave function $(\Psi_{MPS}^{(CCSD)})$,[57] the method can be viewed as an approximate CC ansatz with the MPS reference function

$$|\Psi_{DMRG\text{-}TCCSD}\rangle \approx e^{(T_{ext}^{(1)}+T_{ext}^{(2)})}|\Psi_{MPS}^{(CCSD)}\rangle \quad (6)$$

However, it uses a single Slater determinant as a Fermi vacuum that introduces a certain bias, which might deteriorate the performance of the method in exactly degenerate situations. In such cases, the method will break the spatial symmetry of the degenerate components. For the same reason, the TCCSD method, despite being size-extensive, does not fulfill the size-

DOI: 10.1021/acs.jpclett.6b01908
J. Phys. Chem. Lett. 2016, 7, 4072−4078

consistency exactly;[58] however, with growing size of the active space, the error will decrease, and in the limit of including all orbitals, the error must vanish because TCCSD then becomes identical to FCI. We have performed a test of size-consistency of the method by comparison of the energy of the N_2 dimer separated by 100 au with respect to double of the N atom energy. While standard (closed-shell) CCSD fails to converge at all for the separated dimer, TCCSD(6,6) has an error of 20.7 kcal/mol, which monotonically decreases with the size of the active space, yielding 20.0, 14.7, and 13.4 kcal/mol for the spaces (10,14), (10,16), and (10,18), respectively. The advantage of employing DMRG together with TCC is that it enables using large active spaces (up to 40 orbitlas in generic cases), decreasing significantly any such errors. Even if not suppressed completely, we still believe that the TCCSD method can be very useful in computational scenarios where size-consistency is not a critical issue, as demonstrated on our numerical examples.

In what follows, we denote the DMRG-TCCSD method by the abbreviation TCCSD(e,o), where the numbers inside of the brackets specify the DMRG active space, namely, e refers to the number of electrons and o to the number of orbitals.

The chromium dimer (Cr_2) has been known for a long time as a particularly challenging small system in QC. In order to adequately describe its intricate dissociation curve, the used method has to provide the best possible treatment of both nondynamic and dynamic correlation. Over the decades, the problem has been tackled by many groups.[34,45,59−70] Our aim was not to calculate the whole dissociation curve but rather test the DMRG-TCCSD method on a single-point energy calculation for which the large-scale DMRG extrapolated energy has recently been published.[45] These results are considered as a FCI benchmark.

Following,[45] we performed a single-point calculation, with the chromium atoms being placed 1.5 Å apart. According to the single-orbital entanglement entropy profiles, we chose three active spaces: CAS(12,12) for $s_i > 0.2$; CAS(12,19) for $s_i > 0.05$; and CAS(12,21) for s_i just under the 0.05 (after these two orbitals, a drop in s_i values was observed). The first CAS includes all of the valence orbitals (4s and 3d); the other spaces are augmented by double-shell orbitals. In particular, CAS(12,19) adds two 5s and five 4d orbitals, and CAS(12,21) adds another two 4d orbitals.

The resulting DMRG, TCCSD, and, for comparison, also CCSD, CCSD(T), and CCSDTQ[45] energies are shown in Table 1. The amount of retrieved correlation energy (with respect to the extrapolated DMRG energies[45]) for CC and TCCSD methods is plotted in Figure 1. The calculations systematically ameliorate with the augmenting active space, and in the case of the largest TCCSD(12,21) calculation, we were able to retrieve more than 99% of the overall correlation energy. This is a significant improvement upon stand-alone CCSD or DMRG calculations, and it even surpasses the considerably more demanding CCSDTQ method.

The next system that we chose for tests of the DMRG-TCCSD method is the nitrogen molecule (N_2). It is well-known that a proper description of the triple bond breaking process in N_2 requires reliable multireference treatment. For example, the single-reference CCSD method fails by predicting an unphysical hump on the potential energy surface (PES) of the $X^1\Sigma_g^+$ electronic state for about twice the equilibrium distance. On the other hand, as has been shown by Kinoshita et al.[15] already, TCCSD(6,6) corrects this unphysical behavior [see Figure 3 of the Supporting Information (SI)].

Table 1. TCCSD Energies (E+2086 in au) of the Cr_2 Molecule (r = 1.5 Å) with SV Basis for Different Active Spaces, with Their Respective DMRG ($\chi = 10^{-5}$)[a] Energies with CCSD, CCSD(T), and CCSDTQ Energies for Comparison

method	E + 2086
DMRG(12,12)	−0.071746
TCCSD(12,12)	−0.424826
DMRG(12,19)	−0.228125
TCCSD(12,19)	−0.428037
DMRG(12,21)	−0.252552
TCCSD(12,21)	−0.437171
CCSD	−0.344277
CCSD(T)[45]	−0.422229
CCSDTQ[45]	−0.430244
DMRG(48,42)[b45]	−0.444784

[a]For the definition of χ, see the Computational Details section. [b]Extrapolated DMRG energies serving as a FCI benchmark.

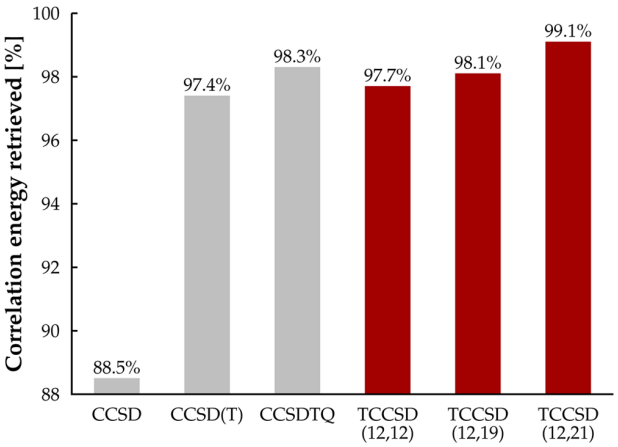

Figure 1. Amount of correlation energy retrieved (with respect to the extrapolated DMRG energies[45]) by TCCSD for the Cr_2 molecule (r = 1.5 Å) with SV basis. CCSD, CCSD(T), and CCSDTQ[45] energies are shown for comparison.

In order to accurately calculate spectroscopic parameters like vibrational frequencies (ω_e) or anharmonicities ($\omega_e x_e$), a high-quality PES is required, which makes them good tests for the DMRG-TCCSD method.

As in the previous example, the DMRG active space was selected according to the single-orbital entanglement entropy values. We have selected 19 orbitals, which complied with s_i > 0.02. The final DMRG(10,19) and TCCSD(10,19) results (vibrational frequencies, anharmonicities, and equilibrium bond lengths) together with the single-reference CCSD and TCCSD(6,6) results are shown in Table 2.

As can be seen, the TCCSD(10,19) method gives the best agreement with the experimental vibrational frequencies and anharmonicities, improving the CCSD and DMRG(10,19) vibrational frequencies by more than 53 and 48 cm^{-1}, respectively, and anharmonicities by more than 1.1 and 0.2 cm^{-1}, respectively. It also gives the vibrational frequencies and anharmonicities superior to TCCSD(6,6) by more than 6 cm^{-1} in the case of the vibrational frequency and 0.3 cm^{-1} for the anharmonicity. Only the TCCSD(10,19) equilibrium bond

DOI: 10.1021/acs.jpclett.6b01908
J. Phys. Chem. Lett. 2016, 7, 4072−4078

Table 2. Spectroscopic Parameters of the $X^1\Sigma_g^+$ Electronic State of N_2 Calculated with the cc-pVTZ Basis Together with the Experimental Values Taken from Reference 71 along with Vibrational Frequencies (ω_e) and Anharmonicities ($\omega_e x_e$), Bond Lengths, and Absolute Values of Deviations from the Experimental Results

	ω_e (cm^{-1})	$\lvert\Delta\omega_e\rvert$ (cm^{-1})	$\omega_e x_e$ (cm^{-1})	$\lvert\Delta\omega_e x_e\rvert$ (cm^{-1})	r_0 (Å)	$\lvert\Delta r_0\rvert$ (Å)
CCSD	2423.3	64.7	12.75	1.57	1.0967	0.0010
TCCSD(6,6)	2376.3	17.7	13.57	0.75	1.1009	0.0032
DMRG(10,19)	2298.8	59.8	13.72	0.60	1.1112	0.0135
TCCSD(10,19)	2347.3	11.3	13.91	0.41	1.1036	0.0059
experiment	2358.57		14.324		1.09768	

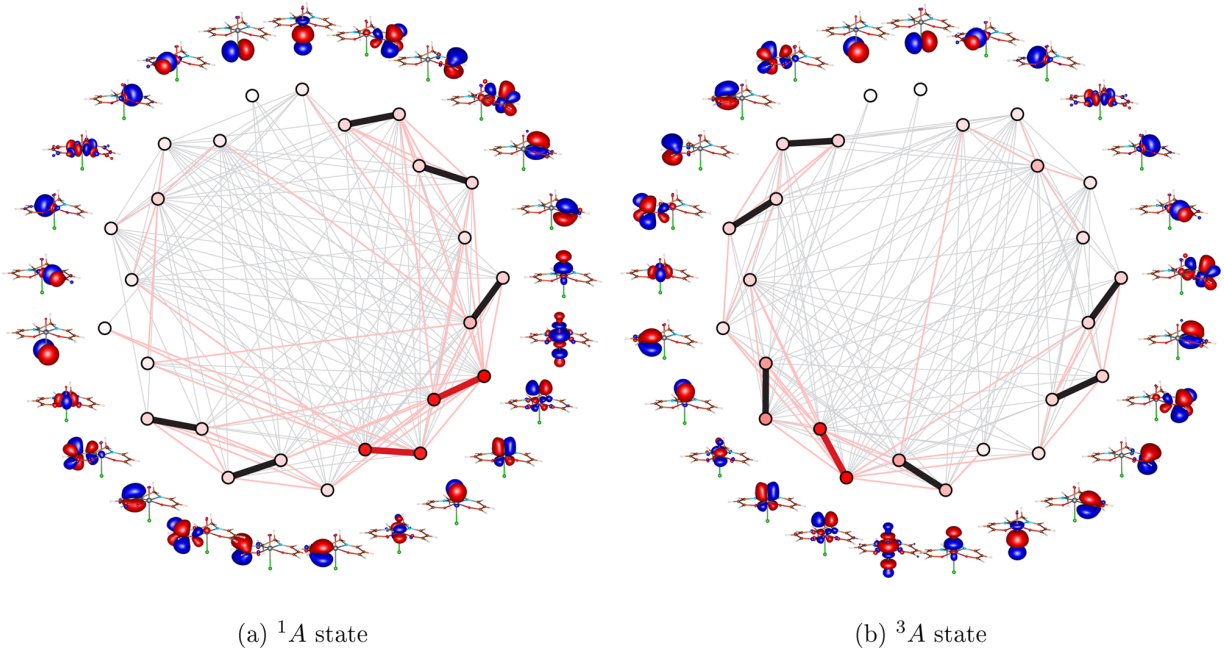

(a) ^1A state (b) ^3A state

Figure 2. CAS split-localized orbitals and their mutual information (M = 512) for ^{1}A and ^{3}A states of oxo-Mn(Salen) with the 6-31G* basis. The mutual information is color-coded: the thick red lines correspond to the strongest correlations (order of magnitude 1), followed by black (10^{-1}), pink (10^{-2}), and gray (10^{-3}). One-site entropy values are represented by a color gradient of the respective dot, red being the largest value and white being zero.

length is slightly worse than the CCSD value, which is however justifiable as the CCSD methods works well around the energy minimum where the wave function exhibits single-reference nature. Nevertheless, the error of 0.006 Å for the TCCSD-(10,19) equilibrium bond length represents fairly good accuracy. The TCCSD(6,6) dissociation energy (D_e) computed as the difference of the N_2 energy at the optimum geometry and the double of the N atom energy equals 213.7 kcal/mol and lies 11 kcal/mol under the experimental value (D_e^{exp} = 225 kcal/mol[71]). It improves the CASSCF(6,6) dissociation energy by 10 kcal/mol and the CCSD dissociation energy by 6.5 kcal/mol ($D_e^{CASSCF(6,6)}$ = 203.8 kcal/mol; D_e^{CCSD} = 207.2 kcal/mol).

The last system that we have computed is oxo-Mn(Salen). It catalyzes the enantioselective epoxidation of unfunctional olefins[72,73] and has been studied extensively with different multireference methods,[74−76] most recently also with the DMRG methodology.[45,77,78] Despite huge efforts, the energetic ordering of the lowest singlet and triplet states is still not clear, and proper answer requires studies of the effect of dynamic correlation. The ordering of the lowest spin states is an important issue indeed because different reaction paths have been suggested depending on the spin state.[79] To the best of our knowledge, we report the first "post-DMRG" computations of this system.

In the case of oxo-Mn(Salen), we followed the work of Olivares-Amaya et al.[45] in selection of the active space. The active space contained 5 Mn 3d orbitals, 10 π orbitals of the equatorial conjugated rings (C, N, O atoms), 4 equatorial 2p orbitals forming Mn−N and Mn−O σ bonds, 3 2p orbitals for axial O, as well as Cl atoms, which resulted in CAS(34,25). The split-localized molecular orbitals forming the DMRG active space with their respective mutual information are presented in Figure 2. Our TCCSD and DMRG ^{1}A and ^{3}A energies together with previous DMRG and DMRG-SCF results are listed in Table 3. As can be seen, our DMRG(34,25) results agree with the DMRG-SCF results of Wouters et al.[77] in predicting the ^{3}A state to be the ground state.[80] In our case, the singlet−triplet gap is higher in absolute value, which can be assigned to the fact that we did not optimize the orbitals. However, inclusion of the dynamic correlation through the TCCSD approach decreases the gap, suggesting that the ^{3}A state is lower in energy than the ^{1}A state by 3.6 kcal/mol.

In this Letter, we have presented a novel method for accurate treatment of strongly correlated molecules that , in the spirit of TCC,[7,15,16,19] combines the CC theory, in particular, CCSD,

DOI: 10.1021/acs.jpclett.6b01908
J. Phys. Chem. Lett. 2016, 7, 4072−4078

Table 3. TCCSD ^{1}A and ^{3}A Energies (E + 2251 in au) and Energy Differences [$\Delta E = E(^3\text{A}) - E(^1\text{A})$ in kcal/mol] of oxo-Mn(Salen) with the 6-31G* Basis along with DMRG and Previous DMRG and DMRG-SCF Results for Comparison

method	$E(^1\text{A})$	$E(^3\text{A})$	ΔE
DMRG-SCF(28,22)[77]	−0.5498	−0.5578	−5.0
DMRG(32,24)[45]	−0.304712	−0.304128	0.4
DMRG-SCF(26,21)[a][78]	−0.796326	−0.795396	0.6
DMRG(34,25)	−0.410926	−0.431039	−12.6
TCCSD(34,25)	−2.727314	−2.733037	−3.6

[a]The cc-pVDZ basis set was employed.

with the DMRG method. In this approach, DMRG is responsible for proper description of the nondynamic electron correlation and CCSD is supposed to deal with the major part of the remaining dynamic correlation.

Despite being conceptually simple, the first results of the benchmark calculations on the Cr_2, N_2, and oxo-Mn(Salen) molecules are indeed very encouraging. In the case of Cr_2 (r = 1.5 Å), for which the extrapolated DMRG energy is available, we were able to recover more than 99% of the correlation energy with the TCCSD(12,21) method, compared to 88.5% of the standard CCSD method. Regarding the N_2 example, with the TCCSD(10,19) method, we were able to obtain the vibrational frequency and the equilibrium bond length with errors of about 0.5%. More importantly, this method provided the anharmonicity, which is more sensitive to the shape of the potential energy curve further from the energy minimum, with an error less than 3%, compared to 11% error of the standard CCSD method. In the case of oxo-Mn(Salen), we have presented the first "post-DMRG" calculations whose aim was to shed more light on the energy ordering of the lowest spin states. Our results are in agreement with the results of Wouters et al.,[77] predicting the triplet state to be 3.6 kcal/mol lower than the singlet one.

The DMRG-TCCSD method in fact represents the simplest version of DMRG externally corrected CC approaches. An alternative (and potentionally even more accurate) method that deserves future investigations is the reduced multireference CCSD method[8−11] employing the DMRG connected triples and quadruples in the active space.

COMPUTATIONAL DETAILS

We have extended the Budapest QC-DMRG code[81] for computations of active space CC amplitudes and interfaced it with the Orca program system,[82] in which we have implemented the TCCSD method.

In all of the production DMRG calculations, we employed the DBSS procedure[25,83] with the truncation criterion set on entropy $\chi = S_{max} - S$, where S_{max} denotes the entanglement entropy of the augmented block before the truncation and S the truncated one. We tested the effect of the truncation error χ on the final TCCSD N_2 spectroscopic parameters and found that $\chi = 10^{-5}$ is sufficient for the presented accuracy. This truncation criterion was used throughout the work, and it resulted in bond dimensions varying in the range of 1000−6000. Note that χ is a tighter criterion than the more common $\delta\epsilon_{TR} = 1 - \sum \lambda_i^2$, with λ_i being the Schmidt values, in our case by almost 2 orders of magnitude. The orbitals for the DMRG active spaces were chosen according to their single-orbital entanglement entropies[41,49,78] calculated with fixed bond dimensions M = 512 (see Figures 2 and 5 of the SI). In the case of N_2, the single-orbital entropies were averaged over 10 points, from which the spectroscopic parameters were computed. The Fiedler method[43,48] was used for optimization of the orbital ordering. The DMRG runs were initialized using the CI-DEAS procedure,[30,41] and the energy convergence threshold measured between the two subsequent sweeps was set to 10^{-6} au.

In the case of Cr_2, the RHF orbitals computed in Ahlrichs's SV basis were used for the subsequent DMRG and TCCSD calculations (see Figure 1 of the SI). For N_2, we used the CASSCF(6,6)/cc-pVTZ orbitals with the active space consisting of six 2p orbitals in all DMRG and TCCSD calculations (see Figure 4 of the SI). Likewise, we excluded two 1s orbitals from the TCCSD correlation treatment. The N_2 spectroscopic parameters were calculated employing the Dunham analysis.[84] In the case of oxo-Mn(Salen) we used the singlet CASSCF-(10,10)/6-31G* geometry of Ivanic et al.[74] (see Figure 6 of the SI). As in ref 45, we employed the triplet 6-31G* ROHF orbitals, which were for easier selection of the DMRG active space split-localized: for the ^{1}A state, all of the valence and 32 virtual orbitals; for ^{3}A, all of the valence, 2 singly occupied, and 31 virtual orbitals. Again, the core orbitals were excluded from correlation treatment.

ASSOCIATED CONTENT

Supporting Information

The Supporting Information is available free of charge on the ACS Publications website at DOI: 10.1021/acs.jpclett.6b01908.

DMRG active space orbitals for N_2 and Cr_2 examples with mutual information and single-orbital entanglement entropy plots, plot of the N_2 PES, employed oxo-Mn(Salen) geometry, and oxo-Mn(Salen) orbitals involved in the characteristic singlet to triplet excitation (PDF)

AUTHOR INFORMATION

Corresponding Authors

*E-mail: libor.veis@jh-inst.cas.cz (L.V.).
*E-mail: legeza.ors@wigner.mta.hu (O.L.).
*E-mail: jiri.pittner@jh-inst.cas.cz (J.P.).

Author Contributions

⊥L.V. and A.A. contributed equally to this work.

Notes

The authors declare no competing financial interest.

ACKNOWLEDGMENTS

We would like to thank Ch. Krumnow, R. Schneider, and Sz. Szalay for helpful discussions and F. Wennmohs for the Orca technical assistance. This work has been supported by the Czech Science Foundation (Grant No. 16-12052S), by the Czech Ministry of Education, Youth and Sports from the Large Infrastructures for Research, Experimental Development and Innovations project "IT4Innovations National Supercomputing Center - LM2015070", DAAD/16/07 project, Hungarian−Czech Joint Research Project MTA/16/05, and the Hungarian Research Fund (OTKA) (Grant No. NN110360).

REFERENCES

(1) Čížek, J. On the Correlation Problem in Atomic and Molecular Systems. Calculation of Wavefunction Components in Ursell-Type Expansion Using Quantum-Field Theoretical Methods. *J. Chem. Phys.* **1966**, *45*, 4256.

DOI: 10.1021/acs.jpclett.6b01908
J. Phys. Chem. Lett. 2016, 7, 4072−4078

(2) Gauss, J. Coupled Cluster Theory. In *The Encyclopedia of Computational Chemistry*; Schleyer, P. v. R., Allinger, N. L., Clark, T., Gasteiger, J., Kollman, P. A., Schaefer, H. F., III, Scheiner, P. R., Eds.; Wiley: Chichester, U.K., 1998.
(3) The CCSD(T) method,[85] which includes connected single, double, and perturbative triple excitations, is often referred to as the gold standard of QC.
(4) Many important compounds belong to this class, for example, reaction intermediates or transition metal complexes.
(5) Bartlett, R. J.; Musial, M. Coupled-cluster theory in quantum chemistry. *Rev. Mod. Phys.* **2007**, *79*, 291.
(6) *Recent Progress in Coupled Cluster Methods*; Čársky, P., Paldus, J., Pittner, J., Eds; Springer: Berlin, Germany, 2010.
(7) Lyakh, D. I.; Musial, M.; Lotrich, V. F.; Bartlett, R. J. Multireference Nature of Chemistry: The Coupled-Cluster View. *Chem. Rev.* **2012**, *112*, 182−243.
(8) Li, X.; Paldus, J. Reduced multireference CCSD method: An effective approach to quasidegenerate states. *J. Chem. Phys.* **1997**, *107*, 6257.
(9) Li, X. Benchmark study of potential energies and vibrational levels using the reduced multireference coupled cluster method. The HF molecule. *J. Mol. Struct.: THEOCHEM* **2001**, *547*, 69−81.
(10) Li, X. Energy versus amplitude corrected coupled-cluster approaches. I. *J. Chem. Phys.* **2001**, *115*, 5759−5773.
(11) Li, X.; Paldus, J. Energy versus amplitude corrected coupled-cluster approaches. II. Breaking the triple bond. *J. Chem. Phys.* **2001**, *115*, 5774−5783.
(12) Paldus, J.; Planelles, J.; Li, X. Valence bond corrected single reference coupled cluster approach II. Application to PPP model systems. *Theor. Chim. Acta* **1994**, *89*, 13.
(13) Piecuch, P.; Tobola, R.; Paldus, J. Approximate account of connected quadruply excited clusters in single-reference coupled-cluster theory via cluster analysis of the projected unrestricted Hartree-Fock wave function. *Phys. Rev. A: At., Mol., Opt. Phys.* **1996**, *54*, 1210.
(14) Li, X.; Peris, G.; Planelles, J.; Rajadall, F.; Paldus, J. Externally corrected singles and doubles coupled cluster methods for open-shell systems. *J. Chem. Phys.* **1997**, *107*, 90.
(15) Kinoshita, T.; Hino, O.; Bartlett, R. J. Coupled-cluster method tailored by configuration interaction. *J. Chem. Phys.* **2005**, *123*, 074106.
(16) Lyakh, D. I.; Lotrich, V. F.; Bartlett, R. J. The 'tailored' CCSD(T) description of the automerization of cyclobutadiene. *Chem. Phys. Lett.* **2011**, *501*, 166−171.
(17) Melnichuk, A.; Bartlett, R. J. Relaxed active space: fixing tailored-CC with high order coupled cluster. I. *J. Chem. Phys.* **2012**, *137*, 214103.
(18) Melnichuk, A.; Bartlett, R. J. Relaxed active space: Fixing tailored-CC with high order coupled cluster. II. *J. Chem. Phys.* **2014**, *140*, 064113.
(19) Hino, O.; Kinoshita, T.; Chan, G. K.-L.; Bartlett, R. J. Tailored coupled cluster singles and doubles method applied to calculations on molecular structure and harmonic vibrational frequencies of ozone. *J. Chem. Phys.* **2006**, *124*, 114311.
(20) White, S. R.; Noack, R. M. Real-space quantum renormalization groups. *Phys. Rev. Lett.* **1992**, *68*, 3487−3490.
(21) White, S. R. Density matrix formulation for quantum renormalization groups. *Phys. Rev. Lett.* **1992**, *69*, 2863−2866.
(22) White, S. R. Density-matrix algorithms for quantum renormalization groups. *Phys. Rev. B: Condens. Matter Mater. Phys.* **1993**, *48*, 10345−10356.
(23) White, S. R.; Martin, R. L. Ab initio quantum chemistry using the density matrix renormalization group. *J. Chem. Phys.* **1999**, *110*, 4127−4130.
(24) Chan, G. K.-L.; Head-Gordon, M. Highly correlated calculations with a polynomial cost algorithm: A study of the density matrix renormalization group. *J. Chem. Phys.* **2002**, *116*, 4462−4476.
(25) Legeza, Ö.; Röder, J.; Hess, B. Controlling the accuracy of the density-matrix renormalization-group method: The dynamical block state selection approach. *Phys. Rev. B: Condens. Matter Mater. Phys.* **2003**, *67*, 125114.
(26) Legeza, Ö.; Noack, R.; Sólyom, J.; Tincani, L. Applications of Quantum Information in the Density-Matrix Renormalization Group. In *Computational Many-Particle Physics*; Fehske, H., Schneider, R., Weisse, A., Eds.; Springer: Berlin, Heidelberg, Germany, 2008; Vol. *739*.
(27) Marti, K. H.; Reiher, M. The Density Matrix Renormalization Group Algorithm in Quantum Chemistry. *Z. Phys. Chem.* **2010**, *224*, 583−599.
(28) Chan, G. K.-L.; Sharma, S. The Density Matrix Renormalization Group in Quantum Chemistry. *Annu. Rev. Phys. Chem.* **2011**, *62*, 465−481.
(29) Wouters, S.; Van Neck, D. The density matrix renormalization group for ab initio quantum chemistry. *Eur. Phys. J. D* **2014**, *68*, 272.
(30) Szalay, S.; Pfeffer, M.; Murg, V.; Barcza, G.; Verstraete, F.; Schneider, R.; Legeza, Ö. Tensor product methods and entanglement optimization for ab initio quantum chemistry. *Int. J. Quantum Chem.* **2015**, *115*, 1342.
(31) Yanai, T.; Kurashige, Y.; Mizukami, W.; Chalupský, J.; Lan, T. N.; Saitow, M. Density matrix renormalization group for ab initio Calculations and associated dynamic correlation methods: A review of theory and applications. *Int. J. Quantum Chem.* **2015**, *115*, 283−299.
(32) Kurashige, Y.; Chan, G. K.-L.; Yanai, T. Entangled quantum electronic wavefunctions of the Mn4CaO5 cluster in photosystem IIm. *Nat. Chem.* **2013**, *5*, 660−666.
(33) Sharma, S.; Sivalingam, K.; Neese, F.; Chan, G. K.-L. Low-energy spectrum of iron−sulfur clusters directly from many-particle quantum mechanics. *Nat. Chem.* **2014**, *6*, 927.
(34) Kurashige, Y.; Yanai, T. Second-order perturbation theory with a density matrix renormalization group self-consistent field reference function: Theory and application to the study of chromium dimer. *J. Chem. Phys.* **2011**, *135*, 094104.
(35) Saitow, M.; Kurashige, Y.; Yanai, T. Multireference configuration interaction theory using cumulant reconstruction with internal contraction of density matrix renormalization group wave function. *J. Chem. Phys.* **2013**, *139*, 044118.
(36) Neuscamman, E.; Yanai, T.; Chan, G. K.-L. A review of canonical transformation theory. *Int. Rev. Phys. Chem.* **2010**, *29*, 231−271.
(37) Sharma, S.; Chan, G. Communication: A flexible multi-reference perturbation theory by minimizing the Hylleraas functional with matrix product states. *J. Chem. Phys.* **2014**, *141*, 111101.
(38) Notice also that due to the two-body nature of the electronic Hamiltonian, TCCSD energy within the active space will reproduce the CASCI energy.
(39) Schollwöck, U. The density-matrix renormalization group. *Rev. Mod. Phys.* **2005**, *77*, 259−315.
(40) Schollwöck, U. The density-matrix renormalization group in the age of matrix product states. *Ann. Phys.* **2011**, *326*, 96−192.
(41) Legeza, Ö.; Sólyom, J. Optimizing the density-matrix renormalization group method using quantum information entropy. *Phys. Rev. B: Condens. Matter Mater. Phys.* **2003**, *68*, 195116.
(42) Moritz, G.; Hess, B.; Reiher, M. Convergence behavior of the density-matrix renormalization group algorithm for optimized orbital orderings. *J. Chem. Phys.* **2005**, *122*, 024107.
(43) Fertitta, E.; Paulus, B.; Barcza, G.; Legeza, Ö. Investigation of metal-insulator-like transition through the ab initio density matrix renormalization group approach. *Phys. Rev. B: Condens. Matter Mater. Phys.* **2014**, *90*, 245129.
(44) Krumnow, C.; Veis, L.; Legeza, Ö.; Eisert, J. *Fermionic orbital optimization in tensor network states*. arXiv:1504.00042v3 [quant-ph].
(45) Olivares-Amaya, R.; Hu, W.; Nakatani, N.; Sharma, S.; et al. The ab-initio density matrix renormalization group in practice. *J. Chem. Phys.* **2015**, *142*, 034102.
(46) Legeza, Ö.; Sólyom, J. Two-Site Entropy and Quantum Phase Transitions in Low-Dimensional Models. *Phys. Rev. Lett.* **2006**, *96*, 116401.
(47) Rissler, J.; Noack, R. M.; White, S. R. Measuring orbital interaction using quantum information theory. *Chem. Phys.* **2006**, *323*, 519−531.

DOI: 10.1021/acs.jpclett.6b01908
J. Phys. Chem. Lett. 2016, 7, 4072−4078

(48) Barcza, G.; Legeza, Ö.; Marti, K. H.; Reiher, M. Quantum-information analysis of electronic states of different molecular structures. *Phys. Rev. A: At., Mol., Opt. Phys.* **2011**, *83*, 012508.
(49) Boguslawski, K.; Tecmer, P.; Legeza, Ö.; Reiher, M. Entanglement Measures for Single- and Multireference Correlation Effects. *J. Phys. Chem. Lett.* **2012**, *3*, 3129−3135.
(50) Boguslawski, K.; Tecmer, P.; Barcza, G.; Legeza, Ö.; Reiher, M. Orbital Entanglement in Bond-Formation Processes. *J. Chem. Theory Comput.* **2013**, *9*, 2959−2973.
(51) Barcza, G.; Noack, R. M.; Sólyom, J.; Legeza, Ö. Entanglement patterns and generalized correlation functions in quantum many-body systems. *Phys. Rev. B: Condens. Matter Mater. Phys.* **2015**, *92*, 125140.
(52) Moritz, G.; Reiher, M. Decomposition of density matrix renormalization group states into a Slater determinant basis. *J. Chem. Phys.* **2007**, *126*, 244109.
(53) Boguslawski, K.; Marti, K. H.; Reiher, M. Construction of CASCI-type wave functions for very large active spaces. *J. Chem. Phys.* **2011**, *134*, 224101.
(54) Zgid, D.; Nooijen, M. Obtaining the two-body density matrix in the density matrix renormalization group method. *J. Chem. Phys.* **2008**, *128*, 144115.
(55) The term $O(M^3n^3)$ is usually the dominant one.
(56) It might seem at first sight that it will scale as $O(M^2n^5)$ [$O(n^4)$ CI coefficients each requiring $O(M^2n)$ operations when contracting the MPS matrices]. However, when the formation of two-index intermediates and construction of different terms during the whole sweep are used in the same way as those for the construction of DMRG two-body reduced density matrices,[54] the scaling can be reduced to $O(M^2n^4)$.
(57) Even though this approximation may not be perfect, the method performs very well, as shown in the examples, due to the fact that energy expressed in intermediate normalization requires only T1 and T2 amplitudes and the active space ones are very accurate, indeed.
(58) The underlying DMRG is size-consistent, provided that the active space has been properly chosen to include orbitals to which bonds dissociate in the fragments (analogous situation to CASSCF).
(59) Angeli, C.; Bories, B.; Cavallini, A.; Cimiraglia, R. Third-order multireference perturbation theory: The nn -electron valence state perturbation-theory approach. *J. Chem. Phys.* **2006**, *124*, 054108.
(60) Goodgame, M. M.; Goddard, W. A., III Modified Generalized Valence-Bond Method: A Simple Correction for the Electron Correlation Missing in Generalized Valence-Bond Wave Functions; Prediction of Double-Well States for Cr2 and Mo2. *Phys. Rev. Lett.* **1985**, *54*, 661.
(61) Andersson, K.; Roos, B. O.; Malmqvist, P.-A.; Widmark, P.-O. The Cr2 potential energy curve studied with multiconfigurational second-order perturbation theory. *Chem. Phys. Lett.* **1994**, *230*, 391.
(62) Bauschlicher, C. W.; Partridge, H. Cr2 revisited. *Chem. Phys. Lett.* **1994**, *231*, 277.
(63) Roos, B. O.; Andersson, K. Multiconfigurational perturbation theory with level shift — the Cr2 potential revisited. *Chem. Phys. Lett.* **1995**, *245*, 215.
(64) Stoll, H. The Cr2 potential curve: a multireference pair functional treatment. *Mol. Phys.* **1996**, *88*, 793.
(65) Dachsel, H.; Harrison, R. J.; Dixon, D. A. Multireference Configuration Interaction Calculations on Cr2: Passing the One Billion Limit in MRCI/MRACPF Calculations. *J. Phys. Chem. A* **1999**, *103*, 152.
(66) Roos, B. O. The Ground State Potential for the Chromium Dimer Revisited. *Collect. Czech. Chem. Commun.* **2003**, *68*, 265.
(67) Celani, P.; Stoll, H.; Werner, H.-J.; Knowles, P. J. The CIPT2 method: Coupling of multi-reference configuration interaction and multi-reference perturbation theory. Application to the chromium dimer. *Mol. Phys.* **2004**, *102*, 2369.
(68) Zgid, D.; Ghosh, D.; Neuscamman, E.; Chan, G. K.-L. A study of cumulant approximations to nn-electron valence multireference perturbation theory. *J. Chem. Phys.* **2009**, *130*, 194107.
(69) Müller, T. Large-Scale Parallel Uncontracted Multireference-Averaged Quadratic Coupled Cluster: The Ground State of the Chromium Dimer Revisited. *J. Phys. Chem. A* **2009**, *113*, 12729.
(70) Moritz, G.; Reiher, M. Construction of environment states in quantum-chemical density-matrix renormalization group calculations. *J. Chem. Phys.* **2006**, *124*, 034103.
(71) Lofthus, A.; Krupenie, P. H. The spectrum of molecular nitrogen. *J. Phys. Chem. Ref. Data* **1977**, *6*, 113.
(72) Zhang, W.; Loebach, J. L.; Wilson, S. R.; Jacobsen, E. N. Enantioselective epoxidation of unfunctionalized olefins catalyzed by salen manganese complexes. *J. Am. Chem. Soc.* **1990**, *112*, 2801.
(73) Irie, R.; Noda, K.; Ito, Y.; Matsumoto, N.; Katsuki, T. Catalytic asymmetric epoxidation of unfunctionalized olefins. *Tetrahedron Lett.* **1990**, *31*, 7345.
(74) Ivanic, J.; Collins, J. R.; Burt, S. K. J. Theoretical Study of the Low Lying Electronic States of oxoX(salen) (X = Mn, Mn-, Fe, and Cr-) Complexes. *J. Phys. Chem. A* **2004**, *108*, 2314−2323.
(75) Sears, J. S.; Sherrill, C. D. The electronic structure of oxo-Mn(salen): Single-reference and multireference approaches. *J. Chem. Phys.* **2006**, *124*, 144314.
(76) Ma, D.; Li Manni, G.; Gagliardi, L. The generalized active space concept in multiconfigurational self-consistent field methods. *J. Chem. Phys.* **2011**, *135*, 044128.
(77) Wouters, S.; Bogaerts, T.; Van Der Voort, P.; Van Speybroeck, V.; Van Neck, D. Communication: DMRG-SCF study of the singlet, triplet, and quintet states of oxo-Mn(Salen). *J. Chem. Phys.* **2014**, *140*, 241103.
(78) Stein, C. J.; Reiher, M. Automated Selection of Active Orbital Spaces. *J. Chem. Theory Comput.* **2016**, *12*, 1760−1771.
(79) Abashkin, Y. G.; Collins, J. R.; Burt, S. K. Salen)Mn(III)-Catalyzed Epoxidation Reaction as a Multichannel Process with Different Spin States. Electronic Tuning of Asymmetric Catalysis: A Theoretical Study. *Inorg. Chem.* **2001**, *40*, 4040.
(80) At our first attempt, we perfectly reproduced the DMRG results of Olivares-Amaya et al.[45] (ΔE differed by less than 0.1 kcal/mol, which is because our CAS was bigger by one occupied orbital); however, we found out that we did not converge to the global ^{3}A state ROHF minimum, resulting in a wrong characteristic excitation of the ^{3}A state (it is unfortunately not mentioned in ref 45). The correct character of the ^{3}A state, which corresponds to the global ROHF minimum, is shown in Figure 7 of the SI. The TCCSD method, nevertheless, predicted the ^{3}A state to be the ground state even in this case with $\Delta E = -0.4$ kcal/mol.
(81) Legeza, Ö. *QC-DMRG-Budapest*, a program for quantum chemical DMRG calculations; 2011.
(82) Neese, F. The ORCA program system. *WIREs Comput. Mol. Sci.* **2012**, *2*, 73−78.
(83) Legeza, Ö.; Sólyom, L. Quantum data compression, quantum information generation, and the density-matrix renormalization-group method. *Phys. Rev. B: Condens. Matter Mater. Phys.* **2004**, *70*, 205118.
(84) Dunham, J. L. The Energy Levels of a Rotating Vibrator. *Phys. Rev.* **1932**, *41*, 721.
(85) Raghavachari, K.; Trucks, G. W.; Pople, J. A.; Head-Gordon, M. Historical perspective on: A fifth-order perturbation comparison of electron correlation theories. *Chem. Phys. Lett.* **1989**, *157*, 479.

DOI: 10.1021/acs.jpclett.6b01908
J. Phys. Chem. Lett. 2016, 7, 4072−4078

JCTC Journal of Chemical Theory and Computation

Article

Cite This: J. Chem. Theory Comput. 2018, 14, 2439−2445

pubs.acs.org/JCTC

The Intricate Case of Tetramethyleneethane: A Full Configuration Interaction Quantum Monte Carlo Benchmark and Multireference Coupled Cluster Studies

Libor Veis,*[,†] Andrej Antalík,*[,†,‡] Örs Legeza,*[,¶] Ali Alavi,*[,§,∥] and Jiří Pittner*[,†]

[†]J. Heyrovský Institute of Physical Chemistry, Academy of Sciences of the Czech Republic, v.v.i., Dolejškova 3, 18223 Prague 8, Czech Republic

[‡]Faculty of Mathematics and Physics, Charles University, 11636 Prague, Czech Republic

[¶]Strongly Correlated Systems "Lendület" Research group, Wigner Research Centre for Physics, H-1525 Budapest, Hungary

[§]Department of Chemistry, University of Cambridge, Cambridge CB2 1EW, United Kingdom

[∥]Max Planck Institüt für Festkörperforschung, 70569 Stuttgart, Germany

ABSTRACT: We have performed a full configuration interaction (FCI) quality benchmark calculation for the tetramethyleneethane molecule in the cc-pVTZ basis set employing a subset of complete active space second order perturbation theory, CASPT2(6,6), natural orbitals for the FCI quantum Monte Carlo calculation. The results are in an excellent agreement with the previous large scale diffusion Monte Carlo calculations by Pozun et al. and available experimental results. Our computations verified that there is a maximum on the potential energy surface (PES) of the ground singlet state (^{1}A) 45° torsional angle, and the corresponding vertical singlet−triplet energy gap is 0.01 eV. We have employed this benchmark for the assessment of the accuracy of Mukherjee's coupled clusters with up to triple excitations (MkCCSDT) and CCSD tailored by the density matrix renormalization group method (DMRG). Multireference MkCCSDT with CAS(2,2) model space, though giving good values for the singlet−triplet energy gap, is not able to properly describe the shape of the multireference singlet PES. Similarly, DMRG(24,25) is not able to correctly capture the shape of the singlet surface, due to the missing dynamic correlation. On the other hand, the DMRG-tailored CCSD method describes the shape of the ground singlet state with excellent accuracy but for the correct ordering requires computation of the zero-spin-projection component of the triplet state (^{3}B$_1$).

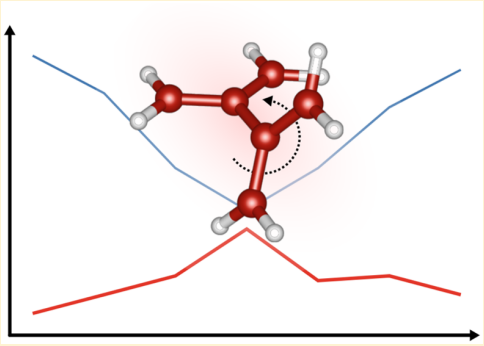

1. INTRODUCTION

Tetramethyleneethane (TME), the simplest disjoint non-Kekulé diradical first synthesized by Dowd,[1] due to its complex electronic structure has been often used as a benchmark system for the state-of-the-art multireference computational methods.[2−6] Its complexity comes out of the fact that it contains a nearly degenerate pair of frontier orbitals, which tend to be localized on separate allyl subunits[5] and are occupied by two electrons. Moreover, TME possesses a degree of freedom corresponding to the rotation about the central C−C bond (maintaining D_2 symmetry, see Figure 1) and the energetic ordering of these two frontier orbitals and consequently their occupation in the lowest singlet state changes along the rotation[a]. As a result, determining the relative stability of the lowest singlet and triplet states turned out to be a big challenge for both experimental and theoretical methods.

The first experimental electron paramagnetic resonance (EPR) results predicted TME to have a triplet ground state,[1] when stabilized in a matrix with a torsional angle being approximately 45°.[7,8] The predicted triplet ground state attracted much interest in TME for its potential use as an organic magnet.[9] However, photoelectron spectroscopy of the TME$^-$ ion strongly suggested TME to have a singlet ground state at the torsional angle corresponding to 90°,[10] similar to the EPR experiments on TME derivatives.[11,12]

Several theoretical studies using different level of approximations[2−4,13−17] have step by step contributed to the understanding of the electronic structure of the TME diradical. Nevertheless, only the work of Pozun et al. employing the large scale diffusion Monte Carlo (DMC) calculations[5] finally reliably established the magnitude of the singlet−triplet gap and also the shape of the singlet potential energy surface (PES).

The main conclusions tell us that the correct theoretical description of the multireference singlet state (^{1}A) requires all of the following conditions being fulfilled: a flexible-enough atomic basis set, a proper description of the static correlation with the minimum active space comprising of six π-orbitals, and a proper treatment of the dynamic correlation (at least at the level of the second-order perturbation theory). All of this makes

Received: January 9, 2018
Published: March 23, 2018

DOI: 10.1021/acs.jctc.8b00022
J. Chem. Theory Comput. 2018, 14, 2439−2445

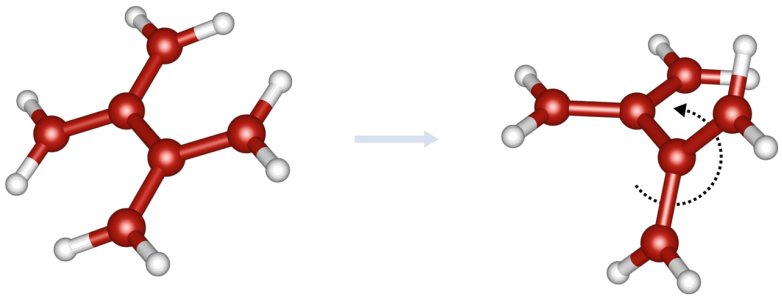

Figure 1. Studied process of a rotation of the TME allyl subunits about the central C−C bond. Carbon atoms are colored red; hydrogens are white.

TME a very delicate molecule and indeed a perfect benchmark system for state-of-the-art multireference methods. Moreover, TME serves as a model system for more complicated disjoint diradicals.

In the present work, we compute the singlet, as well as triplet, twisting PESs of TME. First, we provide full configuration interaction (FCI) quality data by the FCI quantum Monte Carlo (FCIQMC) method,[18−21] whose accuracy is justified by the excellent agreement with DMC results of Pozun et al.[5] and available experimental data. Second, we compare the results of the Hilbert space Mukherjee's multireference coupled clusters (MR MkCC)[22−30] and the recently developed coupled clusters with single and double excitations tailored by the density matrix renormalization group method (DMRG-TCCSD)[31,32] against the FCIQMC benchmark.

The paper is organized as follows: in section 2, we give a very brief overview of the used computational approaches and the actual computational details. Section 3 summarizes the results with discussion, and the section 4 closes with conclusions and outlook.

2. OVERVIEW OF COMPUTATIONAL APPROACHES

In this section, for completeness, we sketch out main concepts and ideas of the employed computational approaches.

2.1. FCI Quantum Monte Carlo. The FCIQMC method,[18,19,21,33] originally developed by one of us, is a stochastic approach performing a long time integration of the imaginary-time Schrödinger equation, which is capable of converging onto a FCI solution for much larger orbital spaces than the exact diagonalization allows. In contrast to DMC, FCIQMC samples the *Slater determinant space* by an ensemble of walkers that move around randomly.

Master equations governing walkers' population dynamics are given by

$$-\frac{\mathrm{d}N_i}{\mathrm{d}\tau} = (H_{ii} - S)N_i + \sum_{j\neq i} H_{ij}N_j \tag{1}$$

where τ is the imaginary time, N_i is the walker population on determinant i, S is the energy shift parameter controlling the total walker population, and H_{ij} are the Hamiltonian matrix elements in the basis of Slater determinants. When employing the stochastic approach, individual walkers evolve according to a simple set of rules, which include spawning, death and cloning, and most importantly annihilation processes.[18]

We have used a semistochastic method with real walker weights,[20] in which a part of the imaginary-time propagation (eq 1) is performed exactly (deterministic space) and the rest stochastically. Such an approach in fact greatly reduces stochastic errors.

2.2. Mukherjee's Coupled Clusters. The MR MkCC approach formulated by Mukherjee et al.[22] and later on developed by others, including one of us,[6,23−30,34,35] is a state specific Hilbert-space multireference coupled cluster method. Consequently, the MkCC wave function, $|\Psi_{\mathrm{MkCC}}\rangle$, is expressed by means of the Jeziorski−Monkhorst ansatz

$$|\Psi_{\mathrm{MkCC}}\rangle = \sum_{\mu=1}^{M} c_\mu \, \mathrm{e}^{T(\mu)}|\Phi_\mu\rangle \tag{2}$$

In eq 2, $|\Phi_\mu\rangle$ are the reference functions spanning the model space (in our case complete) and $T(\mu)$ are the reference-dependent cluster operators. The c_μ coefficients as well as the desired energy are obtained by diagonalization of the effective Hamiltonian matrix, whose elements read

$$H^{\mathrm{eff}}_{\mu\nu} = \langle\Phi_\mu|H\mathrm{e}^{T(\nu)}|\Phi_\nu\rangle \tag{3}$$

with H being the Hamiltonian operator.

The MkCC method is superior to the related Hilbert-space multireference method based on the Brillouin−Wigner CC theory due to its exact size extensivity. Though not completely free of problems, the MkCC approach is reliable for small model spaces, and it is indeed the method of choice for electronic structure studies of diradicals. In the present work, we have employed the MR MkCC methods including single and double (MkCCSD) and single, double, and triple excitations (MkCCSDT).

2.3. DMRG-Based Tailored Coupled Clusters. The tailored CC (TCC) approach was formulated by Kinoshita et al.[36] and belongs to the class of so-called externally corrected CC methods. The TCC wave function expansion employs the split-amplitude ansatz used previously by Piecuch et al.[37,38]

$$|\Psi_{\mathrm{TCC}}\rangle = \mathrm{e}^{T}|\Phi_0\rangle = \mathrm{e}^{T_{\mathrm{ext}}+T_{\mathrm{CAS}}}|\Phi_0\rangle = \mathrm{e}^{T_{\mathrm{ext}}}\mathrm{e}^{T_{\mathrm{CAS}}}|\Phi_0\rangle \tag{4}$$

that is, the cluster operator is split up into its active space part (T_{CAS}) and the remaining external part (T_{ext}). Since $|\Phi_0\rangle$ is a single-determinant reference wave function, both of the aforementioned cluster operators mutually commute, which keeps the methodology very simple.

The T_{CAS} amplitudes are supposed to be responsible for a proper description of the static correlation. They are computed from the complete active space configuration interaction (CASCI) wave function coefficients and are kept frozen during the CC iterations. Only the T_{ext} part, which is responsible for a proper description of the dynamic correlation, is being optimized.

DOI: 10.1021/acs.jctc.8b00022
J. Chem. Theory Comput. 2018, 14, 2439−2445

Recently, some of us have developed the DMRG-TCCSD method, that is, coupled clusters with single and double excitations tailored by matrix product state (MPS) wave functions (wave functions produced by the DMRG algorithm[39,40]).[31] This approach replaces CASCI of the original TCC method by DMRG and thus allows employing much larger active spaces. It has proven itself to be a reliable method suitable for difficult multireference problems requiring larger active spaces.[31]

2.4. Computational Details. We have performed constrained geometry optimizations for seven values of the torsional angle along the twisting process. Geometries were optimized for both states (^{1}A, ^{3}B$_1$) with the complete active space second order perturbation theory (CASPT2) as implemented in the MOLPRO package.[41] The CASPT2 calculations were carried out using the active space comprising of six π orbitals, CAS(6,6) and cc-pVTZ basis.[42] Only the first 60 CASPT2(6,6) natural orbitals sorted according to their occupation numbers[b] were kept for the correlation treatment by the FCIQMC, MR MkCC, DMRG, and DMRG-TCCSD methods; the rest were dropped. We have chosen this strategy rather than employing a smaller basis, for example, 6-31G/6-31G* (still manageable by the massively parallel FCIQMC implementation[33]), as it was clearly demonstrated[5] that a triple-ζ basis with f functions on the C atoms is essential for the proper description of the singlet (^{1}A) PES (see section 3 for further comments).

For the FCIQMC calculations, we have employed the following computational protocol: (1) equilibration computations with 10 million walkers; (2) generation of FCIQMC natural orbitals[21] (for faster convergence with the number of walkers) with 50-million-walker computations; (3) subsequent 100, 500, and 1000-million-walker computations with the FCIQMC natural orbitals. We have used the initiator version of the FCIQMC method as implemented in the NECI program package.[43] Moreover, to greatly reduce stochastic errors, we have employed a semistochastic method with real walker weights[20] and, in case of the largest 1000-million-walker computations, 50 thousand most populated determinants in the deterministic space.

MR MkCC calculations were performed with the complete model space comprising of the frontier orbitals, CAS(2,2).

In all production DMRG calculations (those used for generation of the active space CC amplitudes), we have employed the dynamical block state selection (DBSS) procedure[44,45] with the truncation error criterion set to 5×10^{-6}, which resulted in bond dimensions varying in the range of 1000−8000. The orbitals for DMRG active spaces were chosen according to their single-orbital entropies (S_i), in particular for CAS(6,6) $S_i > 0.3$, in case of CAS(12,12) $S_i > 0.1$, and for CAS(24,25) $S_i > 0.075$. The DMRG active space orbitals were split-localized.[46] The Fiedler method[47,48] was used for optimization of the orbital ordering, and DMRG runs were initialized using the CI-DEAS procedure.[49,50]

In all DMRG-TCCSD calculations, we have employed the frozen core approximation. Apart from the high spin triplet ($m_s = 1$), for the reasons discussed below, we have also calculated the low spin triplet components ($m_s = 0$). Such calculations were realized by swapping (rotation) of the open-shell β spin−orbitals and finally closed-shell computations employing the unrestricted versions of the DMRG[c] and TCCSD codes (the molecular orbital integrals become spin-dependent).

3. RESULTS AND DISCUSSION

The FCIQMC PESs of the singlet (^{1}A) and triplet states (^{3}B$_1$) corresponding to the twisting process are shown in Figure 2.

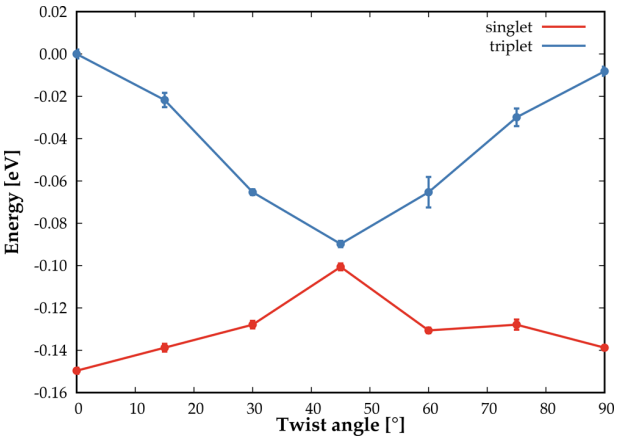

Figure 2. FCIQMC singlet (^{1}A) and triplet state (^{3}B$_1$) twisting PESs of TME. Vertical lines correspond to errors calculated by the blocking analysis.[54]

We do not present the absolute energies as they may not be fully converged with the number of walkers;[d] however 1000 million walkers was the maximum we could afford with 2000 CPU cores, and the relative energies are definitely not affected, giving an excellent agreement with the DMC energies by Pozun et al.[5] and available experimental data (see Table 2).

One can observe a very similar shape of the singlet PES as demonstrated by Pozun et al.,[5] that is, with its maximum corresponding to the torsional angle of 45°. The height of this "hump" $[E(45°) - E(0°)]$ calculated by the FCIQMC method equals 0.05 eV. Pozun et al.[5] demonstrated that a triple-ζ basis with f functions on the C atoms is essential to obtain a correct shape of the singlet PES with the maximum at 45°. We have performed additional FCIQMC calculations for the torsional angles of 0°, 45°, and 90° with the hybrid 6-31G/6-31G* including polarization functions only on the two central C atoms (74 molecular orbitals in total) to verify this conclusion. In fact, the energy difference between the points at 45° and 0° that we obtained was zero within the statistical errors, which is in agreement with ref 5.

The magnitude of the TME singlet−triplet energy gap is indeed very small, corresponding to 0.01 eV as obtained by the FCIQMC method. This is also the reason for the originally wrong ground state triplet assignment by EPR spectroscopy.[1] Weak EPR signal was apparently caused by small population of the triplet state allowed by the rotation about the central C−C bond.

In Figure 3, we present the MR MkCCSD, MkCCSDT, and DMRG(24,25) singlet (^{1}A) and triplet state (^{3}B$_1$) TME PESs. TCCSD PESs are shown in Figure 4.

As can be observed in Figure 3, the MR MkCCSD method gives wrong state ordering for all points along the twisting process except for one (0°). Inclusion of triple excitations (MR MkCCSDT) in fact corrects this behavior. Nevertheless, neither the MR MkCCSD nor the MR MkCCSDT method with CAS(2,2) model space is able to properly describe the PES of the singlet state with the apparent maximum at the torsional angle of 45°. There is actually an indication of an

DOI: 10.1021/acs.jctc.8b00022
J. Chem. Theory Comput. 2018, 14, 2439−2445

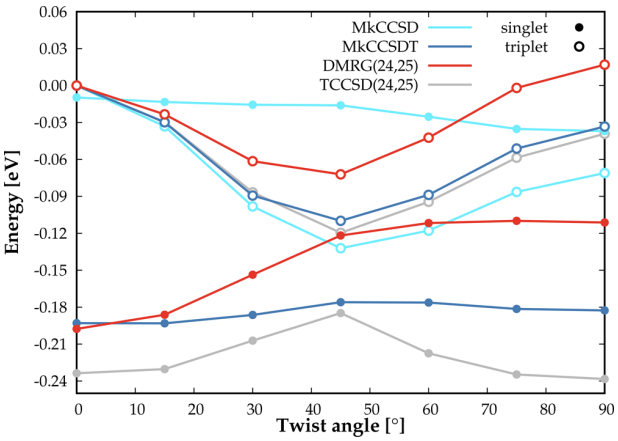

Figure 3. MR MkCCSD, MkCCSDT, DMRG(24,25), and TCCSD-(24,25) singlet (^{1}A) and triplet state (^{3}B$_1$) twisting PESs of TME. The triplet TCCSD(24,25) results correspond to the low spin (m_s = 0) component.

arising maximum on the MR MkCCSDT singlet PES close to 45°; however, it is still too flat. Either enlargement of the model space as suggested by Pozun et al.[5] or inclusion of higher (quadruple) excitations is probably necessary for the correct singlet state description. We have not pursued any of these possibilities, mainly due to considerably higher computational demands. Moreover, MR MkCC methods (as well as the other Hilbert space MR CC methods) are known to suffer from the so-called "proper residual problem",[55−57] where numerous residual components of the projected Schrödinger equation are not equal to zero (Schrödinger is not satisfied). This effect is more pronounced for larger model spaces, and it is also the reason why the most successful applications of the MR MkCCSD method were limited to the CAS(2,2) model space,[57] and larger model spaces [in our case ideally CAS(6,6)] are not recommended.

Figure 3 also depicts the DMRG(24,25) PESs. One can see the correct ordering of both spin states; however, the singlet (^{1}A) PES also does not possess the right shape. The singlet state energy is correctly increasing when going from the torsional angle of 0° to 45° but does not sufficiently decrease for 45° to 90°. Apparently, the missing dynamic correlation has an important effect on this part of the singlet PES, changing its shape qualitatively.

The TCC results from Figure 4 indicate that the TCCSD method is successful in recovering a major part of the missing dynamic correlation and thus properly describes the singlet PES. The effect of enlarging CAS is graphically depicted in Figure 4a and numerically by comparison with the FCIQMC benchmark in Table 1. One can observe that the value of the

Table 1. TME Singlet State (^{1}A) Twisting Energy Barrier (kcal/mol), Calculated by the TCCSD Method with Various CASs and the Energy Differences from the FCIQMC Benchmark

method	E	ΔE
TCCSD(6,6)	2.527	1.395
TCCSD(12,12)	1.577	0.445
TCCSD(24,25)	1.127	−0.005

twisting energy barrier $[E(45°) - E(0°)]$ is decreasing with enlarging CAS and also improving toward the FCIQMC benchmark, eventually giving an excellent agreement for TCCSD(24,25) with the error of −0.005 kcal/mol.

Nevertheless, the shape of the singlet PES is only a part of the story. In case of the spin state ordering, even the TCCSD method is not completely free of problems. When calculating the high spin triplet component (m_s = 1), TCCSD(24,25) gives a wrong ordering of both spin states near the torsional angle of 45° (see Figure 4b). The reason for this behavior is obviously the fact that at 45°, both spin states very much differ in their character; triplet is dominated by a single determinant, whereas singlet is strongly multireference with two determinants ($HOMO^2LUMO^0$ and $HOMO^0LUMO^{2e}$) of practically equal weights. This is actually the worst case scenario for the TCC method, which even though we call it a multireference CC, strictly speaking uses a single reference determinant and may be slightly biased in such "degenerate" situations. Taking into account that the TME singlet−triplet energy gap is really small

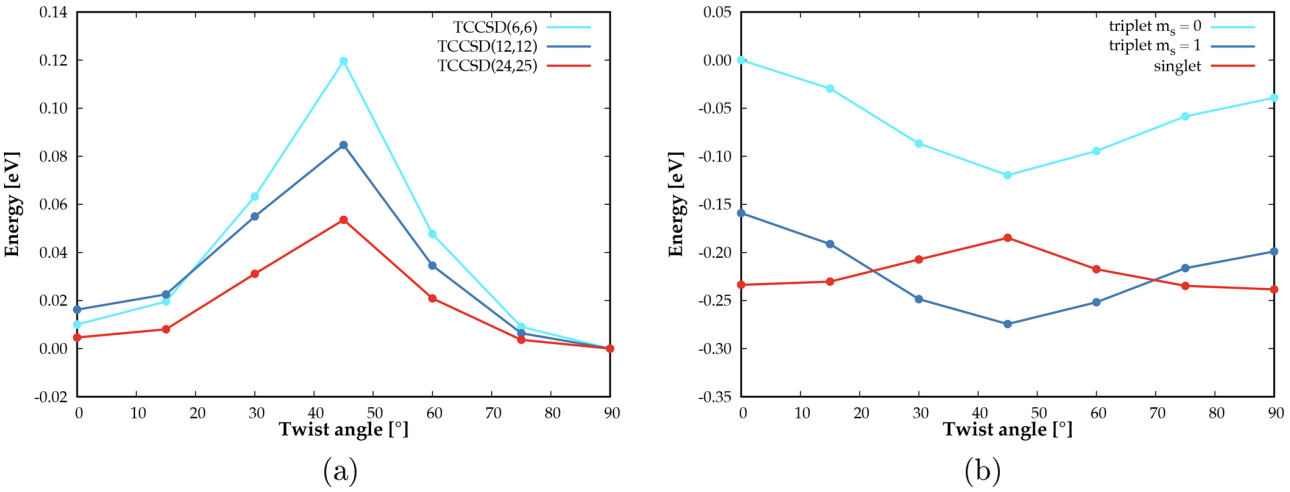

Figure 4. TCCSD PESs of TME. (a) Singlet state (^{1}A) PES calculated with different CAS sizes. (b) Singlet and triplet state (^{3}B$_1$) PESs calculated by the TCCSD(24,25) method.

DOI: 10.1021/acs.jctc.8b00022
J. Chem. Theory Comput. 2018, 14, 2439−2445

(0.2 kcal/mol by FCIQMC), the aforementioned fact results in wrong state ordering.

To verify our assumptions, we have also calculated the low spin triplet component ($m_s = 0$). It is strongly multireference as well, since it can be qualitatively described by a combination of two determinants ($HOMO^{\alpha}LUMO^{\beta}$ and $HOMO^{\beta}LUMO^{\alpha}$) with equal weights. Our aim was to eliminate to some extent the bias toward one of two equally important determinants by calculating the states of a similar character. Figure 4b shows that such an approach gives correct spin state ordering.

Last but not least, Table 2 compares the singlet−triplet energy gaps for the torsional angles of 45° and 90° calculated by different methods with the DMC result of Pozun et al.[5] and available experimental data. One can notice results of a similar quality for the MR MkCCSDT and $TCCSD(24,25)_{m_s=0}$ methods, where the fact that the former method includes single, double, and triple excitations whereas the latter includes only single and double excitations should be emphasized.

Table 2. TME Singlet-Triplet Energy Gaps in eV, Corresponding to the Torsional Angles of 45° and 90° Calculated by Different Methods

	ΔE_{T-S}	
method	45°	90°
MkCCSD	−0.12	−0.03
MkCCSDT	0.07	0.15
DMRG(24,25)	0.05	0.13
$TCCSD(24,25)_{m_s=1}$	−0.09	0.04
$TCCSD(24,25)_{m_s=0}$	0.07	0.20
FCIQMC	0.01	0.13
best available	0.02[a]	0.13 ± 0.013[b]

[a]DMC result/[5] [b]Photoelectron spectroscopy result.[10]

4. CONCLUSIONS

We have presented the FCIQMC benchmark data for the twisting process of the TME diradical, which give excellent agreement with the previous DMC and available experimental results. Our computations verified that there is a maximum on the PES of the ground singlet state (^1A) corresponding to the torsional angle of 45°. At this geometry, there is also the smallest vertical singlet−triplet energy gap of 0.01 eV as provided by FCIQMC. Compared to the previous study, we provide the data along the whole PES.

Against the FCIQMC benchmark data, we have critically assessed the accuracy of the MR MkCC and TCC methods. We have found out that the MR MkCCSD method is not able to correctly predict the ordering of both lowest lying spin states and that the MR MkCCSDT, though giving good values for the singlet−triplet energy gap, is due to the small CAS(2,2) model space, not able to properly describe the shape of the multireference singlet PES. On the other hand, the TCCSD method describes the ground singlet state with excellent accuracy but, for the correct ordering, requires computation of the low-spin component of the triplet state ($^3B_1$) due to the single-reference bias of TCC.

Finally, we would like to note that a multireference generalization of the tailored CC method is in our view an attractive approach worth exploring. We believe that such a method, based on the Jeziorski−Monkhorst ansatz (eq 2), that is, employing different sets of CC amplitudes for each reference determinant, and MR cluster analysis[58] of the MPS wave function, could help to remove the aforementioned single-reference bias of TCC.

AUTHOR INFORMATION

Corresponding Authors

*E-mail: libor.veis@jh-inst.cas.cz.
*E-mail: andrej.antalik@jh-inst.cas.cz.
*E-mail: legeza.ors@wigner.mta.hu.
*E-mail: A.Alavi@fkf.mpg.de.
*E-mail: jiri.pittner@jh-inst.cas.cz.

ORCID

Libor Veis: 0000-0002-4229-6335
Andrej Antalík: 0000-0002-8422-8410

Notes

The authors declare no competing financial interest.

ACKNOWLEDGMENTS

We thank J. Brabec for helpful discussions. This work has been supported by the Czech Science Foundation (Grant No. 16-12052S), Charles University (Project GA UK No. 376217), Czech Ministry of Education, Youth and Sports (Project No. LTAUSA17033), the Hungarian-Czech Joint Research Project MTA/16/05, the Hungarian National Research, Development and Innovation Office (Grant No. K120569), and the Hungarian Quantum Technology National Excellence Program (Project No. 2017-1.2.1-NKP-2017-00001). The FCIQMC calculations were carried out on the Salomon supercomputer in Ostrava; we therefore acknowledge the support by the Czech Ministry of Education, Youth and Sports from the Large Infrastructures for Research, Experimental Development and Innovations project "IT4Innovations National Supercomputing Center - LM2015070".

ADDITIONAL NOTES

[a]At the torsional angle matching 45°, the occupation of both frontier orbitals is approaching one.
[b]This number of natural orbitals corresponds approximately to the occupation number threshold of 0.2×10^{-2}.
[c]Huge flexibility of the Budapest QC-DMRG program[51] allows among others use of unrestricted molecular orbital integrals, as well as more general relativistic ones[52] or those appearing in nuclear structure calculations.[53]
[d]The MR MkCCSDT energies are in fact lower by approximately 10 mHartree; nevertheless, the CC method is generally not variational, and the error coming out from this fact is questionable.
[e]We use the standard notation of HOMO being the highest occupied molecular orbital and LUMO the lowest unoccupied molecular orbital.

REFERENCES

(1) Dowd, P. Tetramethyleneethane. *J. Am. Chem. Soc.* **1970**, *92*, 1066−1068.
(2) Pittner, J.; Nachtigall, P.; Čársky, P.; Hubač, I. State-specific Brillouin-Wigner multireference coupled cluster study of the singlet-triplet separation in the tetramethyleneethane diradical. *J. Phys. Chem. A* **2001**, *105*, 1354−1356.
(3) Bhaskaran-Nair, K.; Demel, O.; Šmydke, J.; Pittner, J. Multireference state-specific Mukherjee's coupled cluster method with noniterative triexcitations using uncoupled approximation. *J. Chem. Phys.* **2011**, *134*, 154106.

DOI: 10.1021/acs.jctc.8b00022
J. Chem. Theory Comput. 2018, 14, 2439−2445

(4) Chattopadhyay, S.; Chaudhuri, R. K.; Mahapatra, U. S. Ab Initio Multireference Investigation of Disjoint Diradicals: Singlet versus Triplet Ground States. *ChemPhysChem* **2011**, *12*, 2791−2797.
(5) Pozun, Z. D.; Su, X.; Jordan, K. D. Establishing the Ground State of the Disjoint Diradical Tetramethyleneethane with Quantum Monte Carlo. *J. Am. Chem. Soc.* **2013**, *135*, 13862−13869.
(6) Demel, O.; Pittner, J.; Neese, F. A Local Pair Natural Orbital-Based Multireference Mukherjee's Coupled Cluster Method. *J. Chem. Theory Comput.* **2015**, *11*, 3104−3114.
(7) Dowd, P.; Chang, W.; Paik, Y. H. Tetramethyleneethane, a ground-state triplet. *J. Am. Chem. Soc.* **1986**, *108*, 7416−7417.
(8) Dowd, P.; Chang, W.; Paik, Y. H. 2,3-Dimethylenecyclohexa-1,3-diene diradical is a ground-state triplet. *J. Am. Chem. Soc.* **1987**, *109*, 5284−5285.
(9) Berson, J. A. In *Magnetic Properties of Organic Materials*; Lahti, P. M., Ed.; Marcel Dekker, Inc: New York, 1999.
(10) Clifford, E. P.; Wenthold, P. G.; Lineberger, W. C.; Ellison, G. B.; Wang, C. X.; Grabowski, J. J.; Vila, F.; Jordan, K. D. Properties of tetramethyleneethane (TME) as revealed by ion chemistry and ion photoelectron spectroscopy. *J. Chem. Soc., Perkin Trans. 2* **1998**, *2*, 1015−1022.
(11) Bush, L. C.; Heath, R.; Feng, X. W.; Wang, P. A.; Maksimovic, L.; Song, A. I.; Chung, W.-S.; Berinstain, A. B.; Scaiano, J. C.; Berson, J. A. Tuning the Singlet-Triplet Energy Gap in a Non-Kekule Series by Designed Structural Variation. The Singlet States of N-Substituted-3,4-dimethylenepyrrole Biradicals. *J. Am. Chem. Soc.* **1997**, *119*, 1406−1415.
(12) Bush, L. C.; Maksimovic, L.; Feng, X. W.; Lu, H. S. M.; Berson, J. A. Triplet Species from Dihydropyrrolo[3,4-d]pyridazines, the Diazene Precursors of N-Arenesulfonyl-3,4-dimethylenepyrroles. *J. Am. Chem. Soc.* **1997**, *119*, 1416−1427.
(13) Du, P.; Borden, W. T. Ab initio calculations predict a singlet ground state for tetramethyleneethane. *J. Am. Chem. Soc.* **1987**, *109*, 930−931.
(14) Nachtigall, P.; Jordan, K. D. Theoretical study of the low-lying triplet and singlet states of diradicals. 1. Tetramethyleneethane. *J. Am. Chem. Soc.* **1992**, *114*, 4743−4747.
(15) Nachtigall, P.; Jordan, K. D. Theoretical study of the low-lying triplet and singlet states of tetramethyleneethane: prediction of a triplet below singlet state at the triplet equilibrium geometry. *J. Am. Chem. Soc.* **1993**, *115*, 270−271.
(16) Filatov, M.; Shaik, S. Tetramethyleneethane (TME) Diradical: Experiment and Density Functional Theory Reach an Agreement. *J. Phys. Chem. A* **1999**, *103*, 8885−8889.
(17) Rodriguez, E.; Reguero, M.; Caballol, R. The Controversial Ground State of Tetramethyleneethane. An ab Initio CI Study. *J. Phys. Chem. A* **2000**, *104*, 6253−6258.
(18) Booth, G. H.; Thom, A. J.; Alavi, A. Fermion Monte Carlo without fixed nodes: A game of life, death, and annihilation in Slater determinant space. *J. Chem. Phys.* **2009**, *131*, 054106.
(19) Cleland, D.; Booth, G. H.; Alavi, A. Communications: Survival of the fittest: Accelerating convergence in full configuration-interaction quantum Monte Carlo. *J. Chem. Phys.* **2010**, *132*, 041103.
(20) Petruzielo, F. R.; Holmes, A. A.; Changlani, H. J.; Nightingale, M. P.; Umrigar, C. J. Semistochastic Projector Monte Carlo Method. *Phys. Rev. Lett.* **2012**, *109*, 230201.
(21) Overy, C.; Booth, G.; Blunt, N. S.; Shepherd, J.; Cleland, D.; Alavi, A. Unbiased reduced density matrices and electronic properties from full configuration interaction quantum Monte Carlo. *J. Chem. Phys.* **2015**, *141*, 244117.
(22) Mahapatra, U.; Datta, B.; Mukherjee, D. A size-consistent state-specific multireference coupled cluster theory: Formal developments and molecular applications. *J. Chem. Phys.* **1999**, *110*, 6171.
(23) Evangelista, F.; Allen, W.; Schaefer, H. F., III High-order excitations in state-universal and state-specific multireference coupled cluster theories: Model systems. *J. Chem. Phys.* **2006**, *125*, 154113.
(24) Evangelista, F.; Allen, W.; Schaefer, H. F., III Coupling term derivation and general implementation of state-specific multireference coupled cluster theories. *J. Chem. Phys.* **2007**, *127*, 024102.
(25) Evangelista, F.; Simmonett, A.; Allen, W.; Schaefer, H. F., III; Gauss, J. Triple excitations in state-specific multireference coupled cluster theory: Application of Mk-MRCCSDT and Mk-MRCCSDT-n methods to model systems. *J. Chem. Phys.* **2008**, *128*, 124104.
(26) Evangelista, F.; Prochnow, E.; Gauss, J.; Schaefer, H. F., III Perturbative triples corrections in state-specific multireference coupled cluster theory. *J. Chem. Phys.* **2010**, *132*, 074107.
(27) Das, S.; Mukherjee, D.; Kallay, M. Full implementation and benchmark studies of Mukherjee's state-specific multireference coupled-cluster ansatz. *J. Chem. Phys.* **2010**, *132*, 074103.
(28) Bhaskaran-Nair, K.; Demel, O.; Pittner, J. Multireference state-specific Mukherjee's coupled cluster method with noniterative triexcitations. *J. Chem. Phys.* **2008**, *129*, 184105.
(29) Bhaskaran-Nair, K.; Demel, O.; Pittner, J. Multireference Mukherjee's coupled cluster method with triexcitations in the linked formulation: Efficient implementation and applications. *J. Chem. Phys.* **2010**, *132*, 154105.
(30) Demel, O.; Bhaskaran-Nair, K.; Pittner, J. Uncoupled multi-reference state-specific Mukherjee's coupled cluster method with triexcitations. *J. Chem. Phys.* **2010**, *133*, 134106.
(31) Veis, L.; Antalik, A.; Brabec, J.; Neese, F.; Legeza, O.; Pittner, J. Coupled Cluster Method with Single and Double Excitations Tailored by Matrix Product State Wave Functions. *J. Phys. Chem. Lett.* **2016**, *7*, 4072.
(32) Faulstich, F. M.; Laestadius, A.; Kvaal, S.; Legeza, O.; Schneider, R. Analysis of The Coupled-Cluster Method Tailored by Tensor-Network States in Quantum Chemistry. 2018; arXiv:1802.05699. arXiv.org ePrint archive. http://arxiv.org/abs/1802.05699 (accessed Mar 3, 2018).
(33) Booth, G. H.; Smart, S. D.; Alavi, A. Linear-scaling and parallelizable algorithms for stochastic quantum chemistry. *Mol. Phys.* **2014**, *112*, 1855.
(34) Brabec, J.; Bhaskaran-Nair, K.; Kowalski, K.; Pittner, J.; van Dam, H. J. Towards large-scale calculations with State-Specific Multireference Coupled Cluster methods: Studies on dodecane, naphthynes, and polycarbenes. *Chem. Phys. Lett.* **2012**, *542*, 128−133.
(35) Brabec, J.; Pittner, J.; van Dam, H.; Apra, E.; Kowalski, K. Parallel Implementation of Multireference Coupled-Cluster Theories Based on the Reference-Level Parallelism. *J. Chem. Theory Comput.* **2012**, *8*, 487.
(36) Kinoshita, T.; Hino, O.; Bartlett, R. J. Coupled-cluster method tailored by configuration interaction. *J. Chem. Phys.* **2005**, *123*, 074106.
(37) Piecuch, P.; Oliphant, N.; Adamowicz, L. A state-selective multireference coupled-cluster theory employing the single-reference formalism. *J. Chem. Phys.* **1993**, *99*, 1875.
(38) Piecuch, P.; Adamowicz, L. State-selective multireference coupled-cluster theory employing the single-reference formalism: Implementation and application to the H8 model system. *J. Chem. Phys.* **1994**, *100*, 5792.
(39) White, S. R. Density matrix formulation for quantum renormalization groups. *Phys. Rev. Lett.* **1992**, *69*, 2863−2866.
(40) Schollwöck, U. The density-matrix renormalization group in the age of matrix product states. *Ann. Phys.* **2011**, *326*, 96−192.
(41) Werner, H.-J.; Knowles, P. J.; Knizia, G.; Manby, F. R.; Schütz, M. et al. MOLPRO, version 2015.1, a package of ab initio programs. 2015; see http://www.molpro.net.
(42) Dunning, T. H. Gaussian basis sets for use in correlated molecular calculations. I. The atoms boron through neon and hydrogen. *J. Chem. Phys.* **1989**, *90*, 1007−1023.
(43) Booth, G.; Alavi, A. NECI. https://github.com/ghb24/NECI_STABLE, 2017.
(44) Legeza, Ö.; Röder, J.; Hess, B. Controlling the accuracy of the density-matrix renormalization-group method: The dynamical block state selection approach. *Phys. Rev. B: Condens. Matter Mater. Phys.* **2003**, *67*, 125114.
(45) Legeza, Ö.; Sólyom, L. Quantum data compression, quantum information generation, and the density-matrix renormalization-group method. *Phys. Rev. B: Condens. Matter Mater. Phys.* **2004**, *70*, 205118.

DOI: 10.1021/acs.jctc.8b00022
J. Chem. Theory Comput. 2018, 14, 2439−2445

(46) Olivares-Amaya, R.; Hu, W.; Nakatani, N.; Sharma, S.; et al. The ab-initio density matrix renormalization group in practice. *J. Chem. Phys.* **2015**, *142*, 034102.
(47) Barcza, G.; Legeza, Ö.; Marti, K. H.; Reiher, M. Quantum-information analysis of electronic states of different molecular structures. *Phys. Rev. A: At., Mol., Opt. Phys.* **2011**, *83*, 012508.
(48) Fertitta, E.; Paulus, B.; Barcza, G.; Legeza, Ö. Investigation of metal-insulator-like transition through the *ab initio* density matrix renormalization group approach. *Phys. Rev. B: Condens. Matter Mater. Phys.* **2014**, *90*, 245129.
(49) Legeza, Ö.; Sólyom, J. Optimizing the density-matrix renormalization group method using quantum information entropy. *Phys. Rev. B: Condens. Matter Mater. Phys.* **2003**, *68*, 195116.
(50) Szalay, S.; Pfeffer, M.; Murg, V.; Barcza, G.; Verstraete, F.; Schneider, R.; Legeza, Ö. Tensor product methods and entanglement optimization for ab initio quantum chemistry. *Int. J. Quantum Chem.* **2015**, *115*, 1342.
(51) Legeza, Ö.; Veis, L.; Mosoni, T. QC-DMRG-Budapest, a program for quantum chemical DMRG calculations.
(52) Knecht, S.; Legeza, Ö.; Reiher, M. Communication: Four-component density matrix renormalization group. *J. Chem. Phys.* **2014**, *140*, 041101.
(53) Legeza, Ö.; Veis, L.; Poves, A.; Dukelsky, J. Advanced density matrix renormalization group method for nuclear structure calculations. *Phys. Rev. C: Nucl. Phys.* **2015**, *92*, 051303.
(54) Flyvbjerg, H.; Petersen, H. G. Error estimates on averages of correlated data. *J. Chem. Phys.* **1989**, *91*, 461.
(55) Hanrath, M. An exponential multireference wave-functionAnsatz. *J. Chem. Phys.* **2005**, *123*, 084102.
(56) Kong, L. *Int. J. Quantum Chem.* **2009**, *109*, 441−447.
(57) Lyakh, D. I.; Musial, M.; Lotrich, V. F.; Bartlett, R. J. Multireference Nature of Chemistry: The Coupled-Cluster View. *Chem. Rev.* **2012**, *112*, 182−243.
(58) Paldus, J.; Li, X. Analysis of the multireference state-universal coupled-cluster ansatz. *J. Chem. Phys.* **2003**, *118*, 6769−6783.

DOI: 10.1021/acs.jctc.8b00022
J. Chem. Theory Comput. 2018, 14, 2439−2445

JCTC Journal of Chemical Theory and Computation

Article

Cite This: J. Chem. Theory Comput. 2019, 15, 2206−2220

pubs.acs.org/JCTC

Numerical and Theoretical Aspects of the DMRG-TCC Method Exemplified by the Nitrogen Dimer

Fabian M. Faulstich,[*,†] Mihály Máté,[‡,∥] Andre Laestadius,[†] Mihály András Csirik,[‡] Libor Veis,[¶] Andrej Antalik,[¶,⊥] Jiří Brabec,[¶] Reinhold Schneider,[§] Jiří Pittner,[¶] Simen Kvaal,[†] and Örs Legeza[‡]

[†]Hylleraas Centre for Quantum Molecular Sciences, Department of Chemistry, University of Oslo, P.O. Box 1033 Blindern, N-0315 Oslo, Norway

[‡]Strongly Correlated Systems "Lendület" Research Group, Wigner Research Center for Physics, H-1525, P.O. Box 49, Budapest, Hungary

[¶]J. Heyrovský Institute of Physical Chemistry, Academy of Sciences of the Czech Republic, v.v.i., Dolejškova 3, 18223 Prague 8, Czech Republic

[§]Modeling, Simulation and Optimization in Science, Department of Mathematics, Technische Universität Berlin, Sekretariat MA 5-3, Straße des 17. Juni 136, 10623 Berlin, Germany

[∥]Department of Physics of Complex Systems, Eötvös Loránd University, Pf. 32, H-1518 Budapest, Hungary

[⊥]Faculty of Mathematics and Physics, Charles University, 11636 Prague, Czech Republic

ABSTRACT: In this article, we investigate the numerical and theoretical aspects of the coupled-cluster method tailored by matrix-product states. We investigate formal properties of the used method, such as energy size consistency and the equivalence of linked and unlinked formulation. The existing mathematical analysis is here elaborated in a quantum chemical framework. In particular, we highlight the use of what we have defined as a complete active space-external space gap describing the basis splitting between the complete active space and the external part generalizing the concept of a HOMO−LUMO gap. Furthermore, the behavior of the energy error for an optimal basis splitting, i.e., an active space choice minimizing the density matrix renormalization group-tailored coupled-cluster singles doubles error, is discussed. We show numerical investigations on the robustness with respect to the bond dimensions of the single orbital entropy and the mutual information, which are quantities that are used to choose a complete active space. Moreover, the dependence of the ground-state energy error on the complete active space has been analyzed numerically in order to find an optimal split between the complete active space and external space by minimizing the density matrix renormalization group-tailored coupled-cluster error.

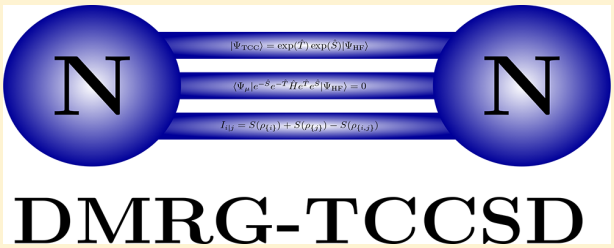

I. INTRODUCTION

The coupled-cluster (CC) theory has played a revolutionary role in establishing a new level of high accuracy in electronic structure calculations and quantum-chemical simulations. Despite the immense progress made in the field, computational schemes aiming at describing quasi-degenerate electronic structures of chemical systems are still unreliable. These multiconfiguration systems, also called strongly correlated systems, form one of the most challenging computational problems in quantum chemistry. Since these systems appear in various research areas, a reliable computational scheme is of major interest for the natural sciences. Recently, the computational advantages of the novel density matrix renormalization group-tailored coupled-cluster (DMRG-TCC) method restricted to single (S) and double (D) excitations were demonstrated on large and statically correlated systems by Veis et al.[1,2] Furthermore, computations have shown that the use of the DMRG-TCCSD method is indispensable for the DMRG in order to determine the proper structure of the low lying energy spectrum in strongly correlated systems.[2] In addition to these computational features, the DMRG-TCC approach is a promising candidate for a black-box quasi multireference scheme as considerable parts of the program already provide a routine procedure up to a numerical threshold. This would increase the accessibility for a broad class of researchers from various fields of study.

Although DMRG implementations already allow high precision multireference calculations on large complete active spaces (CAS), covering the majority of strongly correlated orbitals,[3] there is still a need for further analysis and developments in order to achieve a multireference routine procedure. In the setting of the DMRG-TCC method, a CAS DMRG solution is improved by means of an additional CC calculation performed on the remaining (external) orbital space. This CC correction, improving the description of dynamical

Received: September 20, 2018
Published: February 25, 2019

DOI: 10.1021/acs.jctc.8b00960
J. Chem. Theory Comput. 2019, 15, 2206−2220

correlation by the approximate solution, leaves the CAS part, i.e., the DMRG solution, invariant. We emphasize, however, that the presented implementation of the external CC corrections only take correlations with a single reference determinant into account, i.e., the considered CC amplitude equations are formulated with respect to one reference determinant. Despite the method's dependence on the reference determinant (in its current version), we have noticed significant improvements for systems with multireference character ($\sim 0.05 E_h$) via the CCSD correction on the external part compared to the single reference CCSD method on the full space. Nonetheless, the simplistic approach of the DMRG-TCC method to the multireference problem comes with a price. The DMRG-TCC, as a CAS method, does not correlate external amplitudes with the CAS amplitudes, i.e., contributions from the external part to excited determinants within the CAS are not present. Furthermore, in situations where the choice of a reference determinant becomes unclear, e.g., strong open-shell systems, the DMRG-TCC method could run into potential problems since it is based on a single reference formulation. Although the total spin can be fixed for the CAS part in the DMRG calculations (spin-adapted DMRG[4−7]), for the full orbital space it cannot be controlled through the external CC corrections presented in this work.

Common approaches to the strong correlation problem are provided by the multireference coupled-cluster (MRCC) theory based on the Jeziorski−Monkhorst ansatz.[8−10] The underlying idea of this ansatz is to include higher cluster excitations that are physically relevant but often more difficult to access in the usual single reference approach. To that end multiple determinants are employed in the reference state.[11] These multireference approaches can be roughly divided into three categories:[12] first, valence-universal approaches[13−21] (often also called genuine MRCC approaches); second, state-universal approaches;[22−27] and third, state-specific approaches.[28−49] Methods within the first two categories commonly suffer from so-called intruder states,[50−53] which leads to divergent behavior. Such methods furthermore require solving for a manifold of eigenstates, including several solutions that are irrelevant to the problem. These downsides can be overcome by state-specific approaches, however, they rely on an explicit inclusion of higher excitations. For a more detailed description of these active fields of research, we refer the reader to ref 9 and the references therein. An alternative multireference CC method that makes use of matrix product states and a modified DMRG algorithm is the linearized CCSD theory of Sharma and Alavi.[54] Furthermore, the pair CCD (pCCD) method—a CCD approach preserving electron pairs—besides being computationally inexpensive, can describe strong correlation, which the single reference CCD theory cannot. Nonetheless, the pCCD scheme lacks adequate dynamical correlation which was improved (by adding certain amplitudes) based on seniority of a determinant (number of unpaired electrons).[55] However, pairing merely the double excitations is not sufficient to describe the dissociation of the triple bond in the nitrogen dimer,[55] which is the content of this article. Higher order pairing schemes, however, allow a more effective treatment of strong correlations and are worth mentioning at this point.[56−62]

The mathematical analysis of CC schemes is far from being complete, especially with regard to multireference methods; however, many important steps have already been taken. The list of fundamental and mathematical chemistry articles aiming to describe the existence and nature of solutions of CC equations is too long to be summarized here. We will limit our discussion to a short selection of publications addressing such fundamental issues of chemistry.

As a system of polynomial equations the CC equations can have real or, if the cluster operator is truncated, complex solutions.[63,64] A standard tool to compute a solution of these nonlinear equations is the Newton−Raphson and the quasi-Newton method. However, these methods may diverge if the Jacobian or the approximated Jacobian become singular.[65] This is in particular the case when strongly correlated systems are considered. These and other related aspects of the CC theory have been addressed by Živković and Monkhorst[63,66] and Piecuch et al.[64] Significant advances in the understanding of the nature of multiple solutions of single-reference CC have been made by Kowalski and Jankowski[67] and by Piecuch and Kowalski.[68] An interesting attempt to address the existence of a cluster operator and cluster expansion in the open-shell case was done by Jeziorski and Paldus.[69]

The first advances within the rigorous realm of local functional analysis were performed by Schneider and Rohwedder, providing analyses of the closed-shell CC method for nonmulticonfiguration systems.[70−72] Since then, the local analysis of CC schemes was extended by Laestadius and Kvaal analyzing the extended CC method[73] and revisiting the bivariational approach[74,75] and Faulstich et al. providing the first local mathematical analysis of a multireference scheme, namely the CC method tailored by tensor network states (TNS-TCC).[76] As this mathematical branch of CC theory is very young, channeling abstract mathematical results into the quantum-chemistry community is a highly interdisciplinary task merging both fields. A first attempt in this direction was done by Laestadius and Faulstich linking the physical assumption of a HOMO−LUMO gap to the somewhat abstract Gårding inequality and in that context presenting key aspects of refs 70−73 from a more quantum chemical point of view.[77]

With this article, we aim to bridge the mathematical results in ref 76 of the TNS-TCC method into the quantum-chemistry community and extend these results with a numerical study on the complete active space dependence of the DMRG-TCCSD error. Furthermore, we derive formal properties of the TCC method.

II. DMRG-TCC METHOD

As a post-Hartree−Fock method, the TCC approach was introduced by Kinoshita et al. in ref 28 as an alternative to other multireference methods. It divides the cluster operator into a complete active space part, denoted $\hat{S}$, and an external (ext) part $\hat{T}$, i.e., the wave function is parametrized as

$$|\Psi_{\mathrm{TCC}}\rangle = \exp(\hat{T})\exp(\hat{S})|\Psi_{\mathrm{HF}}\rangle$$

Separating the cluster operator into several parts goes back to Piecuch et al.[78,79] Note that the operators $\hat{S}$, $\hat{T}$ commute since this separation is merely a partition of the overall cluster operator. In this formulation the linked CC equations are given by

$$\begin{cases} E^{(\mathrm{TCC})} = \langle \Psi_{\mathrm{HF}}|e^{-\hat{S}}e^{-\hat{T}}\hat{H}e^{\hat{T}}e^{\hat{S}}|\Psi_{\mathrm{HF}}\rangle \\ 0 = \langle \Psi_{\mu}|e^{-\hat{S}}e^{-\hat{T}}\hat{H}e^{\hat{T}}e^{\hat{S}}|\Psi_{\mathrm{HF}}\rangle \end{cases} \quad (1)$$

Computing $|\Psi_{\mathrm{CAS}}\rangle = e^{\hat{S}}|\Psi_{\mathrm{HF}}\rangle$ first and keeping it fixed for the dynamical correction via the CCSD method restricts the above equations to $|\Psi_{\mu}\rangle$ not in the CAS, i.e., $\langle\Psi|\Psi_{\mu}\rangle = 0$ for all $|\Psi\rangle$ in the CAS (we say that $|\Psi_{\mu}\rangle$ is in the L^2-orthogonal complement of

DOI: 10.1021/acs.jctc.8b00960
J. Chem. Theory Comput. 2019, 15, 2206−2220

the CAS). We emphasize that this includes mixed states, e.g., $|\Psi_{IJ}^{AB}\rangle$ where $|\Psi_I^A\rangle$ is an element of the CAS but $|\Psi_J^B\rangle$ is not. We consider a CAS of N-electron Slater-determinants formed from the set of spin-orbitals $B_{\mathrm{CAS}} = \{\chi_1, ..., \chi_k\}$. This is, in the mathematical sense, a subspace of the full configuration interaction (FCI) space, i.e., the space of all N-electron Slater-determinants formed from the entire set of spin-orbitals $B = \{\chi_1, ..., \chi_k, ..., \chi_K\}$. We here assume the spin-orbitals to be eigenfunctions of the system's Fock operator. Note that the following analysis can be applied to any single-particle operator fulfilling the properties used in ref 76—not only the Fock operator. This mathematical analysis, among other things, rests on the structure of a one-particle operator with a distinct (and furthermore steerable) CAS-ext gap. As described below (in connection to Assumption A), choosing the Fock operator might lead to the inclusion of diffuse functions in the CAS.

Based on the single reference approach, the TCC method needs a large CAS to cover most of the static correlations. Since the size of the CAS scales exponentially with respect to the number of particles N, i.e., $\dim(\mathrm{CAS}) \in O(k^N)$ (for more details we refer the reader to ref 70), an efficient approximation scheme for strongly correlated systems is indispensable for the TCC method to have practical significance. One of the most efficient schemes for static correlation is the DMRG method.[80] Going back to the physicists White and Martin,[3] it was introduced to quantum chemistry as an alternative to the CI or CC approach. However, the major disadvantage of the DMRG is that in order to compute dynamical correlation high bond dimensions (tensor ranks) may be necessary, making the DMRG a potentially costly method.[2,80] Nevertheless, as a TNS-TCC method, the DMRG-TCC approach is an efficient method since the CAS is supposed to cover the statically correlated orbitals of the system. This avoids the DMRG method's weak point and allows to employ a much larger CAS compared to the traditional CI-TCC method. We remark here that some terminology has different meaning in mathematics, physics, and chemistry. The number of legs of a tensor is called the order of the tensor in mathematics, while it is called the rank of the tensor in physics. The rank of the matrix corresponds to the number of nonzero singular values after matricization in mathematics, i.e., the Schmidt number in physics.

A notable advantage of the TCC approach over some MRCC methods is that all excitation operators commute by construction. This is due to the fact that the Hartee−Fock method yields a single reference solution $|\Psi_{\mathrm{HF}}\rangle$, which implies that separating the cluster operator corresponds to a partition of excitation operators. Hence, $\hat{S}$ and $\hat{T}$ commute. This makes the DMRG-TCC method's analysis much more accessible than internally contracted MRCC methods and therewith facilitates establishing sound mathematical results.[76] We remark, however, that the computationally most demanding step of the DMRG-TCC calculation is the DMRG part, and its cost increases rapidly with k. Alternative to the dynamical correction via the CC approach, the DMRG-MRCI method in ref 81 utilizes an internally contracted CI algorithm different from a conventional CI calculation.

III. FORMAL PROPERTIES OF THE DMRG-TCC METHOD

It is desired that quantum-chemical computations possess certain features representing the system's chemical and physical behavior. Despite their similarity, the CC and TCC method have essentially different properties, which are here elaborated. A basic property of the CC method is the equivalence of linked and unlinked CC equations. We point out that this equivalence is in general not true for the DMRG-TCCSD scheme. This is a consequence of the CAS ansatz since it yields mixed states, i.e., two particle excitations with one excitation into the CAS. The respective overlap integrals in the unlinked CC equations will then not vanish unless the single excitation amplitudes are equal to zero. Generalizing this result for rank complete truncations of order n we find that all excitation amplitudes need to be zero but for the nth one. This is somewhat surprising as the equivalence of linked and unlinked CC equations holds for rank complete truncations of the single-reference CC method.

For the sake of simplicity we show this results for the DMRG-TCCSD method. The general case can be proven in similar a fashion. We define the matrix representation $\mathbf{T}$ with elements $T_{\mu,\nu} = \langle\Psi_\mu|e^{\hat{T}}|\Psi_\nu\rangle$ for $\mu, \nu \notin$ CAS. Note that, as $\hat{T}$ increases the excitation rank, $\mathbf{T}$ is an atomic lower triangular matrix and therefore not singular. Assuming that the linked CC equations hold, the nonsingularity of $\mathbf{T}$ yields

$$\begin{aligned} A_\mu &:= \sum_{\nu\notin\mathrm{CAS}} T_{\mu,\nu}\langle\Psi_\nu|e^{-\hat{T}}\hat{H}e^{\hat{T}}|\Psi_{\mathrm{HF}}\rangle \\ &= \sum_{\nu\notin\mathrm{CAS}} \langle\Psi_\mu|e^{\hat{T}}|\Psi_\nu\rangle\langle\Psi_\nu|e^{-\hat{T}}\hat{H}e^{\hat{T}}|\Psi_{\mathrm{HF}}\rangle \\ &= 0 \end{aligned}$$

As the full projection manifold is complete under de-excitation, we obtain that

$$A_\mu = \langle\Psi_\mu|\hat{H}e^{\hat{T}}|\Psi_{\mathrm{HF}}\rangle - \sum_{\gamma\in\mathrm{CAS}} \langle\Psi_\mu|e^{\hat{T}}|\Psi_\gamma\rangle\langle\Psi_\gamma|\hat{H}e^{\hat{T}}|\Psi_{\mathrm{HF}}\rangle \quad (2)$$

Note that the first term on the r.h.s. in eq 2 together with the Hartree−Fock contribution from the sum, i.e., $E_0\langle\Psi_\mu|e^{\hat{T}}|\Psi_{\mathrm{HF}}\rangle$, describe the unlinked CC equations. To analyze the remaining terms on the r.h.s. in eq 2 we expand the inner products, i.e.,

$$\langle\Psi_\mu|e^{\hat{T}}|\Psi_\gamma\rangle = \langle\Psi_\mu|\Psi_\gamma\rangle + \langle\Psi_\mu|\hat{T}|\Psi_\gamma\rangle + \frac{1}{2}\langle\Psi_\mu|\hat{T}^2|\Psi_\gamma\rangle + ...$$

The first term in this expansion vanishes due to orthogonality. The same holds true for all terms where $\hat{T}$ enters to the power of two or higher since an excitation of order two or higher acting on an at least singly excited Slater-determinant $|\Psi_\gamma\rangle$ yields an at least 3-fold excited Slater-determinant. However, as the external space contains mixed states, we find that $\langle\Psi_\mu|\hat{T}|\Psi_\gamma\rangle$ is not necessarily zero, namely, for $\langle\Psi_\mu| = \langle\Psi_\alpha| \wedge \langle\Psi_\beta|$ and $|\Psi_\gamma\rangle = |\Psi_\beta\rangle$ with $\alpha \in$ ext and $\beta \in$ CAS. This proves the claim.

Subsequently, we elaborate the size consistency of the DMRG-TCCSD method. Let two DMRG-TCCSD wave functions for the individual subsystems A and B be

$$\begin{aligned} |\Psi_{\mathrm{DMRG-TCC}}^{(A)}\rangle &= \exp(\hat{S}_A)\exp(\hat{T}_A)|\Psi_{\mathrm{HF}}^{(A)}\rangle \\ |\Psi_{\mathrm{DMRG-TCC}}^{(B)}\rangle &= \exp(\hat{S}_B)\exp(\hat{T}_B)|\Psi_{\mathrm{HF}}^{(B)}\rangle \end{aligned}$$

The corresponding energies are given by

$$E_A = \langle\Psi_{\mathrm{HF}}^{(A)}|\hat{\bar{H}}_A|\Psi_{\mathrm{HF}}^{(A)}\rangle, \quad E_B = \langle\Psi_{\mathrm{HF}}^{(B)}|\hat{\bar{H}}_B|\Psi_{\mathrm{HF}}^{(B)}\rangle$$

and the amplitudes fulfill

$$0 = \langle\Psi_\mu^{(A)}|\hat{\bar{H}}_A|\Psi_{\mathrm{HF}}^{(A)}\rangle, \quad 0 = \langle\Psi_\mu^{(B)}|\hat{\bar{H}}_B|\Psi_{\mathrm{HF}}^{(B)}\rangle$$

in terms of the effective, similarity-transformed Hamiltonians

DOI: 10.1021/acs.jctc.8b00960
J. Chem. Theory Comput. 2019, 15, 2206−2220

$$\hat{\bar{H}}_A = \exp(-\hat{S}_A - \hat{T}_A)\hat{H}_A\exp(\hat{S}_A + \hat{T}_A)$$

$$\hat{\bar{H}}_B = \exp(-\hat{S}_B - \hat{T}_B)\hat{H}_B\exp(\hat{S}_B + \hat{T}_B)$$

The Hamiltonian of the compound system of the noninteracting subsystems can be written as $\hat{H}_{AB} = \hat{H}_A + \hat{H}_B$. Since the TCC approach corresponds to a partitioning of the cluster amplitudes we note that $\hat{\bar{H}}_{AB} = \hat{\bar{H}}_A + \hat{\bar{H}}_B$ for

$$\hat{\bar{H}}_{AB} = \exp(-\hat{S}_A - \hat{S}_B - \hat{T}_A - \hat{T}_B)\hat{H}_{AB} \times \exp(\hat{S}_A + \hat{S}_B + \hat{T}_A + \hat{T}_B)$$

With $|\Psi_{\mathrm{HF}}^{(AB)}\rangle = |\Psi_{\mathrm{HF}}^{(A)}\rangle \wedge |\Psi_{\mathrm{HF}}^{(B)}\rangle$, the energy of the compound systems can be written as

$$\begin{aligned} E_{AB} &= \langle\Psi_{\mathrm{HF}}^{(AB)}|\hat{\bar{H}}_{AB}|\Psi_{\mathrm{HF}}^{(AB)}\rangle \\ &= (\langle\Psi_{\mathrm{HF}}^{(A)}| \wedge \langle\Psi_{\mathrm{HF}}^{(B)}|)(\hat{\bar{H}}_A + \hat{\bar{H}}_B)(|\Psi_{\mathrm{HF}}^{(A)}\rangle \wedge |\Psi_{\mathrm{HF}}^{(B)}\rangle) \\ &= \langle\Psi_{\mathrm{HF}}^{(A)}|\hat{\bar{H}}_A|\Psi_{\mathrm{HF}}^{(A)}\rangle + \langle\Psi_{\mathrm{HF}}^{(B)}|\hat{\bar{H}}_B|\Psi_{\mathrm{HF}}^{(B)}\rangle \\ &= E_A + E_B \end{aligned}$$

It remains to show that

$$|\Psi_{\mathrm{DMRG-TCC}}^{(AB)}\rangle = \exp(\hat{S}_A + \hat{S}_B + \hat{T}_A + \hat{T}_B)|\Psi_{\mathrm{HF}}^{(AB)}\rangle$$

solves the Schrödinger equation, i.e., for all $\langle\Psi_\mu^{(\mathrm{AB})}|$, it holds that $\langle\Psi_\mu^{(AB)}|\hat{\bar{H}}_{AB}|\Psi_{\mathrm{HF}}^{(AB)}\rangle = 0$. Splitting the argument into three cases, we note that

$$\langle\Psi_\mu^{(A)}\Psi_{(\mathrm{HF})}^{(B)}|\hat{\bar{H}}_{AB}|\Psi_{\mathrm{HF}}^{(AB)}\rangle = \langle\Psi_\mu^{(A)}|\hat{\bar{H}}_A|\Psi_{\mathrm{HF}}^{(A)}\rangle = 0$$

$$\langle\Psi_{(\mathrm{HF})}^{(A)}\Psi_\mu^{(B)}|\hat{\bar{H}}_{AB}|\Psi_{\mathrm{HF}}^{(AB)}\rangle = \langle\Psi_\mu^{(B)}|\hat{\bar{H}}_B|\Psi_{\mathrm{HF}}^{(B)}\rangle = 0$$

$$\langle\Psi_\mu^{(A)}\Psi_\mu^{(B)}|\hat{\bar{H}}_{AB}|\Psi_{\mathrm{HF}}^{(AB)}\rangle = 0$$

where $\langle\Psi^{(A)}\Psi^{(B)}| = \langle\Psi^{(A)}| \wedge \langle\Psi^{(B)}|$. This proves the energy size consistency for the untruncated TCC method. From this we conclude the energy size consistency for the DMRG-TCCSD scheme, because the truncation only affects the product states $\langle\Psi_\mu^{(A)}\Psi_\mu^{(B)}|$ and these are zero in the above projection.

Looking at TCC energy expression we observe that due to the Slater−Condon rules, these equations are independent of CAS excitations higher than order three, i.e., amplitudes of $\hat{S}_n$ for $n > 3$. More precisely, due to the fact that in the TCCSD case external space amplitudes can at most contain one virtual orbital in the CAS, the TCCSD amplitude expressions become independent of $\hat{S}_4$, i.e.,

$$\langle\Psi_{ij}^{A'A}|\hat{\bar{H}}|\Psi_{klmn}^{B'c'd'e'}\rangle = 0$$

where the primed variables a', b', c', d', e' describe orbitals in the CAS, the nonprimed variable a describes an orbital in the external part and i, j, k, l, m, n are occupied orbitals. Note, this does not imply that we can restrict the CAS computation to a manifold characterizing excitations with rank less or equal to three as for strongly correlated systems these can still be relevant. However, it reduces the number of terms entering the DMRG-TCCSD energy computations significantly.

This work aligns with the originally introduced CI-TCCSD method taking only $\hat{S}_n$ for $n = 1, 2$ into account.[28] We emphasize that the additional consideration of $\hat{S}_3$ corresponds to an exact treatment of the CAS contributions to the energy. Furthermore, this consideration does not change the TCC method's complexity, if the $\hat{S}_3$ amplitudes are available. This is due to the fact that including the CAS triple excitation amplitudes will not exceed the dominating complexities of the CCSD approach[82] nor of the DMRG method. However, the extraction of the CI-triples from the DMRG wave function is costly and a corresponding efficiency investigation is left for future work.

IV. ANALYSIS OF THE DMRG-TCC METHOD

In the sequel we discuss and elaborate mathematical properties of the TCC approach and their influence on the DMRG-TCC method. The presentation here is held brief and the interested reader is referred to ref 76 and the references therein for further mathematical details.

IV.A. Complete Active Space Choice. As pointed out in the previous section, the TCC method relies on a *well-chosen* CAS, i.e., a large enough CAS that covers the system's static correlation. Consequently, we require a quantitative measurement for the quality of the CAS, which presents the first obstacle for creating a nonempirical model since the chemical concept of correlation is not well-defined.[83] In the DMRG-TCC method, we use a quantum information theory approach to classify the spin-orbital correlation. This classification is based on the *mutual-information*

$$I_{i|j} = S(\rho_{\{i\}}) + S(\rho_{\{j\}}) - S(\rho_{\{i,j\}})$$

This two particle entropy is defined via the *von Neumann entropy* $S(\rho) = -\mathrm{Tr}(\rho \ln \rho)$ of the reduced density operators $\rho_{\{X\}}$.[84] Note that the mutual-information describes two-particle correlations. For a more general connection between multiparticle correlations and ξ-correlations, we refer the reader to the work of Szalay et al.[84] We emphasize that in practice this is a basis dependent quantity, which is in agreement with the chemical definition of correlation concepts.[83] We identify pairs of spin-orbitals contributing to a high mutual information value as strongly correlated, the pairs contributing to the plateau region, i.e., a region in which the mutual information profile is constant, as nondynamically correlated and the pairs contributing to the mutual information tail as dynamically correlated (see Figure 3). The mutual-information profile can be well approximated from a prior DMRG computation on the full system. Due to the size of the full system we only compute a DMRG solution of low *bond dimension* (also called *tensor rank*). These low-accuracy calculations, however, already provide a good qualitative entropy profile, i.e., the shapes of profiles obtained for low bond dimension, M, agree well with the ones obtained in the FCI limit. Here, we refer to Figures 2 and 3 showing the single orbital entropy and mutual information profiles, respectively, for various M values and for three different geometries of the N_2 molecule. The orbitals with large entropies can be identified from the low-M calculations providing a routine procedure to form the CAS including the strongly correlated orbitals.[85−87] In practice this is achieved by using the following dimension reduction protocol: We start with a very low bond dimension calculation carried out on the full orbital space. Based on the corresponding entropy profile and an *a priori* defined numerical threshold, a smaller set of orbitals is selected. In a subsequent step the same procedure is repeated on the reduced orbital set but with a larger bond dimension. This iterative dimension reduction protocol is a typical renormalization group based approach to refine the entropy spectrum that is also used in condensed matter physics.

A central observation is that, for $B_{\mathrm{CAS}} = \{\chi_1, ..., \chi_N\}$ (i.e., $k = N$), the DMRG-TCCSD becomes the CCSD method and, for

DOI: 10.1021/acs.jctc.8b00960
J. Chem. Theory Comput. 2019, 15, 2206−2220

$B_{CAS} = \{\chi_1, \cdots, \chi_K\}$ (i.e., $k = K$), it is the DMRG method. We recall that the CCSD method can not resolve static correlation and the DMRG method needs high tensor ranks for dynamically correlated systems. This suggests that the error obtains a minimum for some k with $N \leq k \leq K$, i.e., there exists an optimal choice of k determining the basis splitting and therewith the choice of the CAS. Note that this feature becomes important for large systems since high bond dimensions become simply impossible to compute with available methods.

IV.B. Local Analysis of the DMRG-TCC Method. The CC method can be formulated as *nonlinear Galerkin scheme*,[70] which is a well-established framework in numerical analysis to convert the continuous Schrödinger equation to a discrete problem. For the DMRG-TCC method a first local analysis was performed in ref 76. There, a quantitative error estimate with respect to the basis truncation was established. Faulstich et al. showed under certain assumptions (Assumption A and B in the sequel) that the DMRG-TCC method possesses a locally unique and *quasi-optimal* solution (cf. section 4.1 in ref 76). In case of the DMRG-TCC method the latter means: On a fixed CAS, the CC method tailored by a DMRG solution provides a truncation hierarchy that converges to the best possible dynamical correction to the given CAS. For a fixed basis set the CC solution tailored by a DMRG solution on a fixed CAS is up to a multiplicative constant the best possible solution in the approximation space defined by the basis set. In other words, the CC method provides the best possible dynamical correction for a given CAS solution such as a DMRG solution.

Note that local uniqueness ensures that for a fixed basis set, the computed DMRG-TCC solution is unique in a neighborhood around the exact solution. We emphasize that this result is derived under the assumption that the CAS solution is fixed. Consequently, for different CAS solutions we obtain in general different TCC solutions, i.e., different cluster amplitudes.

Subsequently, parts of the results in ref 76 are explained in a setting adapted to the theoretical chemistry perspective. The TCC function is given by $f(t; s) = \langle \Psi_\mu | e^{-\hat{S}} e^{-\hat{T}} \hat{H} e^{\hat{T}} e^{\hat{S}} | \Psi_{HF} \rangle$, for $|\Psi_\mu\rangle$ not in the CAS. Note that we use the convention where small letters s, t correspond to cluster amplitudes, whereas capital letters $\hat{S}$, $\hat{T}$ describe cluster operators. The corresponding TCC energy expression is given by

$$\mathcal{E}(t; s) = \langle \Psi_{HF} | e^{-\hat{S}} e^{-\hat{T}} \hat{H} e^{\hat{T}} e^{\hat{S}} | \Psi_{HF} \rangle$$

Consequently, the linked TCC eqs 1 then become

$$\begin{cases} E^{(TCC)} = \mathcal{E}(t; s) \\ 0 = f(t; s) \end{cases}$$

Within this framework the locally unique and quasi-optimal solutions of the TCC method were obtained under two assumptions (see Assumption A and B in ref 76).

First, Assumption A requires that the Fock operator $\hat{F}$ is *bounded* and satisfies a so-called *Gårding inequality*. Note that spectral gap assumptions (cf. HOMO−LUMO gap) are standard in the analysis of dynamically correlated systems, and for a more detailed description of these properties in this context, we refer readers to ref 77. Second, in the theoretical framework[76] it is assumed that there exists a CAS-ext gap in the spectrum of the Fock operator, i.e., there is a gap between the kth and the k + 1st orbital energies. The CAS-ext gap (although in practice possibly very small) was sufficient for the analysis since the main purpose was to remove the HOMO−LUMO gap assumption and allow for quasi-degeneracy, which makes the general TCC approach applicable to multiconfiguration systems. Intuitively, this gap assumption means that the CAS captures the static correlation of the system.

However, in practice, an arbitrarily small gap is insufficient and needs to be complemented by a more detailed discussion (see Remark 10 in ref 76). The crucial stability constant is not directly related to the CAS-ext gap $\varepsilon_{k+1} - \varepsilon_k$, nor to the HOMO−LUMO gap $\varepsilon_{N+1} - \varepsilon_N$. Due to the frozen CAS-amplitudes this stability constant becomes much larger and is roughly estimated by $\varepsilon_{k+1} - \varepsilon_N$. This improved stability provides accurate CC amplitudes and the improved gap is not destroyed e.g. by the existence of many diffuse functions around the LUMO-level (Fermi level). In this case, the CAS includes the diffuse functions. This might not be optimal but is the simplest choice and most importantly fulfills the stability condition. The issue of basis set optimization is discussed briefly in the conclusion but a more detailed discussion is left for future work.

Assumption B is concerned with the fluctuation operator $\hat{W} = \hat{H} - \hat{F}$. This operator describes the difference of the Hamiltonian and a single particle operator, here chosen to be the Fock operator. Using the similarity transformed $\hat{W}$ and fixing the CAS amplitudes s, the map

$$t \mapsto e^{-\hat{T}} e^{-\hat{S}} \hat{W} e^{\hat{S}} e^{\hat{T}} | \Psi_{HF} \rangle$$

is assumed to have a *small enough* Lipschitz-continuity constant (see eq 20 in ref 76). The physical interpretation of this Lipschitz condition is at the moment unclear.

IV.C. Error Estimates for the DMRG-TCC Method. A major difference between the CI and CC method is that the CC formalism is not variational. Hence, it is not evident that the CC energy error decays quadratically with respect to the error of the wave function or cluster amplitudes. Note that the TCC approach represents merely a partition of the cluster operator; however, its error analysis is more delicate than the traditional CC method's analysis. The TCC-energy error is measured as a difference to the FCI energy. Let $|\Psi^*\rangle$ describe the FCI solution on the whole space, i.e., $\hat{H}|\Psi^*\rangle = E|\Psi^*\rangle$. Using the exponential parametrization and the above introduced separation of the cluster operator, we have

$$|\Psi^*\rangle = \exp(\hat{T}^*)\exp(\hat{S}^*)|\Psi_{HF}\rangle \tag{3}$$

An important observation is that the TCC approach ignores the coupling from the external space into the CAS. It follows that the FCI solution on the CAS $|\Psi_{FCI}^{CAS}\rangle = \exp(\hat{S}_{FCI})|\Psi_{HF}\rangle$ is an approximation to the projection of $|\Psi^*\rangle$ onto the CAS

$$|\Psi_{FCI}^{CAS}\rangle \approx \hat{P}|\Psi^*\rangle = \exp(\hat{S}^*)|\Psi_{HF}\rangle$$

where $\hat{P} = \sum_{\mu \in CAS} |\Psi_\mu\rangle\langle\Psi_\mu|$ is the L^2-orthogonal projection onto the CAS. For a reasonably sized CAS the FCI solution $|\Psi_{FCI}^{CAS}\rangle$ is rarely computationally accessible and we introduce the DMRG solution on the CAS as an approximation of $|\Psi_{FCI}^{CAS}\rangle$

$$|\Psi_{DMRG}^{CAS}\rangle = \exp(\hat{S}_{DMRG})|\Psi_{HF}\rangle \approx |\Psi_{FCI}^{CAS}\rangle$$

Tailoring the CC method with these different CAS solutions leads in general to different TCC solutions. In the case of $|\Psi_{FCI}^{CAS}\rangle$, the TCC method yields the best possible solution with respect to the chosen CAS, i.e., $f(t_{CC}^*; s_{FCI}) = 0$. This solution is in general different from t_{CC} fulfilling $f(t_{CC}; s_{DMRG}) = 0$ and its truncated version t_{CCSD} satisfying $P_{Gal} f(t_{CCSD}; s_{DMRG}) = 0$, where P_{Gal} denotes the l^2-orthogonal projection onto the corresponding Galerkin space. In the context of the DMRG-TCC theory, the

DOI: 10.1021/acs.jctc.8b00960
J. Chem. Theory Comput. 2019, 15, 2206−2220

Galerkin space represents a truncation in the excitation rank of the cluster operator, e.g., DMRG-TCCD, DMRG-TCCSD, etc.

For the following argument, suppose that an appropriate CAS has been fixed. The total DMRG-TCC energy error ΔE can be estimated as[76]

$$\begin{aligned}\Delta E &= |\mathcal{E}(t_{\mathrm{CCSD}}; s_{\mathrm{DMRG}}) - \mathcal{E}(t^*; s^*)| \\ &\leq \Delta\varepsilon + \Delta\varepsilon_{\mathrm{CAS}} + \Delta\varepsilon^*_{\mathrm{CAS}}\end{aligned} \tag{4}$$

where each term on the r.h.s. in eq 4 is now discussed. As a technical remark, the norms on either the Hilbert space of cluster amplitudes or wave functions are here simply denoted as $\|\cdot\|$. These norms are not just the l^2- or L^2-norm, respectively, but also measure the kinetic energy. It should be clear from context which Hilbert space is in question and we refer to ref 71 for formal definitions. The first term is defined as

$$\Delta\varepsilon = |\mathcal{E}(t_{\mathrm{CCSD}}; s_{\mathrm{DMRG}}) - \mathcal{E}(t_{\mathrm{CC}}; s_{\mathrm{DMRG}})|$$

which describes the truncation error of the CCSD method tailored by $|\Psi^{\mathrm{CAS}}_{\mathrm{DMRG}}\rangle$. We emphasize that the dynamical corrections via the CCSD and the untruncated CC method are here tailored by the same CAS solution. Hence, the energy error $\Delta\varepsilon$ corresponds to a single reference CC energy error, which suggests an analysis similar to that of refs 70 and 72. Indeed, the *Aubin−Nitsche duality method*[88−90] yields a quadratic *a priori* error estimate in $\|t_{\mathrm{CCSD}} - t_{\mathrm{CC}}\|$ (and in terms of the Lagrange mulitpliers; see Theorem 29 in ref 76).

Second, we discuss the term

$$\Delta\varepsilon_{\mathrm{CAS}} = |\mathcal{E}(t_{\mathrm{CC}}; s_{\mathrm{DMRG}}) - \mathcal{E}(t_{\mathrm{CC}}; s_{\mathrm{FCI}})|$$

Here, different CAS solutions with fixed external solutions are used to compute the energies. This suggests that $\Delta\varepsilon_{\mathrm{CAS}}$ is connected with the error

$$\Delta E_{\mathrm{DMRG}} = |\langle\Psi_{\mathrm{HF}}|e^{-\hat{S}_{\mathrm{DMRG}}}\hat{P}\hat{H}\hat{P}e^{\hat{S}_{\mathrm{DMRG}}} - e^{-\hat{S}_{\mathrm{FCI}}}\hat{P}\hat{H}\hat{P}e^{\hat{S}_{\mathrm{FCI}}}|\Psi_{\mathrm{HF}}\rangle| \tag{5}$$

describing the approximation error of the DMRG solution on the CAS (see Lemma 27 in ref 76). Indeed

$$\begin{aligned}\Delta\varepsilon_{\mathrm{CAS}} \lesssim\ & \Delta E_{\mathrm{DMRG}} + \|t_{\mathrm{CC}} - t^*_{\mathrm{CC}}\|^2 \\ & + \|(\hat{S}_{\mathrm{DMRG}} - \hat{S}_{\mathrm{FCI}})|\Psi_{\mathrm{HF}}\rangle\|^2 + \sum_{|\mu|=1}\varepsilon_\mu(t^*_{\mathrm{CC}})^2_\mu\end{aligned} \tag{6}$$

with $\varepsilon_\mu = \varepsilon^{A_1\cdots A_n}_{I_1\ldots I_n} = \sum_{j=1}^n(\lambda_{A_j} - \lambda_{I_j})$, for $1 \leq n \leq k$, where λ_i are the orbital energies. The ε_μ are the (translated) Fock energies, more precisely, $\hat{F}|\Psi_\mu\rangle = (\Lambda_0 + \varepsilon_\mu)|\Psi_\mu\rangle$, with $\Lambda_0 = \sum_{i=1}^N\lambda_i$. Note that the wave function $|\Psi^{\mathrm{CAS}}_{\mathrm{FCI}}\rangle$ is in general not an eigenfunction of $\hat{H}$; however, it is an eigenfunction of the projected Hamiltonian $\hat{P}\hat{H}\hat{P}$. Equation 5 involves the exponential parametrization. This can be estimated by the energy error of the DMRG wave function, denoted $\Delta\mathcal{E}_{\mathrm{DMRG}}$, namely

$$\Delta E_{\mathrm{DMRG}} \leq 2\Delta\mathcal{E}_{\mathrm{DMRG}} + \|\hat{H}\|\|\Psi^{\mathrm{CAS}}_{\mathrm{DMRG}}\rangle - |\Psi^{\mathrm{CAS}}_{\mathrm{FCI}}\rangle\|_{L^2} \tag{7}$$

In section V the energy error of the DMRG wave function is controlled by the threshold value $\delta\varepsilon_{\mathrm{Tr}}$, i.e., $\Delta\mathcal{E}_{\mathrm{DMRG}}(\delta\varepsilon_{\mathrm{Tr}})$. Hence, for well chosen CAS the difference $\|\Psi^{\mathrm{CAS}}_{\mathrm{DMRG}}\rangle - |\Psi^{\mathrm{CAS}}_{\mathrm{FCI}}\rangle\|_{L^2}$ is sufficiently small such that $\Delta E_{\mathrm{DMRG}} \lesssim 2\Delta\mathcal{E}_{\mathrm{DMRG}}$ holds. This again shows the importance of a well-chosen CAS. Furthermore, the last term in eq 6 can be eliminated via orbital rotations, as it is a sum of single excitation amplitudes.

Finally, we consider

$$\Delta\varepsilon^*_{\mathrm{CAS}} = |\mathcal{E}(t_{\mathrm{CC}}; s_{\mathrm{FCI}}) - \mathcal{E}(t^*; s^*)| \tag{8}$$

Since (t^*, s^*) is a stationary point of $\mathcal{E}$ we have $D\mathcal{E}(t^*; s^*) = 0$. A calculation involving Taylor expanding $\mathcal{E}$ around (t^*, s^*) (see Lemma 26 in ref 76) yields

$$\Delta\varepsilon^*_{\mathrm{CAS}} \lesssim \|t_{\mathrm{CC}} - t^*\|^2 + \|s_{\mathrm{FCI}} - s^*\|^2_{l^2} \tag{9}$$

Note that the above error is caused by the assumed basis splitting, namely, the correlation from the external part into the CAS is ignored. Therefore, the best possible solution for a given basis splitting $(t^*_{\mathrm{CC}}, s_{\mathrm{FCI}})$ differs in general from the FCI solution (t^*, s^*).

Combining now the three quadratic bounds gives an overall quadratic *a priori* energy error estimate for the DMRG-TCC method. The interested reader is referred to ref 76 for a more detailed treatment of the above analysis.

IV.D. On the *k*-Dependence of the Error Estimates. The error estimate outlined above is for a fixed CAS, i.e., a particular basis, splitting and bounds the energy error in terms of truncated amplitudes. Because the TCC solution depends strongly on the choice of the CAS, it is motivated to further investigate the k-dependence of the error ΔE. However, the above derived error bound has a highly complicated k-dependence since not only the amplitudes but also the implicit constants (in $\lesssim$) and norms depend on k. Therefore, the analysis in ref 76 is not directly applicable to take the full k-dependence into account.

In the limit where $s_{\mathrm{DMRG}} \to s_{\mathrm{FCI}}$ we obtain that $t_{\mathrm{CC}} \to t^*_{\mathrm{CC}}$ since the TCC method is numerically stable, i.e., a small perturbation in s corresponds to a small perturbation in the solution t. Furthermore, if we assume that $t_{\mathrm{CCSD}} \approx t_{\mathrm{CC}}$, which is reasonable for the equilibrium bond length of N_2, the error can be bound as

$$\Delta E_k \leq C_k\left(\sum_{|\mu|=1}(t_{\mathrm{CCSD}})^2_\mu + \|(t_{\mathrm{CCSD}}, s_{\mathrm{DMRG}}) - (t^*, s^*)\|^2_{l^2}\right) \tag{10}$$

Here the subscript k on ΔE_k and C_k highlights the k-dependence. We remark that we here used the less accurate l^2-structure on the amplitude space compared to the H^1-structure in eq 9. This yields k-independent vectors $(t_{\mathrm{CCSD}}, s_{\mathrm{DMRG}})$ and (t^*, s^*), as well as an k-independent l^2-norm. The k-depenence of C_k will be investigated numerically in more detail in section B.5.

V. SPLITTING ERROR FOR N_2

Including the k-dependence in the above performed error analysis explicitly is a highly nontrivial task involving many mathematical obstacles and is part of our current research. Therefore, we here extend the mathematical results from section IV with a numerical investigation on this k-dependence. Our study is presented for the N_2 molecule using the cc-pVDZ basis, which is a common basis for benchmark computations developed by Dunning and co-workers.[91] Here we remark that in our calculations all electrons are correlated as opposed to the typical frozen-core calculation, where the two 1s orbitals are omitted from the full orbital space. We investigate three different geometries of the nitrogen dimer by stretching the molecule, thus the performance of DMRG-TCCSD method is assessed against DMRG and single reference CC methods for bond lengths $r = 2.118a_0$, $2.700a_0$, and $3.600a_0$. In the equilibrium geometry the system is weakly correlated implying that single reference CC methods yield reliable results. For increasing bond

DOI: 10.1021/acs.jctc.8b00960
J. Chem. Theory Comput. 2019, 15, 2206−2220

length r the system shows multireference character, i.e., static correlations become more dominant. For $r > 3.5a_0$ this results in the breakdown of single reference CC methods.[92] This breakdown can be overcome with the DMRG-TCCSD method once a large and well chosen CAS is formed, we therefore refer to the DMRG-TCCSD method as numerically stable with respect to the bond length along the potential energy surface (PES).

As mentioned before, the DMRG method is in general less efficient to recover dynamic correlations since it requires large computational resources. However, due to the specific CAS choice the computational resource for the DMRG part of the TCC scheme is expected to be significantly lower than a pure DMRG calculation for the same level of accuracy.

V.A. Computational Details. In practice, a routine application of the TCC method to strongly correlated molecular systems, i.e., to multireference problems, became possible only recently since it requires a very accurate solution in a large CAS including all static correlations. Tensor network state methods fulfill such a high accuracy criterion, but the efficiency of the TNS-TCCSD method strongly depends on various parameters of the involved algorithms. Some of these are defined rigorously while others are more heuristic from the mathematical point of view. In this section we present the optimization steps for the most important parameters of the DMRG-TCCSD method and outline how the numerical error study in section V.B is performed.

As elaborated in sections II and IV.A, the CAS choice is essential for the computational success of TNS-TCC methods. In addition, the error of the TNS method used to approximate the CAS part depends on various approximations. These include the proper choice of a finite dimensional basis to describe the chemical compound, the tensor network structure, and the mapping of the molecular orbitals onto the given network.[93] Fortunately, all these can be optimized by utilizing concepts of quantum information theory, introduced in section IV.A (see also the included references). In the following, we restrict the numerical study to the DMRG-TCCSD method but the results presented here should also hold for other TNS approaches.[93−97]

In the DMRG-TCCSD case, the tensor network topology in the CAS corresponds to a single branched tensor tree, i.e., a one-dimensional topology. Thus, permutations of orbitals along such an artificial chain effect the convergence for a given CAS choice.[98,99] This orbital-ordering optimization can be carried out based on spectral graph theory[100,101] by minimizing the entanglement distance,[102] defined as $I_{\mathrm{dist}} = \sum_{ij} I_{ij} |i - j|^2$. In order to speed up the convergence of the DMRG procedure the configuration interaction based dynamically extended active space (CI-DEAS) method is applied.[93,99] In the course of these optimization steps, the single orbital entropy ($S_i = S(\rho_{\{i\}})$) and the two-orbital mutual information (I_{ij}) are calculated iteratively until convergence is reached. The size of the active space is systematically increased by including orbitals with the largest single site entropy values, which at the same time correspond to orbitals contributing to the largest matrix elements of the mutual information. Thus, the decreasingly ordered values of S_i define the so-called CAS vector, which provides a guide in what order to extend the CAS by including additional orbitals. The bond dimensions M (tensor rank) in the DMRG method can be kept fixed or adapted dynamically (dynamic block state selection (DBSS) approach) in order to fulfill an *a priori* defined error margin.[103,104] Accurate extrapolation to the truncation free limit is possible as a function of the truncation error $\delta\varepsilon_{\mathrm{Tr}}$.[103,105]

In our DMRG implementation[106] we use a spatial orbital basis, i.e., the local tensor space of a single orbital is $d = 4$ dimensional. In this $\mathbb{C}^4$-representation an orbital can be empty, singly occupied with either a spin up or spin down electron, or doubly occupied with opposite spins. Note, in contrast to section IV we need $N/2$ spatial orbitals to describe an N-electron wave function and similar changes apply to the size of the basis set so that we use $K \equiv K/2$ from here on. The single orbital entropy therefore varies between 0 and $\ln d = \ln 4$, while the two-orbital mutual information varies between 0 and $\ln d^2 = \ln 16$.

Next we provide a short description how to perform DMRG-TCCSD calculations in practice. Note that we leave the discussion on the optimal choice of k for the following sections.

(1) First the CAS is formed from the full orbital space by setting $k = K$. DMRG calculations are performed iteratively with fixed low bond dimension (or with a large error margin) in order to determine the optimal ordering and the CAS vector as described above. Thus, the corresponding single-orbital entropy and mutual information are also calculated. These calculations already provide a good qualitative description of the entropy profiles with respect to the exact solution, i.e., strongly correlated orbitals can be identified.

(2) Using a given $N/2 < k < K$ we form the CAS from the Hartree−Fock orbitals and the first $k - N/2$ virtual orbitals from the CAS vector, i.e., orbitals with the largest single orbital entropy values. We emphasize that these orbitals contribute to the largest matrix elements in I_{ij}. We carry out the orbital ordering optimization on the given CAS and perform a large-scale DMRG calculation with a low error threshold margin in order to get an accurate approximation of the $|\Psi_{\mathrm{FCI}}^{\mathrm{CAS}}\rangle$. Note that the DMRG method yields a normalized wave function, i.e., the overlap with the reference determinant $|\Psi_{\mathrm{HF}}\rangle$ is not necessarily equal to one.

(3) Using the matrix product state representation of $|\Psi_{\mathrm{DMRG}}^{\mathrm{FCI}}\rangle$ obtained by the DMRG method we determine the zero reference overlap, single and double CI coefficients of the full tensor representation of the wave function. Next, these are used to calculate the $\hat{S}_1$ and $\hat{S}_2$ amplitudes, which form the input of the forthcoming CCSD calculation.

(4) In the following step the cluster amplitudes for the external part, i.e., $\hat{T}_1$ and $\hat{T}_2$, are calculated in the course of the DMRG-TCCSD scheme.

(5) As we discus in the next section, finding the optimal CAS, i.e., k-splitting, is a highly nontrivial problem, and at the present stage we can only present a solution that is considered as a heuristic approach in terms of rigorous mathematics. In practice, we repeat steps 2−4 for a large DMRG-truncation error as a function of $N/2 < k < K$, thus we find local energy minima (see Figure 4) using a relatively cheap DMRG-TCCSD scheme. Around such a local minimum we perform more accurate DMRG-TCCSD calculations by lowering the DMRG-truncation error in order to refine the optimal k. We also monitor the maximum number of DMRG block states required to reach the *a priori* defined DMRG-error margin as a function of k. Since it can happen that several k values lead to low error DMRG-TCCSD energies, while the computational effort increases significantly with increasing k we select the optimal k that leads to low DMRG-TCCSD energy but also minimizes the required DMRG

DOI: 10.1021/acs.jctc.8b00960
J. Chem. Theory Comput. 2019, 15, 2206−2220

block states. Using the optimal k value we perform large-scale DMRG-TCCSD calculation using a relatively tight error bound for the DMRG-truncation error.

We close this section with a brief summary of the numerically accessible error terms and relate them to equations presented in section IV. Note that the error analysis in section IV is presented for a given k, thus here the k dependence is also omitted.

For a given k split, the accuracy of $|\Psi^{\mathrm{CAS}}_{\mathrm{DMRG}}\rangle$ depends on the DMRG truncation error, $\delta\varepsilon_{\mathrm{Tr}}$. As has been shown in refs 103 and 105, the relative error, $\Delta E_{\mathrm{rel}} = (E^{\mathrm{CAS}}_{\mathrm{DMRG}(\delta\varepsilon_{\mathrm{Tr}})} - E^{\mathrm{CAS}}_{\mathrm{FCI}})/E^{\mathrm{CAS}}_{\mathrm{FCI}}$ is a linear function of $\delta\varepsilon_{\mathrm{Tr}}$ on a logarithmic scale. Therefore, extrapolation to the FCI limit can be carried out as a function of $\delta\varepsilon_{\mathrm{Tr}}$. In addition, the error term

$$\Delta\mathcal{E}_{\mathrm{DMRG}}(\delta\varepsilon_{\mathrm{Tr}}) = E^{\mathrm{CAS}}_{\mathrm{DMRG}(\delta\varepsilon_{\mathrm{Tr}})} - E^{\mathrm{CAS}}_{\mathrm{FCI}}$$

appearing in eq 7 can be controlled.

Note that terms appearing in eqs 6 and 7 include FCI solutions of the considered system. However, for small enough and dynamically correlated systems, these FCI solutions can be well approximated. This is in particular the case for the nitrogen dimer near the equilibrium geometry with the here chosen basis set. The CI-coefficients are then extractable from the matrix product state representation of a wave function, e.g., $|\Psi^{\mathrm{CAS}}_{\mathrm{DMRG}}\rangle$ or $|\Psi^{\mathrm{CAS}}_{\mathrm{FCI}}\rangle$. Note that calculating all CI-coefficients scales exponentially with the size of the CAS. However, since the system is dynamically correlated zeroth order, single and double excitation coefficients are sufficient. Hence, the error terms $\||\Psi^{\mathrm{CAS}}_{\mathrm{DMRG}}\rangle - |\Psi^{\mathrm{CAS}}_{\mathrm{FCI}}\rangle\|_{L^2}$ and $\|(\hat{S}_{\mathrm{FCI}} - \hat{S}_{\mathrm{DMRG}(\delta\varepsilon_{\mathrm{Tr}})})|\Psi_{\mathrm{HF}}\rangle\|$ in eqs 6 and 7, respectively, can be well approximated. We remark that this exponential scaling with the CAS size also effects the computational costs of the CAS CI-triples, which are needed for an exact treatment of the TCCSD energy equation. However, investigations of the influence of the CAS CI-triples on the computed energies are left for future work.

V.B. Results and Discussion. In this section, we investigate the overall error dependence of DMRG-TCCSD as a function of k and as a function of the DMRG-truncation error $\delta\varepsilon_{\mathrm{Tr}}$. For our numerical error study we perform steps 1−4 discussed in section V.A for each $N/2 < k < K$. For each geometry $r = 2.118a_0$, $2.700a_0$, and $3.600a_0$, we also carry out very high accuracy DMRG calculations on the full orbital space, i.e., by setting the truncation error to $\delta\varepsilon_{\mathrm{Tr}} = 10^{-8}$ and $k = K$. This data is used as a reference for the FCI solution.

B.1. Entropy Study on the Full Orbital Space. We start our investigation by showing DMRG results for the full orbital space, i.e., the CAS is formed from $k = K = 28$ orbitals, and for various fixed M values and for $\delta\varepsilon_{\mathrm{Tr}} = 10^{-8}$. In the latter case the maximum bond dimension was set to $M = 10\,000$. In Figure 1 a, we show the relative error of the ground-state energy as a function of the DMRG-truncation error on a logarithmic scale. For the FCI energy, E_{FCI}, the CCSDTQPH reference energy is used given in ref 107. It is visible that the relative error is a linear function of the truncation error on a logarithmic scale, thus extrapolation to the truncation free solution can be carried out according to refs 103 and 105.

In Figures 2 and 3, we present the sorted values of the single orbital entropy and of the mutual information obtained for fixed $M = 64, 256, 512$ and with $\delta\varepsilon_{\mathrm{Tr}} = 10^{-8}$ for the three geometries. As can be seen in the figures, the entropy profiles obtained with low-rank DMRG calculations already resemble the main characteristics of the exact profile ($M \simeq 10000$). Therefore, orbitals with large single orbital entropies, also contributing to large matrix elements of I_{ij}, can easily be identified from a low-rank computation. The ordered orbital indices define the CAS

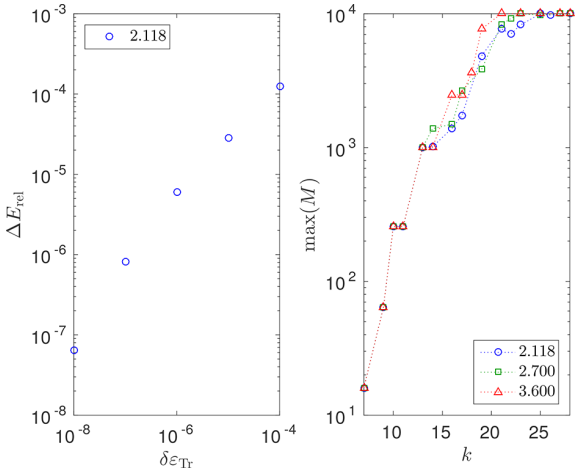

Figure 1. (a) Relative error of the ground-state energy as a function of the DMRG-truncation error on a logarithmic scale obtained for the full orbital space ($k = K$) with $r = 2.118a_0$. (b) Maximum number of block states as a function of k for the *a priori* defined truncation error $\delta\varepsilon_{\mathrm{Tr}} = 10^{-8}$ with $r = 2.118a_0$ (blue), $2.700a_0$ (green), and $3.600a_0$ (red).

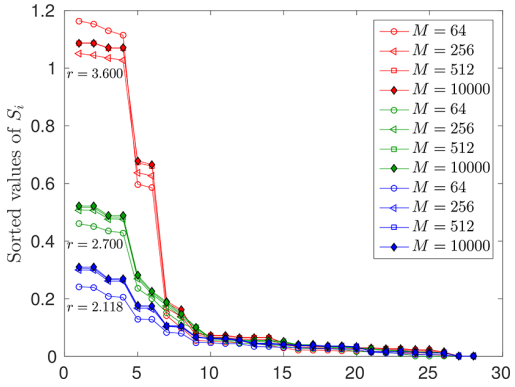

Figure 2. Single orbital entropy for $r = 2.118a_0$ (blue), $2.700a_0$ (green), $3.600a_0$ (red) obtained for the full orbital space ($k = 28$) with DMRG for fixed $M = 64, 256, 512$ and for $\delta\varepsilon_{\mathrm{Tr}} = 10^{-8}$, $M_{\mathrm{max}} = 10\,000$.

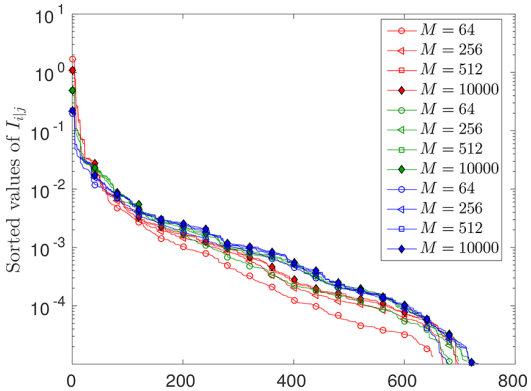

Figure 3. Mutual information for $r = 2.118a_0$ (blue), $2.700a_0$ (green), $3.600a_0$ (red) obtained for the full orbital space ($k = 28$) with DMRG for fixed $M = 64, 256, 512$ and for $\delta\varepsilon_{\mathrm{Tr}} = 10^{-8}$, $M_{\mathrm{max}} = 10\,000$.

DOI: 10.1021/acs.jctc.8b00960
J. Chem. Theory Comput. 2019, 15, 2206−2220

vector, and the CAS for the DMRG-TCCSD can be formed accordingly as discussed in section V.A.

Taking a look at Figure 2, it becomes apparent that S_i shifts upward for increasing r indicating the higher contribution of static correlations for the stretched geometries. Similarly the first 50−100 matrix elements of I_{ij} also take larger values for larger r while the exponential tail, corresponding to dynamic correlations, is less effected. The gap between large and small values of the orbital entropies gets larger and its position shifts rightward for larger r. Thus, for the stretched geometries more orbitals must be included in the CAS during the TCC scheme in order to determine the static correlations accurately. We remark here that the orbitals contributing to the high values of the single orbital entropy and mutual information matrix elements change for the different geometries according to chemical bond forming and breaking processes.[108]

B.2. Numerical Investigation of the Error's k-Dependence. In order to obtain $|\Psi^*\rangle$ in the FCI limit, we perform high-accuracy DMRG calculations with $\delta\varepsilon_{\mathrm{Tr}} = 10^{-8}$. The CAS was formed by including all Hartee−Fock orbitals and its size was increased systematically by including orbitals with the largest entropies according to the CAS vector. Orbitals with degenerate single orbital entropies, due to symmetry considerations, are added to the CAS at the same time. Thus, there are some missing k points in the following figures. For each restricted CAS we carry our the usual optimization steps of a DMRG scheme as discussed in section V.A, with low bond dimension followed by a high-accuracy calculation with $\delta\varepsilon_{\mathrm{Tr}} = 10^{-8}$ using eight sweeps.[93] Our DMRG ground-state energies for $7 < k < 28$ together with the CCSD (corresponding to a DMRG-TCCSD calculation where $k = N/2 = 7$) and CCSDTQ reference energies, are shown in Figure 4 near the equilibrium bond length, $r = 2.118a_0$. The single-reference coupled cluster calculations were performed in NWChem,[109] we employed the cc-pVDZ basis set in the spherical representation. For $k = K = 28$ the CCSDTQPH energy was taken as a reference for the FCI energy.[107]

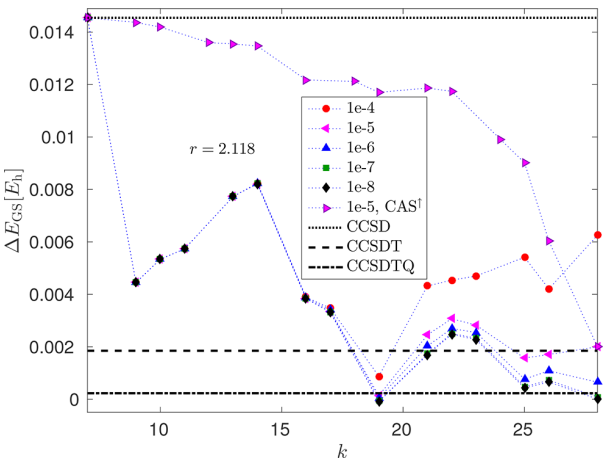

Figure 4. Ground-state energy of the N_2 molecule near the equilibrium geometry, $r = 2.118a_0$, obtained with DMRG-TCCSD for $7 \le k \le 28$ and for various DMRG truncation errors $\delta\varepsilon_{\mathrm{Tr}}$. The CCSD, CCSDT, and CCSDTQ reference energies are shown by dotted, dashed, and dashed−dotted lines, respectively. The CCSDTPQH energy ($k = 28$) is taken as a reference for the FCI energy. For $\delta\varepsilon_{\mathrm{Tr}} = 10^{-5}$ the CAS was additionally formed by taking k orbitals according to increasing values of the single-orbital entropy values, i.e., inverse to the other CAS extensions. This is labeled by CAS$^{\uparrow}$ (see also Sec. V.B.3).

The DMRG energy starts from the Hartree−Fock energy for $k = 7$ and decreases monotonically with increasing k until the full orbital solution with $k = 28$ is reached. It is remarkable, however, that the DMRG-TCCSD energy is significantly below the CCSD energy for all CAS choices, even for a very small $k = 9$. The error, however, shows an irregular behavior taking small values for several different k values. This is due to the fact that the DMRG-TCCSD approach suffers from a methodological error, i.e., certain fraction of the correlations are lost, since the CAS is frozen in the CCSD correction. This supports the hypothesis of a k-dependent constant as discussed in section IV.D. Therefore, whether orbital k is part of the CAS or external part provides a different methodological error. This is clearly seen as the error increases between $k = 10$ and 15 although the CAS covers more of the system's static correlation with increasing k. This is investigated in more detail in section B.4.

Since several k-splits lead to small DMRG-TCCSD errors, the optimal k value from the computational point of view, is determined not only by the error minimum but also by the minimal computational time, i.e., we need to take the computational requirements of the DMRG into account. Note that the size of the DMRG block states contributes significantly to the computational cost of the DMRG calculation. The connection of the block size to the CAS choice is shown in Figure 1b, where the maximal number of DMRG block states is depicted as a function of k for the *a priori* defined truncation error margin $\delta\varepsilon_{\mathrm{Tr}} = 10^{-8}$. Note that $\max(M)$ increases rapidly for $10 < k < 20$. The optimal CAS is therefore chosen such that the DMRG block states are not too large and the DMRG-TCCSD provides a low error, i.e., is a local minimum in the residual with respect to k.

It is important to note that based on Figure 4 the DMRG-TCCSD energy got very close to, or even dropped below, the CCSDT energy for several k values. Since close to the equilibrium geometry the wave function is dominated by a single reference character, it is expected that DMRG-TCCSD leads to even more robust improvements for the stretched geometries, i.e., when the multireference character of the wave function is more pronounced. Our results for the stretched geometries, $r = 2.700a_0$ and $3.600a_0$, are shown in Figures 2, 3, 5, and 6. As mentioned in section B.1, for larger r values static correlations gain importance signaled by the increase in the single orbital entropy in Figure 2. Thus, the multireference character of the wave function becomes apparent through the entropy profiles. According to Figure 5 the DMRG-TCCSD energy for all $k > 7$ values is again below the CCSD computation and for $k > 15$ it is even below the CCSDT reference energy. For $r = 3.600a_0$ the CC computation fluctuates with increasing excitation ranks and CCSDT is even far below the FCI reference energy, revealing the variational breakdown of the single-reference CC method for multireference problems. In contrast to this, the DMRG-TCCSD energy is again below the CCSD energy for all $k > 7$, but above the CCSDT energy. The error furthermore shows a local minimum around $k = 19$. For the stretched geometries static correlations are more pronounced, there are more orbitals with large entropies, thus the maximum number of DMRG block states increases more rapidly with k compared to the situation near the equilibrium geometry (see Figure 1b). Thus, obtaining an error margin within 1 μE_h for $k = 19 \ll 28$ leads to a significant save in computational time and resources. Here we remark that DMRG-TCCSD is a single-reference multireference method thus the choice of the reference determinant can effect its performance. In the our

DOI: 10.1021/acs.jctc.8b00960
J. Chem. Theory Comput. 2019, 15, 2206−2220

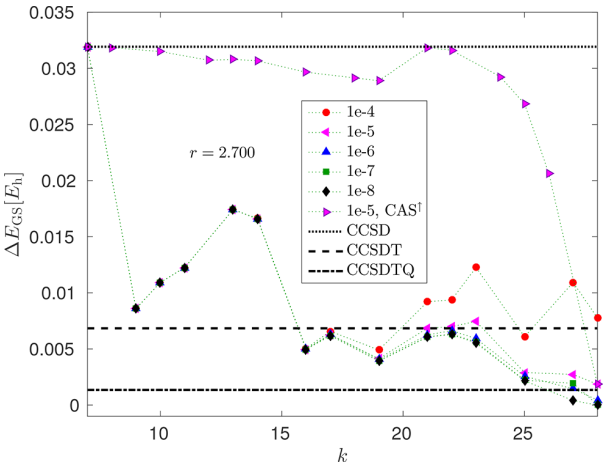

Figure 5. Ground-state energy of the N_2 molecule with bond length $r = 2.7a_0$, obtained with DMRG-TCCSD for $7 \leq k \leq 28$ and for various DMRG truncation errors $\delta\epsilon_{Tr}$. The CCSD, CCSDT, and CCSDTQ reference energies are shown by dotted, dashed, and dashed−dotted lines, respectively. The DMRG energy with $\delta\epsilon_{Tr} = 10^{-8}$ on the full space, i.e., $k = 28$, is taken as a reference for the FCI energy. For $\delta\epsilon_{Tr} = 10^{-5}$, the CAS was additionally formed by taking k orbitals according to increasing values of the single-orbital entropy, i.e., inverse to the other CAS extensions. This is labeled by CAS$^{\uparrow}$ (see also section B.3).

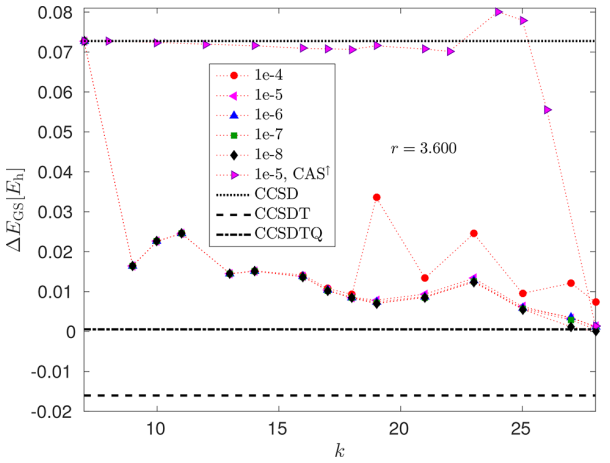

Figure 6. Ground-state energy of the N_2 molecule with bond length $r = 3.6a_0$, obtained with DMRG-TCCSD for $7 \leq k \leq 28$ and for various DMRG truncation errors $\delta\epsilon_{Tr}$. The CCSD, CCSDT, and CCSDTQ reference energies are shown by dotted, dashed, and dashed−dotted lines, respectively. The DMRG energy with $\delta\epsilon_{Tr} = 10^{-8}$ on the full space, i.e., $k = 28$, is taken as a reference for the FCI energy. For $\delta\epsilon_{Tr} = 10^{-5}$, the CAS was additionally formed by taking k orbitals according to increasing values of the single-orbital entropy, i.e., inverse to the other CAS extensions. This is labeled by CAS$^{\uparrow}$ (see also section B.3).

current study, however, we have verified that for $d \leq 4$ and for all k values the weight of the Hartree−Fock determinant was significantly larger than all other determinants.

B.3. Effect of $\delta\epsilon_{Tr}$ on the DMRG-TCCSD. In practice, we do not intend to carry out DMRG calculations in the FCI limit, thus usually a larger truncation error is used. Therefore, we have repeated our calculations for larger truncation errors in the range of 10^{-4} and 10^{-7}. Our results are shown in Figures 4, 5, and 6. For small k the DMRG solution basically provides the Full-CI limit since the *a priori* set minimum number of block states $M_{min} \simeq 64$ already leads to a very low truncation error. Therefore, the error of the DMRG-TCCSD is dominated by the methodological error. For $k > 15$ the effect of the DMRG truncation error becomes visible and for large k the overall error is basically determined by the DMRG solution. For larger $\delta\epsilon_{Tr}$ between 10^{-4} and 10^{-5} the DMRG-TCCSD error shows a minimum with respect to k. This is exactly the expected trend, since the CCSD method fails to capture static correlation while DMRG requires large bond dimension to recover dynamic correlations, i.e., a low truncation error threshold. In addition, the error minima for different truncation error thresholds $\delta\epsilon_{Tr}$ happen to be around the same k values. This has an important practical consequence: the optimal k-split can be determined by performing cheap DMRG-TCCSD calculations using large DMRG truncation error threshold as a function of k.

The figures furthermore indicate that ΔE_{GS} has a high peak for $9 < k < 16$. This can be explained by the splitting of the FCI space since this yields that the correlation from external orbitals with CAS orbitals is ignored. Thus, we also performed calculations for $\delta\epsilon_{Tr} = 10^{-5}$ using a CAS formed by taking k orbitals according to increasing values of the single orbital entropy values in order to demonstrate the importance of the CAS extension. The corresponding error profile as a function of k near the equilibrium geometry is shown in Figure 4 labeled by CAS$^{\uparrow}$. As expected, the improvement of DMRG-TCCSD is marginal compared to CCSD up to a very large $k \simeq 23$ split since ψ^{CAS}_{DMRG} differs only marginally from ψ_{HF}.

B.4. Numerical Investigation on CAS-ext Correlations. Taking another look at Figure 2, we can confirm that already for small k values the most important orbitals, i.e., those with the largest entropies, are included in the CAS. In Figure 7, the sorted

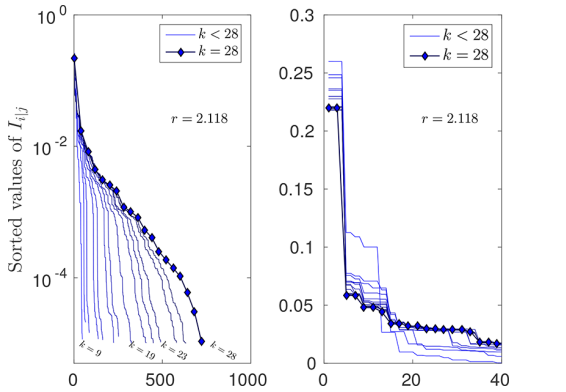

Figure 7. (a) Sorted values of the mutual information obtained by DMRG(k) for $9 \leq k \leq 28$ on a semilogarithmic scale for N_2 at $r = 2.118a_0$. (b) Sorted 40 largest matrix elements of the mutual information obtained by DMRG(k) for $9 \leq k \leq 28$ on a lin−lin scale for N_2 at $r = 2.118a_0$.

values of the mutual information obtained by DMRG(k) for $9 \leq k \leq 28$ is shown on a semilogarithmic scale. It is apparent from the figure that the largest values of $I_{i|j}$ change only slightly with increasing k, thus static correlations are basically included for all restricted CAS. The exponential tail of $I_{i|j}$ corresponding to dynamic correlations, however, becomes more visible only for larger k values. We conclude, for a given k split the DMRG method computes the static correlations efficiently and the missing tail of the mutual information with respect to the full orbital space ($k = 28$) calculation is captured by the TCC scheme.

DOI: 10.1021/acs.jctc.8b00960
J. Chem. Theory Comput. 2019, 15, 2206−2220

Correlations between the CAS and external parts can also be simulated by a DMRG calculation on the full orbital space using an orbital ordering according to the CAS vector. In this case, the DMRG left block can be considered as the CAS and the right block as the external part. For a pure target state, for example, the ground state, the correlations between the CAS and external part is measured by the block entropy, $S(\rho_{\mathrm{CAS}(k)})$ as a function of k. Here $\rho_{\mathrm{CAS}(k)}$ is formed by a partial trace on the external part of $|\Psi^{\mathrm{FCI}}_{\mathrm{DMRG}}\rangle$. The block entropy is shown in Figure 8a. The block entropy decays monotonically for $k > 7$, i.e, the correlations between the CAS and the external part vanish with increasing k. In contrast to this, when an ordering according to CAS$^{\uparrow}$ is used the correlation between CAS and external part remains always strong, i.e., some of the highly correlated orbitals are distributed among the CAS and the external part. Nevertheless, both curves are smooth and they cannot explain the error profile shown in Figure 4.

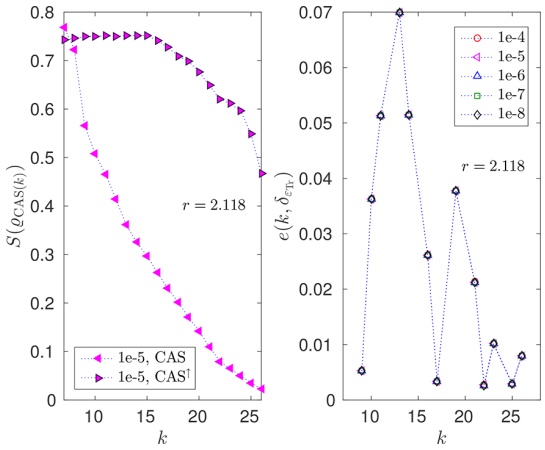

Figure 8. (a) Block entropy, $S(\rho_{\mathrm{CAS}(k)})$, as a function of k for $r = 2.118$ ordering orbitals along the DMRG chain according to the same CAS and CAS$^{\uparrow}$ vectors as used in Figure 4. (b) $e(k, \delta_{\varepsilon_{\mathrm{Tr}}})$ as a function of k of the nitrogen dimer near the equilibrium bond length for DMRG truncation error thresholds $\delta_{\varepsilon_{\mathrm{Tr}}}$ between 10^{-4} and 10^{-8}.

B.5. Numerical Values for the Amplitude Error Analysis. Since correlation analysis based on the entropy functions cannot reveal the error profile shown in Figure 4, here we reinvestigate the error behavior as a function of $N/2 \le k \le K$ but in terms of the CC amplitudes. Therefore, we also present a more detailed description of eq 10 in section IV which includes the following terms:

$$e(k, \delta_{\varepsilon_{\mathrm{Tr}}}) = \sum_{\substack{\mu: \\ |\mu|=1}} (t_{\mathrm{CCSD}}(k, \delta_{\varepsilon_{\mathrm{Tr}}}))^2_\mu + \sum_{\substack{\mu: \\ |\mu|=1,2}} [(t^*_k - t_{\mathrm{CCSD}}(k, \delta_{\varepsilon_{\mathrm{Tr}}}))^2_\mu + (s^*_k - s_{\mathrm{DMRG}}(k, \delta_{\varepsilon_{\mathrm{Tr}}}))^2_\mu] \quad (11)$$

Here the *valid index-pairs* are $\mu = (\boldsymbol{i}, \boldsymbol{a})$, with $\boldsymbol{i} = (i_1, ..., i_n) \in \{1, ..., N/2\}^n$, and $\boldsymbol{a} = (a_1, ..., a_n) \in \{N/2 + 1, ..., K\}^n$. The excitation rank is given by $|\mu| = n$ where $n = 1$ stands for singles, $n = 2$ for doubles, and so on. The μ values are the labels of excitation operators $\hat{\tau}^a_i := \hat{a}^\dagger_a \hat{a}_i$, and $\hat{\tau}^{a_1,...,a_n}_{i_1,...,i_n} := \hat{\tau}^{a_n}_{i_n} ... \hat{\tau}^{a_1}_{i_1}$. The corresponding amplitudes are given as $t^{a_1,...,a_n}_{i_1,...,i_n}$. For invalid index-pairs, i.e., index-pairs that are out of range, the amplitudes are always zero. The various amplitudes appearing in eq 11 are calculated according to the following rules:

(1) The tensor s^*_k: amplitudes in the CAS(k) obtained by DMRG($\delta^*_{\varepsilon_{\mathrm{Tr}}} = 10^{-8}$) solution (represented by CI coefficients c^*) for CAS(K)

$$(s^*_k)^A_i = \frac{c^{*A}_i}{c^*_0}$$

$$(s^*_k)^{A_1,A_2}_{i_1,i_2} = \frac{c^{*A_1,A_2}_{i_1,i_2}}{c^*_0} - \frac{c^{*A_1}_{i_1} c^{*A_2}_{i_2} - c^{*A_2}_{i_1} c^{*A_1}_{i_2}}{c^{*2}_0} \quad (12)$$

where $i, i_1, i_2 \in \{1, ..., N/2\}$ and $a, a_1, a_2 \in \{N/2 + 1, ..., k\}$.

(2) The tensor t^*_k: amplitudes not in the CAS(k) obtained from the DMRG($\delta^*_{\varepsilon_{\mathrm{Tr}}} = 10^{-8}$) solution (represented by CI coefficients c^*) for CAS(K) projected onto CAS(k), i.e., the complement (with respect to valid index-pairs) of s^*_k.

(3) The tensor $s_{\mathrm{DMRG}}(k, \delta_{\varepsilon_{\mathrm{Tr}}})$: amplitudes in the CAS($k$) are obtained by the DMRG($\delta_{\varepsilon_{\mathrm{Tr}}}$) solution (represented by CI coefficients c) for CAS(k). The amplitudes $s_{\mathrm{DMRG}}(k, \delta_{\varepsilon_{\mathrm{Tr}}})^a_i$, $s_{\mathrm{DMRG}}(k, \delta_{\varepsilon_{\mathrm{Tr}}})^{a_1,a_2}_{i_1,i_2}$ are the same as eq 12, but with $c^* \to c$, where $i, i_1, i_2 \in \{1, ..., N/2\}$ and $a, a_1, a_2 \in \{N/2 + 1, ..., k\}$.

(4) The tensor $t_{\mathrm{CCSD}}(k, \delta_{\varepsilon_{\mathrm{Tr}}})$: amplitudes not in the CAS(k) obtained by TCCSD, i.e., the complement (with respect to valid index-pairs) of $s_{\mathrm{DMRG}}(k, \delta_{\varepsilon_{\mathrm{Tr}}})$.

In Figure 8b we show the error $e(k, \delta_{\varepsilon_{\mathrm{Tr}}})$ as a function of k of the nitrogen dimer near the equilibrium bond length. Note that the quantitative behavior is quite robust with respect to the bond dimension since the values only differ marginally. We emphasize that the error contribution in Figure 8 is dominated by second term in eq 11 since this is an order of magnitude larger than the contribution from the first and third terms in eq 11, respectively. The first term in eq 11 is furthermore related to the usual T1 diagnostic in CC,[110] so it is not a surprise that a small value, $\sim 10^{-3}$, was found. Comparing this error profile to the one shown in Figure 4 we can understand the irregular behavior and the peak in the error in ΔE_{GS} between $k = 9$ and 17, and the other peaks for $k > 17$ but the error minimum found for $k = 19$ remains unexplained. Furthermore, we can conclude from Figure 8b that the quotient $\Delta E_{\mathrm{GS}}(k)/e(k, \delta_{\varepsilon_{\mathrm{Tr}}})$ is not constant. This indicates that the constants involved in section IV in particular the constant in eq 10 in section IV.D is indeed k-dependent.

VI. CONCLUSION

In this article we presented a fundamental study of the DMRG-TCCSD method. We showed that, unlike the single-reference CC method, the linked and unlinked DMRG-TCC equations are in general not equivalent. Furthermore, we showed energy size consistency of the TCC, DMRG-TCC, and DMRG-TCCSD method and gave a proof that CAS excitations higher than order three do not enter the TCC energy expression.

In addition to these computational properties of the DMRG-TCCSD method, we presented the mathematical error analysis performed in ref 76 from a quantum chemistry perspective. We showed local uniqueness and quasi optimality of DMRG-TCC solutions and highlighted the importance of the CAS-ext gap—a spectral gap assumption allowing to perform the analysis presented here. Furthermore, we presented a quadratic *a priori*

DOI: 10.1021/acs.jctc.8b00960
J. Chem. Theory Comput. 2019, 15, 2206−2220

error estimate for the DMRG-TCC method, which aligns the error behavior of the DMRG-TCC method with variational methods except for the upper bound condition. We emphasize that the DMRG-TCC solution depends strongly on the CAS choice. Throughout the analysis we neglected this dependence as we assumed an optimal CAS choice as indicated in section IV.A. The explicit consideration of this dependence in the performed error analysis carries many mathematical challenges, which are part of our current research. Therefore, we extended this work with a numerical study of the k-dependence of the DMRG-TCCSD error which showed also that the constants involved in the error estimation are most likely k-dependent. This stresses the importance of further mathematical work to include this dependence explicitly in the analysis.

We furthermore presented computational data of the single-site entropy and the mutual information that are used to choose the CAS. Our computations showed that these properties are qualitatively very robust, i.e., their qualitative behavior is well represented by means of a low-rank approximation, which is a computational benefit. The numerical investigation of the k-dependence of the DMRG-TCCSD error revealed that the predicted trend in section IV.A is correct. We demonstrated that the error indeed first decays ($7 \leq k \leq 9$) and then increases again ($25 \leq k \leq 28$) for low-rank approximations, i.e., 10^{-4} respectively 10^{-5}. This aligns with the theoretical prediction based on the properties of the DMRG and single reference CC method. Additional to this general trend, the error shows oscillations. A first hypothesis is that this behavior is related to the ignored correlations in the transition $k \rightarrow k + 1$. However, this was not able to be proven so far using entropy based measures but a similar irregular behavior can be detected by a cluster amplitude error analysis. Furthermore, such oscillations can be related to a bad reference function. Nonetheless, this scenario has here been ruled out since the Hartree−Fock determinant was found to be dominant in the CAS solution, i.e., the weight of the Hartree−Fock had largest weight in the CAS solution. The irregular behavior of the error minimum found for the DMRG-TCCSD method, therefore, could not be explained within this article and is left for future work. Despite the unknown reason for this behavior, we note that the error minima are fairly robust with respect to the bond dimension. Hence, the DMRG-TCCSD method can be extended with a screening process using low bond-dimension approximations to detect possible error minima.

On the other hand, an important feature that we would like to highlight here is that a small CAS ($k = 9$) yields a significant improvement of the energy and that the energies for all three geometries and all CAS choices outrun the single-reference CC method. In addition, the DMRG-TCCSD method avoids the breakdown of the CC approach even for multireference (strongly correlated) systems and, using concepts of quantum information theory, allows an efficient routine application of the method. Since the numerical error study showed a significant improvement for small CAS, we suspect the DMRG-TCCSD method to be of great use for larger systems with many strongly correlated orbitals as well as a many dynamically correlated orbitals.[1,2]

Finally, we remark, that besides the advantageous properties of the method there is a need for further analysis and developments in order to achieve our ultimate goal, i.e., to provide a black-box implementation of the DMRG-TCC method. Among these we highlight orbital rotations in the CAS through Fermionic mode transformation,[111] an automatic calculation of the best rank-1 representation of the DMRG wave function to be used as a reference state and the investigations of the influence of the CAS CI-triples on the computed energies. All these tasks are in progress.

AUTHOR INFORMATION

Corresponding Author

*E-mail: f.m.faulstich@kjemi.uio.no.

ORCID

Fabian M. Faulstich: 0000-0003-4751-7544
Andre Laestadius: 0000-0001-7391-0396
Libor Veis: 0000-0002-4229-6335
Andrej Antalik: 0000-0002-8422-8410
Jiří Brabec: 0000-0002-7764-9890

Notes

The authors declare no competing financial interest.

ACKNOWLEDGMENTS

This work has received funding from the *Research Council of Norway* (RCN) under CoE Grant No. 262695 (Hylleraas Centre for Quantum Molecular Sciences), from ERC-STG-2014 under grant No. 639508, from the *Hungarian National Research, Development and Innovation Office* (NKFIH) through Grant No. K120569, from the *Hungarian Quantum Technology National Excellence Program* (Project No. 2017-1.2.1-NKP-2017-00001), from the *Czech Science Foundation* (grants no. 16-12052S, 18-18940Y, and 18-24563S), and the *Czech Ministry of Education, Youth and Sports* (project no. LTAUSA17033). Ö.L. also acknowledges financial support form the Alexander von Humboldt Foundation. F.M.F, A.L., Ö.L., and M.A.C. are grateful for the mutual hospitality received during their visits at the Wigner Research Center for Physics in Budapest and the Hylleraas Centre for Quantum Molecular Sciences. Ö.L. and J.P. acknowledge useful discussions with Marcel Nooijen.

REFERENCES

(1) Veis, L.; Antalík, A.; Brabec, J.; Neese, F.; Legeza, Ö.; Pittner, J. Coupled Cluster Method with Single and Double Excitations Tailored by Matrix Product State Wave Functions. *J. Phys. Chem. Lett.* **2016**, *7*, 4072−4078.

(2) Veis, L.; Antalík, A.; Legeza, Ö.; Alavi, A.; Pittner, J. The Intricate Case of Tetramethyleneethane: A Full Configuration Interaction Quantum Monte Carlo Benchmark and Multireference Coupled Cluster Studies. *J. Chem. Theory Comput.* **2018**, *14*, 2439−2445.

(3) White, S. R.; Martin, R. L. Ab Initio Quantum Chemistry Using The Density Matrix Renormalization Group. *J. Chem. Phys.* **1999**, *110*, 4127−4130.

(4) McCulloch, I. P.; Gulácsi, M. The non-Abelian density matrix renormalization group algorithm. *Europhys. Lett.* **2002**, *57*, 852.

(5) Tóth, A.; Moca, C.; Legeza, Ö.; Zaránd, G. Density matrix numerical renormalization group for non-Abelian symmetries. *Phys. Rev. B: Condens. Matter Mater. Phys.* **2008**, *78*, 245109.

(6) Sharma, S.; Chan, G. K.-L. Spin-adapted density matrix renormalization group algorithms for quantum chemistry. *J. Chem. Phys.* **2012**, *136*, 124121.

(7) Keller, S.; Reiher, M. Spin-adapted matrix product states and operators. *J. Chem. Phys.* **2016**, *144*, 134101.

(8) Bartlett, R. J.; Musiał, M. Coupled-cluster theory in quantum chemistry. *Rev. Mod. Phys.* **2007**, *79*, 291−352.

(9) Lyakh, D. I.; Musiał, M.; Lotrich, V. F.; Bartlett, R. J. Multireference Nature of Chemistry: The Coupled-Cluster View. *Chem. Rev.* **2012**, *112*, 182−243.

DOI: 10.1021/acs.jctc.8b00960
J. Chem. Theory Comput. 2019, 15, 2206−2220

(10) Köhn, A.; Hanauer, M.; Mück, L. A.; Jagau, T.-C.; Gauss, J. State-specific multireference coupled-cluster theory. *Wiley Interdiscip. Rev.: Comput. Mol. Sci.* **2013**, *3*, 176−197.
(11) Jeziorski, B.; Monkhorst, H. J. Coupled-cluster method for multideterminantal reference states. *Phys. Rev. A: At., Mol., Opt. Phys.* **1981**, *24*, 1668−1681.
(12) Lee, J.; Small, D. W.; Epifanovsky, E.; Head-Gordon, M. Coupled-cluster valence-bond singles and doubles for strongly correlated systems: Block-tensor based implementation and application to oligoacenes. *J. Chem. Theory Comput.* **2017**, *13*, 602−615.
(13) Lindgren, I.; Mukherjee, D. On the connectivity criteria in the open-shell coupled-cluster theory for general model spaces. *Phys. Rep.* **1987**, *151*, 93−127.
(14) Lindgren, I. Linked-Diagram and Coupled-Cluster Expansions for Multi-Configurational, Complete and Incomplete Model Spaces. *Phys. Scr.* **1985**, *32*, 291.
(15) Mukherjee, D.; Moitra, R. K.; Mukhopadhyay, A. Applications of a non-perturbative many-body formalism to general open-shell atomic and molecular problems: calculation of the ground and the lowest π-π^* singlet and triplet energies and the first ionization potential of trans-butadiene. *Mol. Phys.* **1977**, *33*, 955−969.
(16) Stolarczyk, L. Z.; Monkhorst, H. J. Coupled-cluster method with optimized reference state. *Int. J. Quantum Chem.* **1984**, *26*, 267−291.
(17) Stolarczyk, L. Z.; Monkhorst, H. J. Coupled-cluster method in Fock space. I. General formalism. *Phys. Rev. A: At., Mol., Opt. Phys.* **1985**, *32*, 725−742.
(18) Stolarczyk, L. Z.; Monkhorst, H. J. Coupled-cluster method in Fock space. II. Brueckner-Hartree-Fock method. *Phys. Rev. A: At., Mol., Opt. Phys.* **1985**, *32*, 743.
(19) Stolarczyk, L. Z.; Monkhorst, H. J. Coupled-cluster method in Fock space. III. On similarity transformation of operators in Fock space. *Phys. Rev. A: At., Mol., Opt. Phys.* **1988**, *37*, 1908.
(20) Stolarczyk, L. Z.; Monkhorst, H. J. Coupled-cluster method in Fock space. IV. Calculation of expectation values and transition moments. *Phys. Rev. A: At., Mol., Opt. Phys.* **1988**, *37*, 1926.
(21) Stolarczyk, L. Z.; Monkhorst, H. J. Quasiparticle Fock-space coupled-cluster theory. *Mol. Phys.* **2010**, *108*, 3067−3089.
(22) Jeziorski, B.; Monkhorst, H. J. Coupled-cluster method for multideterminantal reference states. *Phys. Rev. A: At., Mol., Opt. Phys.* **1981**, *24*, 1668.
(23) Datta, D.; Mukherjee, D. An explicitly spin-free compact open-shell coupled cluster theory using a multireference combinatoric exponential ansatz: Formal development and pilot applications. *J. Chem. Phys.* **2009**, *131*, 044124.
(24) Evangelista, F. A.; Allen, W. D.; Schaefer, H. F., III High-order excitations in state-universal and state-specific multireference coupled cluster theories: Model systems. *J. Chem. Phys.* **2006**, *125*, 154113.
(25) Piecuch, P.; Paldus, J. Orthogonally spin-adapted multi-reference Hilbert space coupled-cluster formalism: Diagrammatic formulation. *Theor. Chim. Acta* **1992**, *83*, 69−103.
(26) Kucharski, S.; Balková, A.; Szalay, P.; Bartlett, R. J. Hilbert space multireference coupled-cluster methods. II. A model study on H8. *J. Chem. Phys.* **1992**, *97*, 4289−4300.
(27) Balková, A.; Kucharski, S.; Meissner, L.; Bartlett, R. J. A Hilbert space multi-reference coupled-cluster study of the H 4 model system. *Theor. Chim. Acta* **1991**, *80*, 335−348.
(28) Kinoshita, T.; Hino, O.; Bartlett, R. J. Coupled-cluster method tailored by configuration interaction. *J. Chem. Phys.* **2005**, *123*, 074106.
(29) Fang, T.; Shen, J.; Li, S. Block correlated coupled cluster method with a complete-active-space self-consistent-field reference function: The formula for general active spaces and its applications for multibond breaking systems. *J. Chem. Phys.* **2008**, *128*, 224107.
(30) Datta, D.; Kong, L.; Nooijen, M. A state-specific partially internally contracted multireference coupled cluster approach. *J. Chem. Phys.* **2011**, *134*, 214116.
(31) Hanauer, M.; Köhn, A. Pilot applications of internally contracted multireference coupled cluster theory, and how to choose the cluster operator properly. *J. Chem. Phys.* **2011**, *134*, 204111.
(32) Evangelista, F. A.; Gauss, J. An orbital-invariant internally contracted multireference coupled cluster approach. *J. Chem. Phys.* **2011**, *134*, 114102.
(33) Lyakh, D. I.; Ivanov, V. V.; Adamowicz, L. Automated generation of coupled-cluster diagrams: Implementation in the multireference state-specific coupled-cluster approach with the complete-active-space reference. *J. Chem. Phys.* **2005**, *122*, 024108.
(34) Hanrath, M. An exponential multireference wave-function Ansatz. *J. Chem. Phys.* **2005**, *123*, 084102.
(35) Pittner, J.; Nachtigall, P.; Čársky, P.; Hubač, I. State-Specific Brillouin- Wigner Multireference Coupled Cluster Study of the Singlet-Triplet Separation in the Tetramethyleneethane Diradical. *J. Phys. Chem. A* **2001**, *105*, 1354−1356.
(36) Hubač, I.; Wilson, S. On the use of Brillouin-Wigner perturbation theory for many-body systems. *J. Phys. B: At., Mol. Opt. Phys.* **2000**, *33*, 365.
(37) Hubač, I.; Pittner, J.; Čársky, P. Size-extensivity correction for the state-specific multireference Brillouin-Wigner coupled-cluster theory. *J. Chem. Phys.* **2000**, *112*, 8779−8784.
(38) Pittner, J.; Šmydke, J.; Čársky, P.; Hubač, I. State-specific Brillouin-Wigner multireference coupled cluster study of the F2 molecule: assessment of the a posteriori size-extensivity correction. *J. Mol. Struct.: THEOCHEM* **2001**, *547*, 239−244.
(39) Fang, T.; Li, S. Block correlated coupled cluster theory with a complete active-space self-consistent-field reference function: The formulation and test applications for single bond breaking. *J. Chem. Phys.* **2007**, *127*, 204108.
(40) Chattopadhyay, S.; Mahapatra, U. S.; Mukherjee, D. Development of a linear response theory based on a state-specific multireference coupled cluster formalism. *J. Chem. Phys.* **2000**, *112*, 7939−7952.
(41) Kong, L. Connection between a few Jeziorski-Monkhorst ansatz-based methods. *Int. J. Quantum Chem.* **2009**, *109*, 441−447.
(42) Chattopadhyay, S.; Mahapatra, U. S.; Mukherjee, D. Property calculations using perturbed orbitals via state-specific multireference coupled-cluster and perturbation theories. *J. Chem. Phys.* **1999**, *111*, 3820−3831.
(43) Pittner, J. Continuous transition between Brillouin-Wigner and Rayleigh-Schrödinger perturbation theory, generalized Bloch equation, and Hilbert space multireference coupled cluster. *J. Chem. Phys.* **2003**, *118*, 10876−10889.
(44) Mahapatra, U. S.; Datta, B.; Mukherjee, D. A size-consistent state-specific multireference coupled cluster theory: Formal developments and molecular applications. *J. Chem. Phys.* **1999**, *110*, 6171−6188.
(45) Mášik, J.; Hubač, I.; Mach, P. Single-root multireference Brillouin-Wigner coupled-cluster theory: Applicability to the F 2 molecule. *J. Chem. Phys.* **1998**, *108*, 6571−6579.
(46) Hubač, I.; Neogrády, P. Size-consistent Brillouin-Wigner perturbation theory with an exponentially parametrized wave function: Brillouin-Wigner coupled-cluster theory. *Phys. Rev. A: At., Mol., Opt. Phys.* **1994**, *50*, 4558−4564.
(47) Adamowicz, L.; Malrieu, J.-P.; Ivanov, V. V. New approach to the state-specific multireference coupled-cluster formalism. *J. Chem. Phys.* **2000**, *112*, 10075−10084.
(48) Kállay, M.; Szalay, P. G.; Surján, P. R. A general state-selective multireference coupled-cluster algorithm. *J. Chem. Phys.* **2002**, *117*, 980−990.
(49) Piecuch, P.; Kowalski, K. The state-universal multi-reference coupled-cluster theory: An overview of some recent advances. *Int. J. Mol. Sci.* **2002**, *3*, 676−709.
(50) Schucan, T.; Weidenmüller, H. The effective interaction in nuclei and its perturbation expansion: An algebraic approach. *Ann. Phys.* **1972**, *73*, 108−135.
(51) Kaldor, U. Intruder states and incomplete model spaces in multireference coupled-cluster theory: The $2p^2$ states of Be. *Phys. Rev. A: At., Mol., Opt. Phys.* **1988**, *38*, 6013.
(52) Malrieu, J.; Durand, P.; Daudey, J. Intermediate Hamiltonians as a new class of effective Hamiltonians. *J. Phys. A: Math. Gen.* **1985**, *18*, 809.

DOI: 10.1021/acs.jctc.8b00960
J. Chem. Theory Comput. 2019, 15, 2206−2220

(53) Jankowski, K.; Malinowski, P. A valence-universal coupled-cluster single-and double-excitations method for atoms. III. Solvability problems in the presence of intruder states. *J. Phys. B: At., Mol. Opt. Phys.* **1994**, *27*, 1287.
(54) Sharma, S.; Alavi, A. Multireference linearized coupled cluster theory for strongly correlated systems using matrix product states. *J. Chem. Phys.* **2015**, *143*, 102815.
(55) Henderson, T. M.; Bulik, I. W.; Stein, T.; Scuseria, G. E. Seniority-based coupled cluster theory. *J. Chem. Phys.* **2014**, *141*, 244104.
(56) Lehtola, S.; Parkhill, J.; Head-Gordon, M. Cost-effective description of strong correlation: Efficient implementations of the perfect quadruples and perfect hextuples models. *J. Chem. Phys.* **2016**, *145*, 134110.
(57) Lehtola, S.; Parkhill, J.; Head-Gordon, M. Orbital optimization in the perfect pairing hierarchy: applications to full-valence calculations on linear polyacenes. *Mol. Phys.* **2018**, *116*, 547−560.
(58) Cullen, J. Generalized valence bond solutions from a constrained coupled cluster method. *Chem. Phys.* **1996**, *202*, 217−229.
(59) Goddard, W. A., III; Harding, L. B. The description of chemical bonding from ab initio calculations. *Annu. Rev. Phys. Chem.* **1978**, *29*, 363−396.
(60) Ukrainskii, I. New variational function in the theory of quasi-one-dimensional metals. *Theor. Math. Phys.* **1977**, *32*, 816−822.
(61) Hunt, W.; Hay, P.; Goddard, W., III Self-Consistent Procedures for Generalized Valence Bond Wavefunctions. Applications H_3, BH, H_2O, C_2H_6, and O_2. *J. Chem. Phys.* **1972**, *57*, 738−748.
(62) Hurley, A.; Lennard-Jones, J. E.; Pople, J. A. The molecular orbital theory of chemical valency XVI. A theory of paired-electrons in polyatomic molecules. *Proc. R. Soc. London. Series A. Math. Phys. Sci.* **1953**, *220*, 446−455.
(63) Živković, T. P. Existence and reality of solutions of the coupled-cluster equations. *Int. J. Quantum Chem.* **1977**, *12*, 413−420.
(64) Piecuch, P.; Zarrabian, S.; Paldus, J.; Čížek, J. Coupled-cluster approaches with an approximate account of triexcitations and the optimized-inner-projection technique. II. Coupled-cluster results for cyclic-polyene model systems. *Phys. Rev. B: Condens. Matter Mater. Phys.* **1990**, *42*, 3351.
(65) Atkinson, K. E. *An introduction to numerical analysis*; John Wiley & Sons, 2008.
(66) Živković, T. P.; Monkhorst, H. J. Analytic connection between configuration-interaction and coupled-cluster solutions. *J. Math. Phys.* **1978**, *19*, 1007−1022.
(67) Kowalski, K.; Jankowski, K. Towards complete solutions to systems of nonlinear equations of many-electron theories. *Phys. Rev. Lett.* **1998**, *81*, 1195.
(68) Piecuch, P.; Kowalski, K. In *Computational Chemistry: Reviews of Current Trends*; Leszczynski, J., Ed.; World Scientific, Singapore, 2000; Vol. *5*.
(69) Jeziorski, B.; Paldus, J. Valence universal exponential ansatz and the cluster structure of multireference configuration interaction wave function. *J. Chem. Phys.* **1989**, *90*, 2714−2731.
(70) Schneider, R. Analysis of the Projected Coupled Cluster Method in Electronic Structure Calculation. *Numer. Math.* **2009**, *113*, 433−471.
(71) Rohwedder, T. The Continuous Coupled Cluster Formulation for the Electronic Schrödinger Equation. *ESAIM: Math. Modell. Numer. Anal.* **2013**, *47*, 421−447.
(72) Rohwedder, T.; Schneider, R. Error Estimates for the Coupled Cluster Method. *ESAIM: Math. Modell. Numer. Anal.* **2013**, *47*, 1553−1582.
(73) Laestadius, A.; Kvaal, S. Analysis of the extended coupled-cluster method in quantum chemistry. *SIAM J. on Numer. Anal.* **2018**, *56*, 660−683.
(74) Löwdin, P.-O. On the stability problem of a pair of adjoint operators. *J. Math. Phys.* **1983**, *24*, 70−87.
(75) Arponen, J. Variational principles and linked-cluster exp S expansions for static and dynamic many-body problems. *Ann. Phys.* **1983**, *151*, 311−382.
(76) Faulstich, F. M.; Laestadius, A.; Kvaal, S.; Legeza, Ö.; Schneider, R. Analysis of The Coupled-Cluster Method Tailored by Tensor-Network States in Quantum Chemistry. *arXiv.org* **2018**, No. 1802.05699.
(77) Laestadius, A.; Faulstich, F. M. The coupled-cluster formalism-a mathematical perspective. *Mol. Phys.* **2019**, 1−12.
(78) Piecuch, P.; Oliphant, N.; Adamowicz, L. A state-selective multireference coupled-cluster theory employing the single-reference formalism. *J. Chem. Phys.* **1993**, *99*, 1875−1900.
(79) Piecuch, P.; Adamowicz, L. State-selective multireference coupled-cluster theory employing the single-reference formalism: Implementation and application to the H8 model system. *J. Chem. Phys.* **1994**, *100*, 5792−5809.
(80) Chan, G. K.-L.; Sharma, S. The density matrix renormalization group in quantum chemistry. *Annu. Rev. Phys. Chem.* **2011**, *62*, 465−481.
(81) Saitow, M.; Kurashige, Y.; Yanai, T. Multireference configuration interaction theory using cumulant reconstruction with internal contraction of density matrix renormalization group wave function. *J. Chem. Phys.* **2013**, *139*, 044118.
(82) Myhre, R. H.; Koch, H. The multilevel CC3 coupled cluster model. *J. Chem. Phys.* **2016**, *145*, 044111.
(83) Lyakh, D. I.; Musiał, M.; Lotrich, V. F.; Bartlett, R. J. Multireference nature of chemistry: The coupled-cluster view. *Chem. Rev.* **2012**, *112*, 182−243.
(84) Szalay, S.; Barcza, G.; Szilvási, T.; Veis, L.; Legeza, Ö. The correlation theory of the chemical bond. *Sci. Rep.* **2017**, *7*, 2237.
(85) Legeza, Ö.; Sólyom, J. Optimizing the density-matrix renormalization group method using quantum information entropy. *Phys. Rev. B: Condens. Matter Mater. Phys.* **2003**, *68*, 195116.
(86) Barcza, G.; Legeza, Ö.; Marti, K. H.; Reiher, M. Quantum-information analysis of electronic states of different molecular structures. *Phys. Rev. A: At., Mol., Opt. Phys.* **2011**, *83*, 012508.
(87) Stein, C. J.; Reiher, M. Automated selection of active orbital spaces. *J. Chem. Theory Comput.* **2016**, *12*, 1760−1771.
(88) Aubin, J. P. Behavior of the error of the approximate solutions of boundary value problems for linear elliptic operators by Galerkin's and finite difference methods. *Ann. Sc. Norm. Super. Pisa Cl. Sci. (5)* **1967**, *21*, 599−637.
(89) Nitsche, J. Ein kriterium für die quasi-optimalität des ritzschen verfahrens. *Numer. Math.* **1968**, *11*, 346−348.
(90) Oganesyan, L. A.; Rukhovets, L. A. Study of the rate of convergence of variational difference schemes for second-order elliptic equations in a two-dimensional field with a smooth boundary. *USSR Comput. Math. Math. Phys.* **1969**, *9*, 158−183.
(91) Dunning, T. H., Jr Gaussian basis sets for use in correlated molecular calculations. I. The atoms boron through neon and hydrogen. *J. Chem. Phys.* **1989**, *90*, 1007−1023.
(92) Kowalski, K.; Piecuch, P. Renormalized CCSD (T) and CCSD (TQ) approaches: Dissociation of the N_2 triple bond. *J. Chem. Phys.* **2000**, *113*, 5644−5652.
(93) Szalay, S.; Pfeffer, M.; Murg, V.; Barcza, G.; Verstraete, F.; Schneider, R.; Legeza, Ö. Tensor product methods and entanglement optimization for ab initio quantum chemistry. *Int. J. Quantum Chem.* **2015**, *115*, 1342−1391.
(94) Murg, V.; Verstraete, F.; Legeza, Ö.; Noack, R.-h. M. Simulating strongly correlated quantum systems with tree tensor networks. *Phys. Rev. B: Condens. Matter Mater. Phys.* **2010**, *82*, 205105.
(95) Nakatani, N.; Chan, G. K.-L. Efficient tree tensor network states (TTNS) for quantum chemistry: Generalizations of the density matrix renormalization group algorithm. *J. Chem. Phys.* **2013**, *138*, 134113.
(96) Murg, V.; Verstraete, F.; Schneider, R.; Nagy, P. R.; Legeza, Ö. Tree tensor network state with variable tensor order: an efficient multireference method for strongly correlated systems. *J. Chem. Theory Comput.* **2015**, *11*, 1027−1036.
(97) Gunst, K.; Verstraete, F.; Wouters, S.; Legeza, Ö.; Van Neck, D. T3NS: Three-Legged Tree Tensor Network States. *J. Chem. Theory Comput.* **2018**, *14*, 2026−2033.

DOI: 10.1021/acs.jctc.8b00960
J. Chem. Theory Comput. 2019, 15, 2206−2220

(98) Chan, G. K.-L.; Head-Gordon, M. Highly correlated calculations with a polynomial cost algorithm: A study of the density matrix renormalization group. *J. Chem. Phys.* **2002**, *116*, 4462−4476.
(99) Legeza, Ö.; Sólyom, J. Optimizing the density-matrix renormalization group method using quantum information entropy. *Phys. Rev. B: Condens. Matter Mater. Phys.* **2003**, *68*, 195116.
(100) Barcza, G.; Legeza, Ö.; Marti, K. H.; Reiher, M. Quantum-information analysis of electronic states of different molecular structures. *Phys. Rev. A: At., Mol., Opt. Phys.* **2011**, *83*, 012508.
(101) Fertitta, E.; Paulus, B.; Barcza, G.; Legeza, Ö. Investigation of metal-insulator-like transition through the *ab initio* density matrix renormalization group approach. *Phys. Rev. B: Condens. Matter Mater. Phys.* **2014**, *90*, 245129.
(102) Rissler, J.; Noack, R. M.; White, S. R. Measuring orbital interaction using quantum information theory. *Chem. Phys.* **2006**, *323*, 519−531.
(103) Legeza, Ö.; Röder, J.; Hess, B. A. Controlling the accuracy of the density-matrix renormalization-group method: The dynamical block state selection approach. *Phys. Rev. B: Condens. Matter Mater. Phys.* **2003**, *67*, 125114.
(104) Legeza, Ö.; Sólyom, J. Quantum data compression, quantum information generation, and the density-matrix renormalization-group method. *Phys. Rev. B: Condens. Matter Mater. Phys.* **2004**, *70*, 205118.
(105) Legeza, Ö.; Fáth, G. Accuracy of the density-matrix renormalization-group method. *Phys. Rev. B: Condens. Matter Mater. Phys.* **1996**, *53*, 14349−14358.
(106) Legeza, Ö., Veis, L., Mosoni, T. *QC-DMRG-Budapest, a program for quantum chemical DMRG calculations*; HAS RISSPO: Budapest, 2018.
(107) Chan, G. K.-L.; Kállay, M.; Gauss, J. State-of-the-art density matrix renormalization group and coupled cluster theory studies of the nitrogen binding curve. *J. Chem. Phys.* **2004**, *121*, 6110−6116.
(108) Boguslawski, K.; Tecmer, P.; Barcza, G.; Legeza, Ö.; Reiher, M. Orbital Entanglement in Bond-Formation Processes. *J. Chem. Theory Comput.* **2013**, *9*, 2959−2973.
(109) Valiev, M.; Bylaska, E.; Govind, N.; Kowalski, K.; Straatsma, T.; Dam, H. V.; Wang, D.; Nieplocha, J.; Apra, E.; Windus, T.; de Jong, W. NWChem: A comprehensive and scalable open-source solution for large scale molecular simulations. *Comput. Phys. Commun.* **2010**, *181*, 1477−1489.
(110) Lee, T. J.; Taylor, P. R. A diagnostic for determining the quality of singlereference electron correlation methods. *Int. J. Quantum Chem.* **1989**, *36*, 199−207.
(111) Krumnow, C.; Veis, L.; Legeza, Ö.; Eisert, J. Fermionic orbital optimization in tensor network states. *Phys. Rev. Lett.* **2016**, *117*, 210402.

DOI: 10.1021/acs.jctc.8b00960
J. Chem. Theory Comput. 2019, 15, 2206−2220

The Journal of Chemical Physics ARTICLE scitation.org/journal/jcp

Toward the efficient local tailored coupled cluster approximation and the peculiar case of oxo-Mn(Salen)

Cite as: J. Chem. Phys. 151, 084112 (2019); doi: 10.1063/1.5110477
Submitted: 17 May 2019 • Accepted: 29 July 2019 •
Published Online: 30 August 2019

Andrej Antalík,[1,2] Libor Veis,[1] Jiří Brabec,[1] Ondřej Demel,[1] Örs Legeza,[3] and Jiří Pittner[1,a)]

AFFILIATIONS

[1]J. Heyrovský Institute of Physical Chemistry, Academy of Sciences of the Czech Republic, v.v.i., Dolejškova 3, 18223 Prague 8, Czech Republic
[2]Faculty of Mathematics and Physics, Charles University, Ke Karlovu 3, 12116 Prague 2, Czech Republic
[3]Strongly Correlated Systems "Lendület" Research Group, Wigner Research Centre for Physics, H-1525 Budapest, Hungary

[a)]**Electronic mail:** jiri.pittner@jh-inst.cas.cz

ABSTRACT

We introduce a new implementation of the coupled cluster method with single and double excitations tailored by the matrix product state wave functions (DMRG-TCCSD), which employs the local pair natural orbital (LPNO) approach. By exploiting locality in the coupled cluster stage of the calculation, we were able to remove some of the limitations that hindered the application of the canonical version of the method to larger systems and/or with larger basis sets. We assessed the accuracy of the approximation using two systems: tetramethyleneethane (TME) and oxo-Mn(Salen). Using the default cut-off parameters, we were able to recover over 99.7% and 99.8% of the canonical correlation energy for the triplet and singlet state of TME, respectively. In the case of oxo-Mn(Salen), we found that the amount of retrieved canonical correlation energy depends on the size of the complete active space (CAS)—we retrieved over 99.6% for the larger 27 orbital CAS and over 99.8% for the smaller 22 orbital CAS. The use of LPNO-TCCSD allowed us to perform these calculations up to quadruple-ζ basis set, amounting to 1178 basis functions. Moreover, we examined dependence of the ground state of oxo-Mn(Salen) on the CAS composition. We found that the inclusion of $4d_{xy}$ orbital plays an important role in stabilizing the singlet state at the DMRG-CASSCF level via double-shell effect. However, by including dynamic correlation, the ground state was found to be triplet regardless of the size of the basis set or the composition of CAS, which is in agreement with previous findings by canonical DMRG-TCCSD in smaller basis.

I. INTRODUCTION

Since its introduction to quantum chemistry,[1] the coupled cluster (CC) approach has become one of the most widely used methods for the accurate calculations of dynamic correlation. It offers numerous favorable properties, such as compact description of the wave function, size-extensivity, invariance to rotations within occupied or virtual orbital subspaces, and also a systematic hierarchy of approximations converging toward the full configuration interaction (FCI) limit.[2] For instance, the CCSD(T) method,[3] which includes connected single-, double-, and perturbative triple- excitations, is notoriously referred to as the gold standard of quantum chemistry.[2]

Although the CC method performs well for single reference molecules, it becomes fairly inaccurate or breaks down completely for systems with strongly correlated electrons. Such systems are multireference in nature since they include quasidegenerate frontier orbitals, which are common during dissociation processes, in diradicals, or compounds containing transition metals. Over the years, numerous efforts to generalize the CC ansatz and thus overcome this drawback gave rise to a broad family of multireference CC (MRCC) methods.[4–6]

One such approach, aiming to include static correlation in the CC scheme, is to employ a different methodlike complete active space self-consistent field (CASSCF) or multireference configuration interaction (MRCI) in order to extract the information about the most important excitations.[7–29] The retrieved information can be then introduced to a CC calculation as an external correction. One of such methods is tailored CC with single and double excitations (TCCSD) proposed by Kinoshita *et al.*,[14] which draws on the split-amplitude ansatz, in which the amplitudes corresponding to single and double excitations are split into two parts. The active part is treated by complete active space configuration interaction (CAS-CI), and external amplitudes are iterated using the standard CCSD framework. We recently extended this approach by using the density matrix renormalization group (DMRG) method to obtain the active space amplitudes.[30]

The DMRG method, which originated in solid-state physics,[31–33] is nowadays well established in quantum chemistry for the treatment of strongly correlated systems.[34–42] As a numerical approximation to full configuration interaction (FCI), it can handle significantly larger active spaces compared to the conventional method. However, even then, the prohibitive scaling does not allow us to include dynamic correlation, and it is therefore necessary to employ some "post-DMRG" procedure. Many different attempts have been made to tackle this limitation, for example, DMRG-CASPT2,[43] Cholesky decomposition DMRG-NEVPT2,[44] DMRG-icMRCI,[45] canonical transformation,[46] matrix product state (MPS) based formulation of multireference perturbation theory,[47] DMRG pair-density functional theory,[48] and also our aforementioned CC tailored by MPS wave functions (DMRG-TCCSD).[30]

Even though the DMRG-TCCSD method offers a reasonably efficient treatment of both static and dynamic correlation,[49–51] its applications to larger systems are hampered by the infavorable scaling of the CCSD part of the calculation. To remove this restriction, we decided to implement the method using a local approach. Out of many possibilities how to exploit locality,[52–58] we opted for pair natural orbitals (PNOs) based methods, in particular, the local pair natural orbital (LPNO) approach.[59–61]

The PNOs were introduced by Edmiston and Krauss and were shown to provide a compact parameterization of the virtual space.[62] Over the years, several correlation methods that made use of advantages of the approach offered were developed,[63–66] but the full potential of PNOs could have been unleashed only due to more recent advances in modern hardware and modern integral transformation technologies, particularly the density fitting or resolution of the identity methodology.[67] The approach was further extended to domain LPNO (DLPNO), with even more favorable scaling.[68] Apart from single-reference methods, the LPNO and DLPNO methodologies were also successfully applied to multireference CC techniques.[69–72]

In this paper, we contribute to these efforts by implementing the LPNO version of DMRG-TCCSD. We demonstrate the properties of the method on two systems which were previously studied with its canonical implementation.[30,49] First, we used tetramethyleneethane (TME) as a benchmark system to estimate the amount of correlation energy possible to retrieve by LPNO approach compared to the canonical version of the method. Then, we performed a similar test on oxo-Mn(Salen) in a double-ζ basis set and subsequently performed a calculation using up to a quadruple-ζ basis set, far beyond the capabilities of the canonical implementation. This way, we were able to investigate the effect of dynamic correlation in the basis sets of size previously unfeasible. Moreover, we explored the impact of active space composition on the spin state ordering of oxo-Mn(Salen) in order to shed light into previously varying claims about its ground state.

In the rest of this paper, we will use the acronym TCCSD(e, o) to denote a DMRG-TCCSD calculation, in which the active space of DMRG consists of e electrons in o orbitals. In the same manner, LPNO-TCCSD(e, o) denotes the calculation with the CC part performed employing the LPNO approach.

II. THEORY AND IMPLEMENTATION

A. DMRG-based tailored coupled clusters

The tailored coupled cluster method, which belongs to the class of externally corrected methods, employs the split-amplitude wave function ansazt proposed by Kinoshita *et al.*[14]

$$|\Psi_{\mathrm{TCC}}\rangle = e^{T}|\Phi_0\rangle = e^{T_{\mathrm{ext}}+T_{\mathrm{CAS}}}|\Phi_0\rangle = e^{T_{\mathrm{ext}}}e^{T_{\mathrm{CAS}}}|\Phi_0\rangle, \tag{1}$$

where the cluster operator T is split into two parts: T_{CAS} which contains the active amplitudes obtained from an external calculation and T_{ext} which contains the external amplitudes, with $|\Phi_0\rangle$ being the reference wave function.

In our implementation, we employed the DMRG method to obtain the active amplitudes. Using the DMRG algorithm, we first optimize the wave function, which is provided in matrix product state (MPS) form

$$|\Psi_{\mathrm{MPS}}\rangle = \sum_{\{\alpha\}} \mathbf{A}^{\alpha_1}\mathbf{A}^{\alpha_2}\cdots\mathbf{A}^{\alpha_k}|\alpha_1\alpha_2\cdots\alpha_k\rangle, \tag{2}$$

where $\alpha \in \{|-\rangle, |\downarrow\rangle, |\uparrow\rangle, |\downarrow\uparrow\rangle\}$ and $\mathbf{A}^{\alpha_i}$ are MPS matrices. These are then contracted to obtain CI coefficients for single and double excitations C.[73,74] Using the relations between CI and CC coefficients

$$T^{(1)}_{\mathrm{CAS}} = C^{(1)}, \tag{3}$$

$$T^{(2)}_{\mathrm{CAS}} = C^{(2)} - \frac{1}{2}[C^{(1)}]^2, \tag{4}$$

we are able to acquire their respective amplitudes, which are subsequently introduced into a CC calculation. At this point, these active amplitudes are kept frozen, while the remaining amplitudes T_{ext} are optimized by solving the equations

$$\langle\Phi^a_i|He^{T_{\mathrm{ext}}}e^{T_{\mathrm{CAS}}}|\Phi_0\rangle_c = 0 \quad \{i,a\} \not\subset \mathrm{CAS}, \tag{5}$$

$$\langle\Phi^{ab}_{ij}|He^{T_{\mathrm{ext}}}e^{T_{\mathrm{CAS}}}|\Phi_0\rangle_c = 0 \quad \{i,j,a,b\} \not\subset \mathrm{CAS}, \tag{6}$$

analogous to the standard CCSD equations. This way, the active amplitudes account for static correlation, and by optimizing the external amplitudes, we are able to recover the remaining dynamic correlation.

B. The LPNO approach for DMRG-TCCSD

The first step in LPNO methods is the localization of internal orbitals and subsequent transformation of virtual space to a PNO

basis. This process can be divided into three distinct steps. First, based on the MP2 calculation, pair energies and MP2 amplitudes are calculated. From these, pair density matrices are constructed for pairs of occupied orbitals and by their subsequent diagonalization PNOs are acquired.

Since approximations are made during this procedure, the accuracy of the method is controlled mainly by two cut-off parameters. The first, T_{CutPairs}, limits the number of occupied orbital pairs chosen for CCSD correlation treatment based on their respective pair energies. The remaining weak pairs are then treated solely at the MP2 level. The second, T_{CutPNOs}, determines the truncation of the PNO expansion for a given pair, based on the PNO occupation numbers.

In order to make the LPNO-TCCSD method function properly, we considered crucial to maintain the properties of the canonical TCCSD method as well as the behavior of the original LPNO-CCSD method. Just like the latter, it should maintain smooth dependence of retrieved canonical correlation energy with respect to a change in the cut-off parameters. Moreover, it is necessary to perform the PNO transformation in such a way that the active orbitals in the new basis exactly align with the orbitals in the original MO basis. Failing to do so would result in a mismatch between the orbitals and imported amplitudes. For the same reason, it is required for active orbitals to pass both T_{CutPairs} and T_{CutPNOs} screenings.

Because we implemented LPNO-TCCSD in the spin-unrestricted version of the LPNO-CCSD code, the following steps will be described in the respective formalism.[61] Also, for more compact notation, we will write ${}^{\sigma\sigma'}t_{ij}^{ab} = t_{i_\sigma j_{\sigma'}}^{a_\sigma b_{\sigma'}}$.

First, for each pair of occupied orbitals ij, we construct the MP2 amplitudes

$$ {}^{\alpha\alpha}t_{ij}^{ab} = -\frac{K_{ij}^{ab} - K_{ij}^{ba}}{f_{aa} + f_{bb} - f_{ii} - f_{jj}}, \tag{7} $$

$$ {}^{\alpha\beta}t_{ij}^{ab} = -\frac{K_{ij}^{ab}}{f_{aa} + f_{bb} - f_{ii} - f_{jj}}, \tag{8} $$

from exchange integrals K_{ij}^{ab} and orbital energies f_{pp}. The $\beta\beta$ case is constructed analogously as the $\alpha\alpha$ case. Subsequently, we replace the active amplitudes, for which $\{i, j, a, b\} \subset$ CAS, with the amplitudes imported from a DMRG calculation. At this point, the first cut-off parameter comes into play. For each pair, we calculate an MP2 pair energy, and if it is larger than T_{CutPairs}, the pair is kept for further correlation treatment. To ensure that none of the active amplitudes is discarded, we circumvent this screening for all active pairs and keep them automatically.

In the next step, the PNOs are generated. First, for given pair ij, a pair density matrix is built from the matrix $\mathbf{T}_{\sigma\sigma'}^{ij}$ containing the amplitudes ${}^{\sigma\sigma'}t_{ij}^{ab}$,

$$ \mathbf{D}_{\alpha\alpha}^{ij} = \frac{4(\mathbf{T}_{\alpha\alpha}^{ij})^\dagger \mathbf{T}_{\alpha\alpha}^{ij}}{1 + 2\mathrm{Tr}((\mathbf{T}_{\alpha\alpha}^{ij})^\dagger \mathbf{T}_{\alpha\alpha}^{ij})}, \tag{9} $$

$$ {}^{(\alpha)}\mathbf{D}_{\alpha\beta}^{ij} = \frac{2\mathbf{T}_{\alpha\beta}^{ij}(\mathbf{T}_{\alpha\beta}^{ij})^\dagger}{1 + \mathrm{Tr}(\mathbf{T}_{\alpha\beta}^{ij}(\mathbf{T}_{\alpha\beta}^{ij})^\dagger)}, \tag{10} $$

$$ {}^{(\beta)}\mathbf{D}_{\alpha\beta}^{ij} = \frac{2(\mathbf{T}_{\alpha\beta}^{ij})^\dagger \mathbf{T}_{\alpha\beta}^{ij}}{1 + \mathrm{Tr}((\mathbf{T}_{\alpha\beta}^{ij})^\dagger \mathbf{T}_{\alpha\beta}^{ij})}. \tag{11} $$

Since two sets of PNOs are needed for $\alpha\beta$ pairs, we use the superscripts (α) and (β) to distinguish between them. Once again, the $\beta\beta$ case is analogous to the $\alpha\alpha$ case.

For an inactive pair $\{i,j\} \not\subset$ CAS, we proceed directly to diagonalization of the pair matrix to solve

$$ \mathbf{D}^{ij}\mathbf{d}_a^{ij} = n_a^{ij}\mathbf{d}_a^{ij} \tag{12} $$

and obtain set of PNOs $\mathbf{d}_a^{ij}$ and their respective occupation numbers n_a^{ij}, where barred index refers to the PNO basis. This PNO expansion is then truncated based on the second cut-off parameter. Only PNOs with occupation numbers larger than T_{CutPNOs} are kept, and the remaining orbitals are discarded.

However, the process gets slightly more complicated for active pairs $\{i, j\} \subset$ CAS. To maintain the alignment between the original active orbitals in MO basis and the active orbitals in PNO basis, it is necessary to keep their coefficients untouched during the PNO transformation. We achieve this by setting the active-external elements of a pair density matrix to zero and replacing the active-active part with an identity matrix. In order to also preserve the correct order of the active orbitals, we add "infinitesimaly" small positive numbers ε_a to the active diagonal, for which holds that $\varepsilon_a > \varepsilon_{a+1}$. Thus, the resulting matrix has the block form (see Fig. 1)

$$ \widetilde{\mathbf{D}}^{ij} = \mathbf{D}_{\mathrm{CAS}}^{ij} \oplus \mathbf{D}_{\mathrm{ext}}^{ij}, \tag{13} $$

where

$$ \mathbf{D}_{\mathrm{CAS}}^{ij} = \mathrm{diag}(1+\varepsilon_1, \ldots, 1+\varepsilon_n), \tag{14} $$

$$ (D_{\mathrm{ext}}^{ij})_{ab} = D_{a+n,b+n}^{ij}. \tag{15} $$

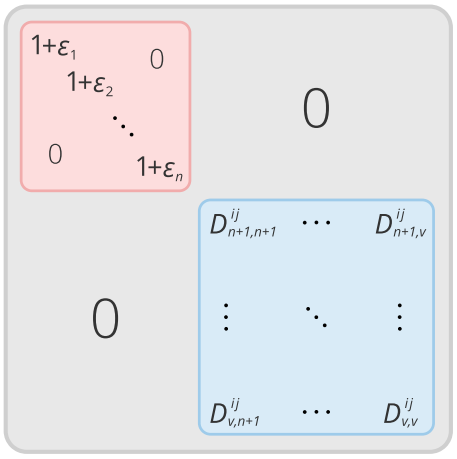

FIG. 1. A pair density matrix $\widetilde{\mathbf{D}}^{ij}$ for an active pair ij. The number of active virtual orbitals is denoted by n, total number of virtuals by v.

This way, we make sure that after solving (12), all active orbitals have the largest eigenvalues, which are in given order at the beginning, and therefore pass the T_{CutPNOs} screening.

The resulting equation for singly excited amplitudes remains formally the same as the equation for the canonical method (5). On the other hand, the equation for doubly excited amplitudes (6) now becomes

$$\langle \Phi_{ij}^{\tilde{a}\tilde{b}} | H e^{T_{\mathrm{ext}}^{(1)} + \tilde{T}_{\mathrm{ext}}^{(2)}} e^{T_{\mathrm{CAS}}} | \Phi_0 \rangle_c = 0 \quad \{i,j,a,b\} \not\subset \mathrm{CAS}, \tag{16}$$

with the active amplitudes formally in PNO basis.

III. COMPUTATIONAL DETAILS

The DMRG calculations were performed by the Budapest QC-DMRG code.[75] The LPNO-TCCSD method was implemented in ORCA program package,[76] which was also used to prepare the orbitals.

In case of TME, we used CASPT2(6,6)/cc-pVTZ geometries for seven values of the dihedral angle from our previous work.[49] The orbitals were prepared by CASSCF(6,6) calculation with the active space containing six $2p_z$ orbitals on carbon atoms.

In case of oxo-Mn(Salen), we used the singlet CASSCF(10,10)/6-31G* optimized geometry by Ivanic *et al.*[77] The orbitals were optimized using the DMRG-CASSCF method[78–80] in Dunning's cc-pVXZ X ∈ {D, T, Q} basis sets.[81–83] The optimization was carried out with fixed bond dimension $M = 1024$ for the smaller CAS(28,22) and $M = 2048$ for CAS(28,27). The composition of these active spaces is discussed further in Sec. IV. The orbitals were then split-localized using the Pipek-Mezey algorithm[84] in the following orbital subspaces: internal, active doubly occupied, active singly occupied, and active virtual.

The orbitals for DMRG were ordered using the Fiedler method[85,86] combined with some manual adjustments. All DMRG runs were initialized by CI-DEAS procedure.[41,87] We employed the dynamical block state selection (DBSS) procedure[36,88] to control the accuracy of the larger oxo-Mn(Salen) calculations with the truncation error criterion set to 10^{-6}. This resulted in block dimension varying between 1000 up to 2500 block states for CAS(28,22) and up to 8200 in case of CAS(28,27). The convergence threshold was set to energy difference between two subsequent sweeps smaller than 10^{-6} a.u.

The core electrons were kept frozen throughout all coupled cluster calculations. Auxiliary basis sets cc-pVQZ/C and cc-pV6Z/C were used for the resolution of the identity approximation for oxo-Mn(Salen) and TME, respectively.[89,90] The default LPNO cut-off parameters were set to $T_{\mathrm{CutPNO}} = 3.33 \times 10^{-7}$, $T_{\mathrm{CutPairs}} = 10^{-4}$, and $T_{\mathrm{CutMKN}} = 10^{-3}$, and these were used unless otherwise stated. The production runs of oxo-Mn(Salen) were performed with ORCA's TightPNO settings, i.e., the cut-off parameters set to $T_{\mathrm{CutPNO}} = 10^{-7}$, $T_{\mathrm{CutPairs}} = 10^{-5}$, and $T_{\mathrm{CutMKN}} = 10^{-4}$. For calculations which purpose was to estimate the dependence of LPNO-TCCSD energies on these parameters, one parameter was varied with remaining parameters fixed to the default value. We assess the amount of retrieved correlation energy by LPNO approach with reference to a DMRG-TCCSD energy calculated with the traditional TCCSD implementation.

IV. RESULTS AND DISCUSSION

A. Tetramethyleneethane

Although small, the tetramethyleneethane molecule is a challenging system due to its complex electronic structure. To correctly describe the character of its singlet state, one needs to employ a theory with a balanced description of both static and dynamic correlations combined with a reasonably large basis set. This is the reason why it often serves as a benchmark system for multireference methods.[49,69,91–94] Moreover, it was already a subject of our previous study with the canonical DMRG-TCCSD method,[49] so it only seems natural to use this system to test the performance of the LPNO approach to TCCSD. For this purpose, we investigate the behavior of the approximation with respect to different geometries corresponding to the rotation about its central C–C bond (see Fig. 2) and different values of the cut-off parameters.

We only present results for a small active space corresponding to six electrons in six 2p orbitals. This decision followed an effort to perform the performance evaluation on three active spaces of different sizes. However, because of the small localization subspaces stemming from a small number of occupied orbitals, many orbitals remained rather delocalized. This resulted in large numbers of PNOs necessary to maintain the accuracy, even for looser cut-off parameters, which ultimately rendered the LPNO approximation useless due to its low efficiency. Therefore, we compare the performance of LPNO-TCCSD with different sized active spaces on oxo-Mn(Salen), which is better suited for this purpose.

At this point, we investigate the amount of correlation energy retrieved by the LPNO-TCCSD method compared to the canonical TCCSD method.

Figure 3 shows the dependence of the retrieved correlation energy with respect to the cut-off parameter T_{CutPairs}, which controls the number of pairs treated by CCSD based on their estimated pair correlation energies. Both singlet and triplet states show the desired behavior and converge toward a certain value. For settings looser than the default value of 10^{-4}, the increasing number of pairs treated by MP2 results in overestimation of the correlation energy. As can be seen, for the triplet state, the method recovers consistently about

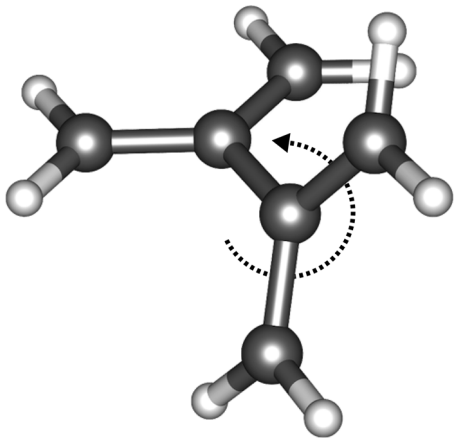

FIG. 2. Dihedral rotation of tetramethylenethane.

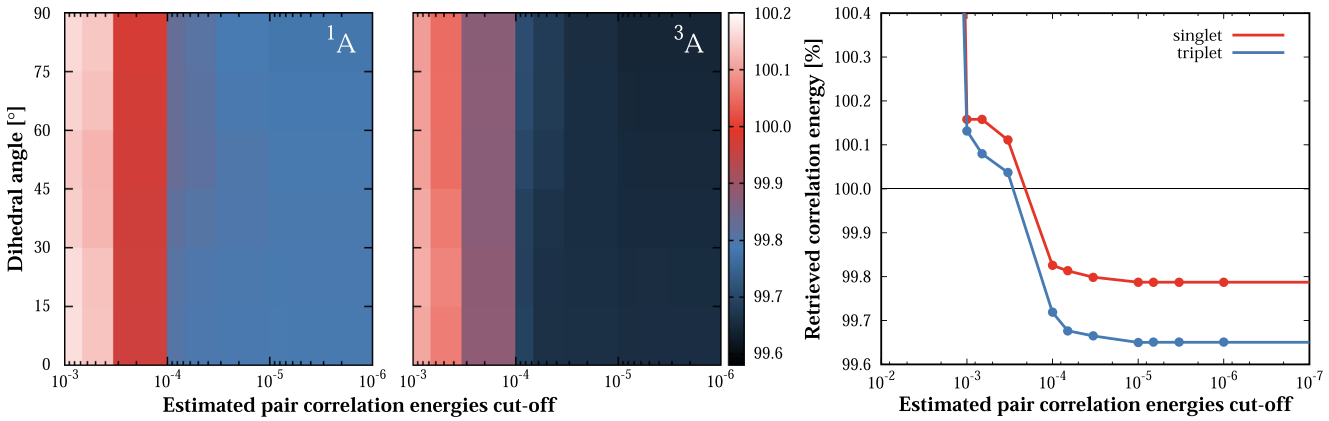

FIG. 3. The percentage of correlation energy of the canonical TCCSD(6,6) calculation recovered by LPNO-TCCSD(6,6) in cc-pVTZ basis with respect to cut-off for estimated pair correlation energies T_{CutPairs}. The color maps on the left show the results for seven studied geometries and ^{1}A and ^{3}A states; the plot on the right shows the results averaged over the geometries.

0.1% of correlation energy less than for the singlet state. This means that the energy difference between the two states is therefore off by about 0.7 kcal/mol compared to a canonical calculation. Regarding the consistency of the approximation across different geometries, the accuracy is mostly consistent, but slight discrepancies are visible around the default value of the cut-off parameter. However, the largest difference in energies at this value is less than 0.03% canonical correlation energies, which corresponds to an energy difference smaller than 0.2 kcal/mol. Note that these differences are relevant for singlet or triplet calculation alone.

Figure 4 shows the dependence on the second studied cut-off parameter T_{CutPNOs}. From 10^{-4}, the recovered energy grows gradually when tightening the parameter resulting in 99.83% and 99.72% of correlation energy recovered at the default value for the singlet and triplet states, respectively. Again, the difference between the geometries is less than 0.03% for each state alone. For the smallest values, the singlet calculation retrieves more than 100% of correlation energy, which is caused by using the default setting for T_{CutPairs}. This means that more pairs are treated only by perturbative correction which overshoots the contributions to correlation energy.

The observed difference in accuracy for these two cases then might arise from the neglect of some of the terms in the current LPNO implementation. However, this behavior should be eradicated in the future DLPNO implementation of the method.

B. oxo-Mn(Salen)

The oxo-Mn(Salen) molecule (Fig. 5) has been a subject of numerous computational studies motivated mainly by its role in catalysis of the enantioselective epoxidation of unfunctional olefins.[95,96] Moreover, its closely lying singlet and triplet states

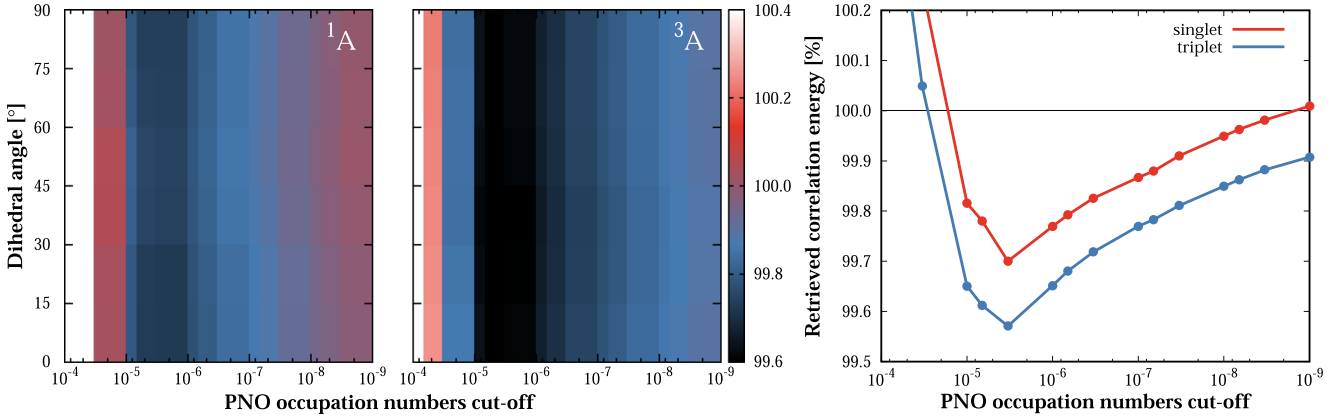

FIG. 4. The percentage of correlation energy of the canonical TCCSD(6,6) calculation recovered by LPNO-TCCSD(6,6) in cc-pVTZ basis with respect to cut-off for PNO occupation numbers T_{CutPNO}. The color maps on the left show the results for seven studied geometries and ^{1}A and ^{3}A states; the plot on the right shows the results averaged over the geometries.

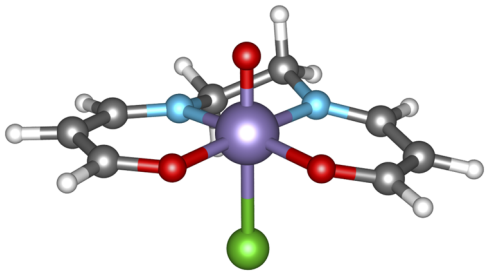

FIG. 5. A molecule of oxo-Mn(Salen).

pose a considerable challenge for multireference methods. Over the years, several multireference studies have been published,[77,97,98] some of which employed the DMRG method,[99–101] and recently, the first DMRG results with dynamic correlation treatment were presented.[30,102] Our aim was to contribute to these efforts by exploring the effect of the active space and basis set dependence on the character of the ground state. With our LPNO implementation, we were able to study the effect of dynamic correlation up to the quadruple-ζ basis set. This would not be possible without the LPNO approximation since the cc-pVQZ basis for this system amounts to 1178 basis functions.

In order to assess the accuracy of the LPNO-TCCSD method with respect to active spaces of different size and investigate the different ground states reported at the CASSCF level, we selected two active spaces. In accordance with the study by Wouters *et al.*,[99] the smaller CAS(28,22) consists of ten π orbitals on equatorial conjugated rings (C, N and O atoms), five 3d orbitals on Mn, three 2p orbitals on the axial O atom, and four 2p orbitals on equatorial N and O atoms forming σ bonds with the Mn atom. On top of these, we added extra five orbitals on Mn resulting in CAS(28,27), namely, $4d_{xy}$, $4d_{yz}$, and $4p_x$, $4p_y$, and 4s, which form σ^* bonds with Mn. The effect of inclusion of these particular orbitals is discussed further in the text. On top of that, we also tried to add 3p orbitals on Cl to the active space since these were included in some of the studies,[30,100] but based on the results of entanglement analysis (one-orbital entropies), we concluded that their effect was negligible.

First, we investigated the behavior of the LPNO approximation in the smallest cc-pVDZ basis. The dependence of recovered correlation energy for both spin states and active spaces with respect to LPNO cut-off parameters is shown in graphs in Fig. 6. When varying T_{CutPairs}, the curves for all four calculations converge smoothly. The singlet and triplet curves exhibit an excellent behavior, with the errors stemming from the approximation canceling out perfectly for both states. In case of the smaller CAS(28,22), this is valid even for less conservative values.

The amount of correlation energy with respect to T_{CutPNOs} parameter changes smoothly toward 100% with smaller values. With the default settings, we were able to recover over 99.85% correlation energy for the smaller and over 99.78% for the larger active space. The method overshoots for T_{CutPNOs} over 3.33×10^{-8} for the same reason as with TME, i.e., the fixed T_{CutPairs} parameter. Also the small consistent gap between singlet and triplet curves disappears with smaller cutoff for estimated pair correlation energies. As can be seen from Table I, although the absolute energies acquired with tighter cutoffs seem to be slightly worse, these settings noticeably improve the reproduction of the canonical singlet-triplet gap.

For this system, the treatment of different spin states is balanced due to more effective cancellation of errors compared to TME. However, a difference in accuracy arises between the larger and smaller CAS, with slightly better retrieval of correlation energy in the latter. Similarly to TME, this can be attributed to a neglect of certain terms in the LPNO implementation of the CC method.

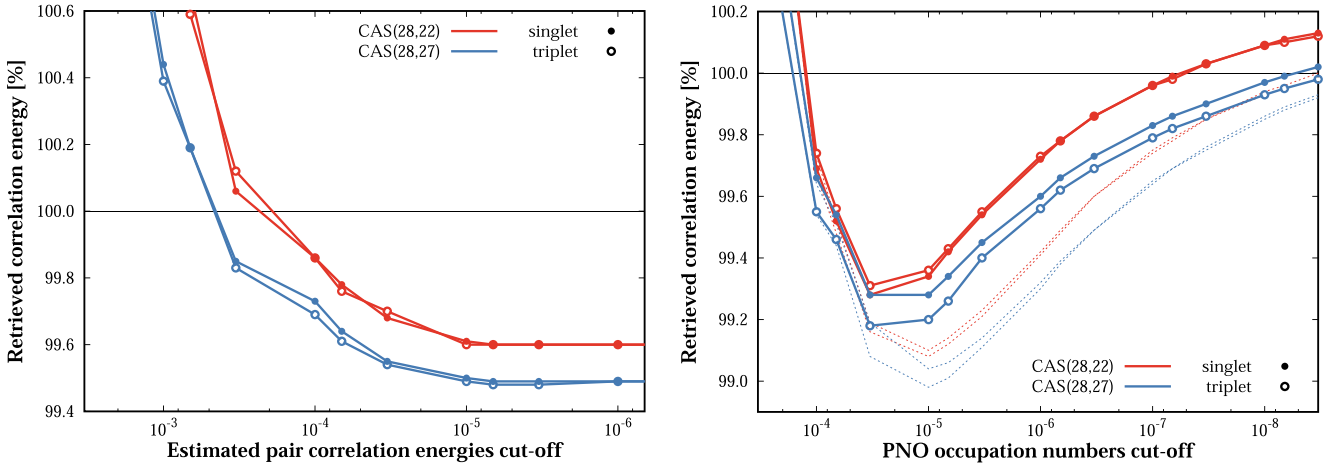

FIG. 6. The percentage of correlation energy of oxo-Mn(Salen) retrieved by LPNO-TCCSD in cc-pVDZ basis with respect to canonical TCCSD calculations as a function of cut-off for estimated pair correlation energies T_{CutPairs} (left) and cut-off for PNO occupation numbers T_{CutPNO} (right). The thin dashed lines in the right plot represent the values for $T_{\mathrm{CutPairs}} = 0$.

TABLE I. Energy differences in kcal/mol between LPNO-TCCSD calculations with different settings of cut-off parameters and equivalent canonical calculations on oxo-Mn(Salen) in cc-pVDZ.

	CAS(28,22)		CAS(28,27)	
	Default	TightPNO	Default	TightPNO
^{1}A	2.53	4.50	4.91	6.47
^{3}A	2.47	4.55	5.51	6.50
ΔE_{T-S}	−0.07	0.04	0.60	0.03

Since the method is based on the original LPNO-CCSD implementation in ORCA, we focused mostly on the accuracy assessment and did not perform an extensive study of time efficiency as the speed-up with respect to canonical method was expected to be very similar to the one achieved by the single-reference CCSD method. As a rough estimate on timing, the LPNO-TCCSD(28,27) calculation with default cutoffs was 20 times faster compared to the canonical calculation, and even with TightPNO settings, an order of magnitude speedup was achieved. The full DMRG procedure took significantly longer time also due to the SCF optimization steps.

After the accuracy assessment, we approached the actual system. The first step was to obtain the energies of Wouters *et al.*[99] with our smaller CAS(28,22) considering that this study reports on the composition of the active space in detail. We successfully reproduced their results establishing the triplet ground state, but since several later studies reported significantly lower energies of both states[101,102] with the CAS of the same size or smaller, we wanted to investigate this further.

Therefore, we included, on top of three orbitals forming the σ^* bonds, additional $4d_{xy}$, $4d_{yz}$ to examine how much the double-shell effect influences the stability of these states. With this active space, we obtained significantly lower energies (partially due to the larger number of variational parameters), and more importantly, the two states switched resulting in the singlet ground state. The energies can be found in Table II.

Based on the diagrams of mutual information plotted in Fig. 7, we assume that the orbitals responsible for considerable decrease in energy are mainly the antibonding σ^* and partially the $4d_{yz}$ orbitals. As expected, these are strongly correlated with the respective bonding orbitals. Since their effect is the same for both states of interest, the remaining $4d_{xy}$ has to cause the change in the ground state. This change can be then easily explained when we consider that in singlet state, the valence $3d_{xy}$ orbital is fully occupied and therefore the $4d_{xy}$ orbital stabilizes the singlet via the double-shell effect. This claim is supported by the fact that mutual information between the two orbitals is fairly large in case of the singlet state. Even though its value in the diagram is of an order of magnitude 10^{-2}, out of the remaining values of the same order, it is in fact one of the largest, namely, 0.086, while in case of the triplet state, its value is merely a fraction, i.e., 0.026. Moreover, this orbital was also present in the study by Stein and Reiher,[101] who obtained the singlet ground state as well, with very similar energy difference between the two states.

When dynamic correlation is added to the calculation by the LPNO-TCCSD method, a significant shift in energies occurs. Looking at the energies of the triplet state, we can observe that the extra orbitals in the larger CAS seem to contribute solely to the dynamic correlation at the CASSCF level since the LPNO-TCCSD energies are virtually the same for both active spaces. Singlet energies, on the other hand, differ depending on the active space, which can be attributed to the effect of aforementioned static correlation from

TABLE II. The singlet and triplet energies of oxo-Mn(Salen) E + 2251 in atomic units and the difference $\Delta E_{T-S} = E(^3A) - E(^1A)$ in kcal/mol. Results for different active spaces and in various basis sets.

	cc-pVDZ			cc-pVTZ			cc-pVQZ		
	^{1}A	^{3}A	ΔE_{T-S}	^{1}A	^{3}A	ΔE_{T-S}	^{1}A	^{3}A	ΔE_{T-S}
DMRG-CASSCF(28,22)[99]	−0.7509	−0.7593	−5.3						
DMRG-CASSCF(26,21)[101]	−0.7963	−0.7954	0.6						
DMRG-CASSCF(28,22)[102]	−0.7991	−0.8002	−0.7	−0.9957	−0.9926	1.9	−1.0449	−1.0418	1.9
DMRG-CASSCF(28,22)	−0.7502	−0.7582	−5.0	−0.9402	−0.9473	−4.5	−0.9891	−0.9961	−4.4
DMRG-CASSCF(28,27)	−0.8803	−0.8791	0.8	−1.0717	−1.0697	1.2	−1.1210	−1.1187	1.5
TCCSD(34,25)[30 a]	−2.7273	−2.7330	−3.6						
MRLCC(28,22)[102]	−3.2830	−3.2600	14.4	−4.1303	−4.1310	−0.5			
NEVPT2(28,22)[102]	−3.0109	−2.9990	7.4	−3.8437	−3.8463	−1.6	−4.1441	−4.1481	−2.4
DLPNO-CCSD[b]	−3.0476	−3.0714	−14.9	−3.8702	−3.8919	−13.6	−4.1479	−4.1700	−13.9
DLPNO-CCSD(T)[b]	−3.1986	−3.2071	−5.3	−4.0742	−4.0794	−3.3	−4.3672	−4.3735	−4.0
LPNO-TCCSD(28,22)	−3.1455	−3.1554	−6.2	−3.9698	−3.9798	−6.3	−4.2479	−4.2578	−6.3
LPNO-TCCSD(28,27)	−3.1491	−3.1550	−3.7	−3.9749	−3.9798	−3.1	−4.2531	−4.2578	−2.9

[a]These values were obtained with split-localized ROHF triplet orbitals.
[b]These calculations were performed with orbitals from the DMRG-CASSCF(28,27) calculation.

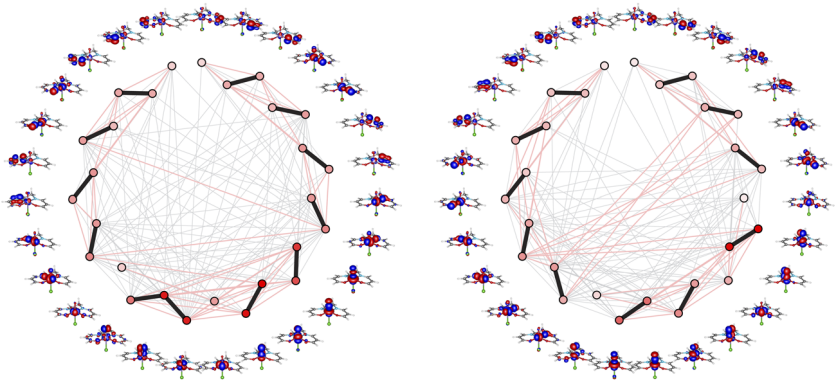

FIG. 7. Split-localized orbitals and their mutual information for ^{1}A (left) and ^{3}A (right) states of oxo-Mn(Salen) with the cc-pVDZ basis in CAS(28,27).[103] The mutual information is color-coded: the black lines correspond to the strongest correlations (10^{-1}), pink (10^{-2}), and gray (10^{-3}). One-site entropy values are represented by a color gradient of the respective dot, red being the largest value and white being zero.

the inclusion of $4d_{xy}$ orbital. Nonetheless, irrespective of the active space, we found the ground state to be a triplet with slightly larger singlet-triplet gap for the smaller CAS. This is in agreement with our previously published results,[30] in which we used canonical TCCSD, but only with orbitals coming from an ROHF calculation.

In addition, we carried out single-reference DLPNO-CCSD and DLPNO-CCSD(T) calculations. These were performed with DMRG-CASSCF(28,27) reference due to the inability to converge UHF calculation for the singlet state. The results show that the single-reference treatment of dynamical correlation favors the triplet ground state. Although the observed gap at the DLPNO-CCSD level is significantly larger than for multireference methods with the additional contributions of perturbative triples, we acquired very similar values to the DMRG-TCCSD(28,27) method.

Furthermore, all results remain consistent with larger basis sets. Going from DZ to QZ basis at the CASSCF level, the ground state of the particular CAS slightly stabilizes. Although no significant change occurs for the singlet-triplet gap by including dynamic correlation in the smaller CAS, the size of the gap decreases for larger CAS. This change roughly corresponds to what was observed at the CASSCF level.

Comparing these results to those published by Sharma *et al.*,[102] we conclude that employing larger basis set does not qualitatively affect the ground state. Since we have shown that the system is quite sensitive to composition of the active space and apart from DZ, their energies agree very reasonably with ours, we suppose there might have been some inconsistency in the active space for DMRG-CASSCF in the smallest studied basis set. Especially our best result LPNO-TCCSD(28,27) is in excellent agreement with the best available NEVPT2(28,22) in cc-pVQZ basis.

Regarding the future endeavors with this system, we would suggest a geometry reoptimization. Although the used geometry serves as a useful benchmark for the reason that it is frequently used by several different groups, since the introduction of dynamic correlation, the optimization at CASSCF(10,10)/6-31G* appears to be fairly inadequate.

V. CONCLUSIONS

We introduced a new version of the DMRG-TCCSD method, which employs the local pair natural orbital approach. The method has been implemented in ORCA presently at the singles and doubles level.

We performed accuracy assessment of the method employing two systems, which were previously studied by the canonical TCCSD method. Regarding tetramethyleneethane, we were able to retrieve over 99.7% for the triplet state and over 99.8% for the singlet state, while using the default settings of cut-off parameters. For oxo-Mn(Salen), the amount of retrieved correlation was dependent on the size of the active space used, ranging from 99.6% for the larger CAS(28,27) to 99.8% for smaller CAS(28,22). Despite this dependence, an excellent agreement was achieved concerning the accuracy between the spin states. Using the default settings resulted in singlet-triplet gap being off by 0.6 kcal/mol and with tighter cut-offs only 0.04 kcal/mol compared to the canonical calculation.

Furthermore, we investigated the previously unexplored problem of varying reports of different ground states of oxo-Mn(Salen) at the CASSCF level. We discovered that this inconsistency most likely originates from the composition of CAS. In particular, we found that the orbital responsible for stabilizing the singlet state is the $4d_{xy}$ orbital via the double-shell effect. However, by employing the dynamic correlation treatment with LPNO-TCCSD, regardless of the basis set, the ground state was unambiguously found to be a triplet.

Regarding the future of the method, we plan to implement the DLPNO version of the TCCSD, which we hope to further enhance capabilities of the method and also include the perturbative triples correction for even more accurate results.

SUPPLEMENTARY MATERIAL

See the supplementary material for additional information on oxo-Mn(Salen)—the split-localized DMRG-CASSCF(28,27) orbitals used for LPNO-TCCSD calculations and the retrieval of correlation energy as the function of both T_{CutPairs} and T_{CutPNO} parameters.

ACKNOWLEDGMENTS

We would like to thank Professor Frank Neese for providing us with access to the ORCA source code, as well as for helpful

discussions, and Dr. Frank Wennmohs for technical assistance with the ORCA code.

This work has been supported by the Czech Science Foundation (Grant Nos. 16-12052S and 18-18940Y), the Czech Ministry of Education, Youth and Sports (Project No. LTAUSA17033), Charles University (Project GA UK No. 376217), the Hungarian National Research, Development and Innovation Office (NKFIH) (Grant Nos. K120569 and KH125597), the Hungarian Quantum Technology National Excellence Program (Project No. 2017-1.2.1-NKP-2017-00001), and the Ministry of Education, Youth and Sports from the Large Infrastructures for Research, Experimental Development and Innovations project IT4Innovations National Supercomputing Center—Grant No. LM2015070. Ö.L. also acknowledges financial support from the Alexander von Humboldt foundation.

REFERENCES

[1] J. Čížek, J. Chem. Phys. **45**, 4256 (1966).
[2] J. Gauss, in *The Encyclopedia of Computational Chemistry*, edited by P. v. R. Schleyer, N. L. Allinger, T. Clark, J. Gasteiger, P. A. Kollman, H. F. Schaefer III, and P. R. Scheiner (Wiley, Chichester, 1998), pp. 615–636.
[3] K. Raghavachari, G. W. Trucks, J. A. Pople, and M. Head-Gordon, Chem. Phys. Lett. **157**, 479 (1989).
[4] R. J. Bartlett and M. Musial, Rev. Mod. Phys. **79**, 291 (2007).
[5] D. P. Tew, C. Hättig, R. A. Bachorz, and W. Klopper, in *Recent Progress in Coupled Cluster Methods*, edited by P. Čársky, J. Paldus, and J. Pittner (Springer Science, New York, 2010), p. 535.
[6] D. I. Lyakh, M. Musial, V. F. Lotrich, and R. J. Bartlett, Chem. Rev. **112**, 182–243 (2012).
[7] X. Li and J. Paldus, J. Chem. Phys. **107**, 6257 (1997).
[8] X. Li and J. Paldus, J. Mol. Struct.: THEOCHEM **547**, 69–81 (2001).
[9] X. Li and J. Paldus, J. Chem. Phys. **115**, 5759–5773 (2001).
[10] X. Li and J. Paldus, J. Chem. Phys. **115**, 5774–5783 (2001).
[11] J. Paldus and J. Planelles, Theor. Chim. Acta **89**, 13 (1994).
[12] P. Piecuch, R. Tobola, and J. Paldus, Phys. Rev. A **54**, 1210 (1996).
[13] X. Li, G. Peris, J. Planelles, F. Rajadell, and J. Paldus, J. Chem. Phys. **107**, 90 (1997).
[14] T. Kinoshita, O. Hino, and R. J. Bartlett, J. Chem. Phys. **123**, 074106 (2005).
[15] D. I. Lyakh, V. F. Lotrich, and R. Bartlett, J. Chem. Phys. Lett. **501**, 166–171 (2011).
[16] A. Melnichuk and R. J. Bartlett, J. Chem. Phys. **137**, 214103 (2012).
[17] A. Melnichuk and R. J. Bartlett, J. Chem. Phys. **140**, 064113 (2014).
[18] P. Piecuch, N. Oliphant, and L. Adamowicz, J. Chem. Phys. **99**, 1875–1900 (1993).
[19] P. Piecuch and L. Adamowicz, J. Chem. Phys. **100**, 5792–5809 (1994).
[20] L. Adamovicz, P. Piecuch, and K. B. Ghose, Mol. Phys. **94**, 225–234 (1998).
[21] P. Piecuch, Mol. Phys. **108**, 2987–3015 (2010).
[22] P. Piecuch, K. Kowalski, I. S. O. Pimienta, and M. J. Mcguire, Int. Rev. Phys. Chem. **21**, 527–655 (2002).
[23] P. Piecuch, K. Kowalski, and I. Pimienta, Int. J. Mol. Sci. **3**, 475–497 (2002).
[24] K. Kowalski and P. Piecuch, J. Chem. Phys. **116**, 7411–7423 (2002).
[25] M. W. Łoch, M. D. Lodriguito, P. Piecuch†, and J. R. Gour, Mol. Phys. **104**, 2149–2172 (2006).
[26] M. D. Lodriguito, K. Kowalski, M. Włoch, and P. Piecuch, J. Mol. Struct.: THEOCHEM **771**, 89–104 (2006).
[27] P. Piecuch, K. Kowalski, I. S. O. Pimienta, P.-D. Fan, M. Lodriguito, M. J. McGuire, S. A. Kucharski, T. Kuś, and M. Musiał, Theor. Chem. Acc. **112**, 349–393 (2004).
[28] K. Kowalski and P. Piecuch, J. Chem. Phys. **115**, 2966–2978 (2001).
[29] K. Kowalski and P. Piecuch, J. Chem. Phys. **113**, 18–35 (2000).
[30] L. Veis, A. Antalik, J. Brabec, F. Neese, O. Legeza, and J. Pittner, J. Phys. Chem. Lett. **7**, 4072 (2016).
[31] S. R. White and R. M. Noack, Phys. Rev. Lett. **68**, 3487–3490 (1992).
[32] S. R. White, Phys. Rev. Lett. **69**, 2863–2866 (1992).
[33] S. R. White, Phys. Rev. B **48**, 10345–10356 (1993).
[34] S. R. White and R. L. Martin, J. Chem. Phys. **110**, 4127–4130 (1999).
[35] G. K.-L. Chan and M. Head-Gordon, J. Chem. Phys. **116**, 4462–4476 (2002).
[36] Ö. Legeza, J. Röder, and B. A. Hess, Phys. Rev. B **67**, 125114 (2003).
[37] Ö. Legeza, R. Noack, J. Sólyom, and L. Tincani, in *Computational Many-Particle Physics*, Lecture Notes in Physics Vol. 739, edited by H. Fehske, R. Schneider, and A. Weisse (Springer Berlin Heidelberg, 2008), pp. 653–664.
[38] K. H. Marti and M. Reiher, Z. Phys. Chem. **224**, 583–599 (2010).
[39] G. K.-L. Chan and S. Sharma, Annu. Rev. Phys. Chem. **62**, 465–481 (2011).
[40] S. Wouters and D. Van Neck, Eur. Phys. J. D **68**, 272 (2014).
[41] S. Szalay, M. Pfeffer, V. Murg, G. Barcza, F. Verstraete, R. Schneider, and Ö. Legeza, Int. J. Quantum Chem. **115**, 1342 (2015).
[42] T. Yanai, Y. Kurashige, W. Mizukami, J. Chalupský, T. N. Lan, and M. Saitow, Int. J. Quantum Chem. **115**, 283–299 (2014).
[43] Y. Kurashige and T. Yanai, J. Chem. Phys. **135**, 094104 (2011).
[44] L. Freitag, S. Knecht, C. Angeli, and M. Reiher, J. Chem. Theory Comput. **13**, 451–459 (2017).
[45] M. Saitow, Y. Kurashige, and T. Yanai, J. Chem. Phys. **139**, 044118 (2013).
[46] E. Neuscamman, T. Yanai, and G. K.-L. Chan, Int. Rev. Phys. Chem. **29**, 231–271 (2010).
[47] S. Sharma and G. Chan, J. Chem. Phys. **141**, 111101 (2014).
[48] P. Sharma, V. Bernales, S. Knecht, D. G. Truhlar, and L. Gagliardi, Chem. Sci. **10**, 1716–1723 (2019).
[49] L. Veis, A. Antalik, O. Legeza, A. Alavi, and J. Pittner, J. Chem. Theory Comput. **14**, 2439 (2018).
[50] F. M. Faulstich, A. Laestadius, S. Kvaal, Ö. Legeza, and R. Schneider, e-print arXiv:1802.05699 (2018).
[51] F. M. Faulstich, M. Máté, A. Laestadius, M. A. Csirik, L. Veis, A. Antalik, J. Brabec, R. Schneider, J. Pittner, S. Kvaal, and Ö. Legeza, J. Chem. Theory Comput. **15**, 2206–2220 (2019).
[52] N. Flocke and R. J. Bartlett, J. Chem. Phys. **121**, 10935 (2004).
[53] D. G. Fedorov and K. Kitaura, J. Chem. Phys. **123**, 134103 (2005).
[54] M. Kobayashi and H. Nakai, J. Chem. Phys. **129**, 044103 (2008).
[55] G. E. Scuseria and P. Y. Ayala, J. Chem. Phys. **111**, 8330–8343 (1999).
[56] S. Li, J. Ma, and Y. Jiang, J. Comput. Chem. **23**, 237–244 (2001).
[57] H. Stoll, Chem. Phys. Lett. **191**, 548–552 (1992).
[58] K. Kristensen, M. Ziółkowski, B. Jansík, T. Kjærgaard, and P. Jørgensen, J. Chem. Theory Comput. **7**, 1677–1694 (2011).
[59] F. Neese, A. Hansen, and D. G. Liakos, J. Chem. Phys. **131**, 064103 (2009).
[60] W. Li, P. Piecuch, J. R. Gour, and S. Li, J. Chem. Phys. **131**, 114109 (2009).
[61] A. Hansen, D. G. Liakos, and F. Neese, J. Chem. Phys. **135**, 214102 (2011).
[62] C. Edmiston and M. Krauss, J. Chem. Phys. **42**, 1119–1120 (1965).
[63] W. Meyer, Int. J. Quantum Chem. **5**, 341–348 (1971).
[64] W. Meyer, Theor. Chem. Acc. **35**, 277–292 (1974).
[65] P. R. Taylor, J. Chem. Phys. **74**, 1256–1270 (1981).
[66] R. Fink and V. Staemmler, Theor. Chem. Acc. **87**, 129–145 (1993).
[67] O. Vahtras, J. Almlöf, and M. Feyereisen, Chem. Phys. Lett. **213**, 514–518 (1993).
[68] C. Riplinger and F. Neese, J. Chem. Phys. **138**, 034106 (2013).
[69] O. Demel, J. Pittner, and F. Neese, J. Chem. Theory Comput. **11**, 3104–3114 (2015).
[70] J. Lang, M. Švaňa, O. Demel, J. Brabec, S. Kedžuch, J. Noga, K. Kowalski, and J. Pittner, Mol. Phys. **115**, 2743–2754 (2017).
[71] J. Brabec, J. Lang, M. Saitow, J. Pittner, F. Neese, and O. Demel, J. Chem. Theory Comput. **14**, 1370–1382 (2018).
[72] J. Lang, J. Brabec, M. Saitow, J. Pittner, F. Neese, and O. Demel, Phys. Chem. Chem. Phys. **21**, 5022–5038 (2019).
[73] G. Moritz and M. Reiher, J. Chem. Phys. **126**, 244109 (2007).

[74]K. Boguslawski, K. H. Marti, and M. Reiher, J. Chem. Phys. **134**, 224101 (2011).
[75]Ö. Legeza, L. Veis, and T. Mosoni, "QC-DMRG-Budapest, a program for quantum chemical DMRG calculations" (unpublished).
[76]F. Neese, Wiley Interdiscip. Rev.: Comput. Mol. Sci. **2**, 73–78 (2012).
[77]J. Ivanic, J. R. Collins, and S. K. J. Burt, J. Phys. Chem. A **108**, 2314–2323 (2004).
[78]D. Ghosh, J. Hachmann, T. Yanai, and G. K.-L. Chan, J. Chem. Phys. **128**, 144117 (2008).
[79]D. Zgid and M. Nooijen, J. Chem. Phys. **128**, 144116 (2008).
[80]T. Yanai, Y. Kurashige, D. Ghosh, and G. K.-L. Chan, Int. J. Quantum Chem. **109**, 2178–2190 (2009).
[81]T. H. Dunning, Jr., J. Chem. Phys. **90**, 1007–1023 (1989).
[82]D. Woon and T. H. Dunning, J. Chem. Phys. **98**, 1358 (1993).
[83]N. Balabanov and K. Peterson, J. Chem. Phys. **123**, 064107 (2005).
[84]J. Pipek and M. G. Mezey, J. Chem. Phys. **90**, 4916 (1989).
[85]G. Barcza, Ö. Legeza, K. H. Marti, and M. Reiher, Phys. Rev. A **83**, 012508 (2011).
[86]E. Fertitta, B. Paulus, G. Barcza, and Ö. Legeza, Phys. Rev. B **90**, 245129 (2014).
[87]Ö. Legeza and J. Sólyom, Phys. Rev. B **68**, 195116 (2003).
[88]Ö. Legeza and L. Sólyom, Phys. Rev. B **70**, 205118 (2004).
[89]F. Weigend, A. Kohn, and C. Hattig, J. Chem. Phys. **116**, 3175 (2002).
[90]D. H. Bross, J. G. Hill, H. J. Werner, and K. A. Peterson, J. Chem. Phys. **139**, 094302 (2013).
[91]J. Pittner, P. Nachtigall, P. Čársky, and I. Hubač, J. Phys. Chem. A **105**, 1354–1356 (2001).
[92]K. Bhaskaran-Nair, O. Demel, J. Šmydke, and J. Pittner, J. Chem. Phys. **134**, 154106 (2011).
[93]S. Chattopadhyay, R. K. Chaudhuri, and U. S. Mahapatra, ChemPhysChem **12**, 2791–2797 (2011).
[94]Z. D. Pozun, X. Su, and K. D. Jordan, J. Am. Chem. Soc. **135**, 13862–13869 (2013).
[95]W. Zhang, J. L. Loebach, S. R. Wilson, and E. N. Jacobsen, J. Am. Chem. Soc. **112**, 2801 (1990).
[96]R. Irie, K. Noda, Y. Ito, N. Matsumoto, and T. Katsuki, Tetrahedron Lett. **31**, 7345 (1990).
[97]J. S. Sears and C. D. Sherrill, J. Chem. Phys. **124**, 144314 (2006).
[98]D. Ma, G. Li Manni, and L. Gagliardi, J. Chem. Phys. **135**, 044128 (2011).
[99]S. Wouters, T. Bogaerts, P. Van Der Voort, V. Van Speybroeck, and D. Van Neck, J. Chem. Phys. **140**, 241103 (2014).
[100]R. Olivares-Amaya, W. Hu, N. Nakatani, and S. Sharma, J. Chem. Phys. **142**, 034102 (2015).
[101]C. J. Stein and M. Reiher, J. Chem. Theory Comput. **12**, 1760 (2016).
[102]S. Sharma, G. Knizia, S. Guo, and A. Alavi, J. Chem. Theory Comput. **13**, 488 (2017).
[103]J. Chalupský, Charmol - program for molecular graphics.

JCTC Journal of Chemical Theory and Computation

pubs.acs.org/JCTC Article

Near-Linear Scaling in DMRG-Based Tailored Coupled Clusters: An Implementation of DLPNO-TCCSD and DLPNO-TCCSD(T)

Jakub Lang, Andrej Antalík, Libor Veis, Jan Brandejs, Jiří Brabec, Örs Legeza, and Jiří Pittner*

Cite This: J. Chem. Theory Comput. 2020, 16, 3028−3040 Read Online

ACCESS | Metrics & More | Article Recommendations

ABSTRACT: We present a new implementation of density matrix renormalization group based tailored coupled clusters method (TCCSD), which employs the domain-based local pair natural orbital approach (DLPNO). Compared to the previous local pair natural orbital (LPNO) version of the method, the new implementation is more accurate, offers more favorable scaling, and provides more consistent behavior across the variety of systems. On top of the singles and doubles, we include the perturbative triples correction (T), which is able to retrieve even more dynamic correlation. The methods were tested on three systems: tetramethyleneethane, oxo-Mn(Salen), and iron(II)−porphyrin model. The first two were revisited to assess the performance with respect to LPNO-TCCSD. For oxo-Mn(Salen), we retrieved between 99.8 and 99.9% of the total canonical correlation energy which is an improvement of 0.2% over the LPNO version in less than 63% of the total LPNO runtime. Similar results were obtained for iron(II)−porphyrin. When the perturbative triples correction was employed, irrespective of the active space size or system, the obtained energy differences between two spin states were within the chemical accuracy of 1 kcal/mol using the default DLPNO settings.

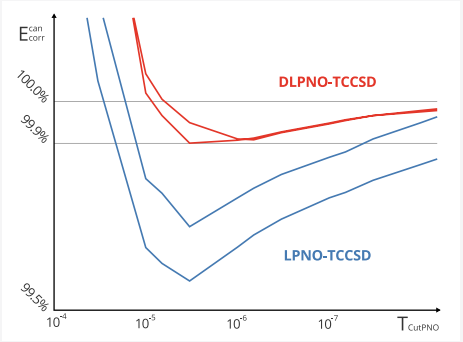

1. INTRODUCTION

Since its introduction to quantum chemistry,[1] the coupled cluster (CC) approach has become one of the most widely used methods for accurate calculations of dynamic correlation. It offers numerous favorable properties, such as compact description of the wave function, size-extensivity, invariance to rotations within occupied or virtual orbital subspaces, and also a systematic hierarchy of approximations converging toward the full configuration interaction (FCI) limit.[2] For instance, the CCSD(T) method,[3] which includes connected single, double, and perturbative triple excitations, is notoriously referred to as the gold standard of quantum chemistry.[2]

Although the CC method performs well for single reference molecules, it becomes fairly inaccurate or breaks down completely for systems with strongly correlated electrons. Such systems are multireference in nature since they include quasi-degenerate frontier orbitals. This situation is common during dissociation processes, in diradicals, or in compounds containing transition metals. Over the years, numerous efforts to generalize the CC ansatz and thus overcome this drawback gave rise to a broad family of multireference CC methods (MRCC).[4−6]

A possible approach for including static correlation in the CC scheme is to employ a different method such as complete active space self-consistent field (CASSCF) or multireference configuration interaction (MRCI) in order to extract the information about the most important excitations.[7−29] The retrieved information can then be introduced to a CC calculation as an external correction. One such method is tailored CC with single and double excitations (TCCSD) proposed by Kinoshita et al.,[14] which draws on the split-amplitude ansatz by Piecuch et al.,[18] in which the cluster operator corresponding to single and double excitations is split into two parts. The active part is imported from a complete active space configuration interaction (CAS-CI) and kept fixed, while the external amplitudes are iterated using the standard CCSD framework. We recently extended this approach by using the density matrix renormalization group (DMRG) method to obtain the active space amplitudes.[30,31] Related externally corrected CC approaches employ fixed T_3 and T_4 amplitudes obtained from MRCI[32] or from stochastic CI[33] and iterate all singles and doubles in their presence. Compared to TCC, this has the advantage that the active space T_1 and T_2 can reflect the dynamic correlation outside of the active space, but one pays the price of a much larger number of the T_3 and T_4 amplitudes involved.

Received: January 20, 2020
Published: April 10, 2020

https://dx.doi.org/10.1021/acs.jctc.0c00065
J. Chem. Theory Comput. 2020, 16, 3028−3040

The DMRG method, which originated in solid-state physics,[34−36] is nowadays well established in quantum chemistry for the treatment of strongly correlated systems.[37−45] As a numerical approximation to FCI, it can handle significantly larger active spaces compared to the conventional methods. However, even then the prohibitive scaling does not allow one to include dynamic correlation and it is therefore necessary to employ some "post-DMRG" procedure. Many different attempts have been made to tackle this limitation for example with the complete active space perturbation theory (CASPT2),[46] Cholesky decomposition n-electron valence state perturbation theory (NEVPT2),[47] MRCI using cumulant reconstruction with internal contraction of DMRG wave function,[48] canonical transformation,[49] matrix product state (MPS) based formulation of multireference perturbation theory,[50] DMRG pair-density functional theory,[51] and also our aforementioned CC tailored by MPS wave functions (DMRG-TCCSD).[30,52,53]

Even though the DMRG-TCCSD method offers a reasonably efficient treatment of both static and dynamic correlation,[54] its application to larger systems is hampered by the unfavorable scaling of the CCSD part of the calculation. With such a steep scaling, even massive parallelization is not sufficient to make the method applicable to molecules with hundreds of atoms. To overcome this issue, Pulay proposed to exploit the locality of the electron correlation.[55,56] Due to its short-range character for non-metallic systems, it is possible to take advantage of sparsity of the Hamiltonian matrix by employing the basis of localized orbitals.

Although the occupied orbital space can be easily localized using a variety of appropriate methods,[57−59] for the virtual space things get slightly more complicated. In their first works on locality, Pulay and Sæbø used projected atomic orbitals (PAOs),[60,61] which were also used by Werner and Schütz in the local CC method.[62−66] In this approach, each localized occupied orbital is assigned a domain of PAOs obtained by projecting out the occupied orbital components from atomic orbitals. The pairs of occupied orbitals are subsequently classified according to their real space distance and treated at either coupled cluster level (strong pairs), perturbative level (weak and distant pairs), or neglected altogether (very distant pairs).

Another idea how to make use of locality is based on the concept of dividing a large system into smaller segments and performing the calculations on each of these subsystems separately. Among such approaches belong the divide−expand−consolidate method,[67,68] the divide-and-conquer method,[69] the incremental method,[70] the local natural orbital method,[71] and the fragment molecular orbital method.[72] The closely related cluster-in-molecule method[73] is based on energy decomposition into contributions corresponding to individual occupied orbitals.

Possibly the most effective way of virtual space truncation is, however, the use of pair natural orbitals (PNOs), which are known to provide compact parametrization of the virtual space. They were first used in the 1960s by Edmiston and Kraus[74] and later by Meyer,[75−79] Ahlrichs and co-workers.[80,81] For many years, the progress in the area of PNO-based methods stalled, until their revival in 2009, when the new local pair natural orbital (LPNO) variants of CEPA and CCSD methods were introduced by Neese et al.[82−85] The cornerstone of this approach, the idea to use PNOs in combination with localized occupied orbitals, was later developed into the more advanced domain-based local pair natural orbital (DLPNO) methods.[86−89]

In these, PNOs were expressed as a linear combination of PAOs in a pair domain, which ultimately removed the bottleneck of previous PNO methods and achieved genuine linear scaling. For instance, the resulting DLPNO-CCSD method is applicable to systems with hundreds of atoms and thousands of basis functions, which renders the prior SCF calculation possibly computationally more demanding than the actual correlation treatment.

Moreover, the PNO-based approaches possess many desirable properties, which allow them to be used in a black box fashion. They provide a very compact description of the virtual space, which makes it computationally feasible to use sufficiently large domains of PAOs, something that would be too costly for a purely PAO-based approach. They use a limited number of cutoff parameters, which do not involve any real space distance and the calculated correlation energy smoothly depends on the values of these parameters.

Currently, PNO-based methods are developed in a number of groups including those of Werner[90−93] and Hättig[94−96] and are widely employed in the context of various systems of chemical interest.[97−106] Apart from single-reference methods, the methodology was also successfully applied to multireference CC techniques.[107−110]

In this article, we build upon the previous investigation of our LPNO-TCCSD method[111] and introduce the newly implemented DLPNO-TCCSD and DLPNO-TCCSD(T) methods. On the basis of our experience, we revisit the molecule of tetramethyleneethane (TME) and address the drawbacks of the former method. The performance of the new approximation is then assessed using two benchmark systems, namely, oxo-Mn(Salen) and a model of iron(II)−porphyrins (FeP).

2. THEORY AND IMPLEMENTATION

2.1. DMRG-Based Tailored Coupled Clusters. The tailored coupled cluster method,[14] which belongs to the class of externally corrected methods, employs the split-amplitude wave function ansatz proposed by Piecuch et al.[18]

$$|\Psi_{\mathrm{TCC}}\rangle = \mathrm{e}^{T}|\Phi_0\rangle = \mathrm{e}^{T_{\mathrm{ext}}+T_{\mathrm{CAS}}}|\Phi_0\rangle = \mathrm{e}^{T_{\mathrm{ext}}}\mathrm{e}^{T_{\mathrm{CAS}}}|\Phi_0\rangle \tag{1}$$

where $|\Phi_0\rangle$ is the reference wave function and the cluster operator T is split into two parts: T_{CAS} which contains the active amplitudes obtained from an external calculation and T_{ext} which contains the external amplitudes, i.e., the amplitudes with at least one index outside the CAS space. Another way to justify this ansatz is the formulation of CC equations on the basis of excitation subalgebras recently introduced by Kowalski.[112,113]

In our implementation, we employed the DMRG method to obtain the active amplitudes. Using the DMRG algorithm, we first optimize the wave function, which is provided in the MPS form

$$|\Psi_{\mathrm{MPS}}\rangle = \sum_{\{\alpha\}} \mathbf{A}^{\alpha_1}\mathbf{A}^{\alpha_2}\ldots\mathbf{A}^{\alpha_k}|\alpha_1\alpha_2\ldots\alpha_k\rangle \tag{2}$$

where $\alpha \in \{|-\rangle, |\downarrow\rangle, |\uparrow\rangle, |\downarrow\uparrow\rangle\}$ and $\mathbf{A}^{\alpha_i}$ are MPS matrices. These are then contracted to obtain CI coefficients for single and double excitations C.[114,115] Using the intermediate normalization and the relations between CI and CC coefficients

https://dx.doi.org/10.1021/acs.jctc.0c00065
J. Chem. Theory Comput. 2020, 16, 3028−3040

$$T_{\mathrm{CAS}}^{(1)} = C^{(1)} \tag{3}$$

$$T_{\mathrm{CAS}}^{(2)} = C^{(2)} - \frac{1}{2}[C^{(1)}]^2 \tag{4}$$

we are able to acquire the respective CC amplitudes, which are subsequently introduced into the CC calculation. At this point, these active amplitudes are kept frozen, while the remaining amplitudes in T_{ext} are optimized by solving the equations

$$\langle \Phi_i^a | H \mathrm{e}^{T_{\mathrm{ext}}} \mathrm{e}^{T_{\mathrm{CAS}}} | \Phi_0 \rangle_c = 0 \qquad \{i, a\} \not\subseteq \mathrm{CAS} \tag{5}$$

$$\langle \Phi_{ij}^{ab} | H \mathrm{e}^{T_{\mathrm{ext}}} \mathrm{e}^{T_{\mathrm{CAS}}} | \Phi_0 \rangle_c = 0 \qquad \{i, j, a, b\} \not\subseteq \mathrm{CAS} \tag{6}$$

analogously to the standard CCSD equations. This way, the active amplitudes account for static correlation, and by optimizing the external amplitudes, we are able to recover the remaining dynamic correlation. The effect of dynamic correlation on T_{CAS} is neglected, which is an approximation inherent in the TCC method.

Due to the two-body Hamiltonian, TCC recovers the DMRG energy for $T_{\mathrm{ext}} = 0$. In the limit of CAS including all orbitals, FCI energy is recovered, although the TCC energy does not behave monotonously when extending the CAS space.[53] Nevertheless, in practice the optimal CAS size related to the energy minimum can be determined with low cost DMRG calculations.[53] In addition, a quadratic error bound valid for DMRG-TCC methods is also derived.[53]

On top of the TCCSD routine, the perturbative triples correction can be applied.[15] However, in order to prevent the double counting of static correlation, it is necessary to omit the terms that include the active amplitudes. This can be straightforwardly achieved by setting all active single and double amplitudes to zero during the calculation of the (T) correction.

2.2. Domain Local Pair Natural Orbital Approximation for TCCSD. The presented method is based on the open-shell DLPNO-CCSD code as implemented in ORCA.[116] In this section, we briefly outline DLPNO-CCSD and describe the modifications that were made to accommodate the tailored version of the method.

As in all PNO-based local methods, the whole process starts with the localization of the occupied orbitals. On the basis of our previous experience,[111] we opt for the split-localization scheme, where the orbitals are separately localized within four distinct orbital subspaces: doubly occupied external, doubly occupied active, singly occupied active, and active virtual. Such choice has been shown to provide a set of orbitals which yield a reasonable convergence behavior of the DMRG procedure,[117] without influencing the DMRG energy.

The next step is the construction of orbital domains. Using the idea of Werner et al.,[118,119] we first construct PAOs

$$|\tilde{\mu}\rangle = \left(1 - \sum_i |i\rangle\right)|\mu\rangle \tag{7}$$

by projecting out the localized occupied and active orbitals $|i\rangle$ from the original set of atomic orbitals $|\mu\rangle$. The acquired orbitals are subsequently normalized, and the orbital domains are constructed on the basis of the differential overlap integrals

$$(\mathrm{DOI})_{i\mu} = \sqrt{\int_{\mathbb{R}^3} |\phi_i|^2 |\phi_{\tilde{\mu}}|^2 \, \mathrm{d}^3 r} \tag{8}$$

between PAOs and the set of occupied and active orbitals. Here, the first prescreening parameter comes into play—for a given occupied orbital i, only PAOs for which $(\mathrm{DOI})_{i\mu} > T_{\mathrm{CutDO}}$ are included within its domain. Also, if an atom contains at least one PAO, all PAOs belonging to this atom are considered for further domain construction.

At this point, the main difference of the TCC approach compared to the conventional DLPNO-CCSD is that all active indices including the active virtuals are formally treated as singly occupied. Moreover, in the following dipole prescreening, it is ensured that every active occupied pair (i.e., a pair with both active indices) automatically survives the dipole prescreening.

After the prescreenings, unrestricted MP2 pair energies $\varepsilon_{ij}^{\mathrm{PAO}}$ are calculated and used to categorize occupied orbital pairs ij into three classes, on the basis of the preset cutoff parameters. Specifically, the active pairs and the pairs with energies larger than T_{CutPairs} are classified as strong, while the rest is either weak or neglected according to a related parameter. The whole process is executed in two consecutive steps. First, a crude screening is performed in smaller domains using loose thresholds, followed by the second screening in which the strong and weak pairs are again distributed between the three categories, but this time with finer thresholds. The strong pairs are then passed to the next stage, while the remaining pair energies are stored as a correction to the final energy

$$\Delta E_{\mathrm{CutPairs}} = \sum_{ij}^{\mathrm{weak}} \varepsilon_{ij}^{\mathrm{PAO}} + \sum_{ip}^{\mathrm{weak}} \varepsilon_{ip}^{\mathrm{PAO}} + \sum_{pq}^{\mathrm{weak}} \varepsilon_{pq}^{\mathrm{PAO}} \tag{9}$$

where i, j are indices of doubly and p, q of singly occupied orbitals. If the perturbative triples correction is invoked, the final weak pairs with energies higher than $0.01 T_{\mathrm{CutPairs}}$ are also saved for later use.

Afterward, using the nonredundant PAOs, the NEVPT2 pair densities, $\mathbf{D}^{ij}$, are constructed for the surviving pairs which do not contain any explicit information about the tailored CAS space. These are diagonalized to obtain PNO expansions $\mathbf{d}^{ij}$, which are then truncated on the basis of the cutoff parameter T_{CutPNO}. Only PNOs with occupation numbers larger than its value are kept, and the remaining orbitals are discarded. The final PAO/PNO transformation matrix for a given pair is then obtained by enlarging the former transformation matrix by a unit matrix

$$\mathbf{S}^{ij} = \mathbf{I}_{N_{\mathrm{CAS}}} \oplus \mathbf{d}^{ij} \tag{10}$$

where N_{CAS} is the number of active SOMOs and virtual orbitals; see Figure 1. While this artificially increases the final number of PNOs, it barely increases the computational time. Singles PNOs are obtained in the same manner from the densities which are computed as

$$\mathbf{D}^{pp} = \mathbf{t}_{pp}^{(1)\dagger} \mathbf{t}_{pp}^{(1)} \tag{11}$$

where the amplitudes are

$$\mathbf{t}_{pp}^{(1)} = \sum_{\tilde{\mu}_{pp}\tilde{\nu}_{pp}} \frac{\langle p\tilde{\mu}_{pp} \| p\tilde{\nu}_{pp} \rangle}{2f_{pp} - \varepsilon_{\tilde{\mu}_{pp}} - \varepsilon_{\tilde{\nu}_{pp}}} \tag{12}$$

where f_{pp} are diagonal Fock matrix elements. Furthermore, the pair energies are recalculated in the new truncated PNO basis, and the differences between them and the original MP2 estimates in the PAO basis

https://dx.doi.org/10.1021/acs.jctc.0c00065
J. Chem. Theory Comput. 2020, 16, 3028−3040

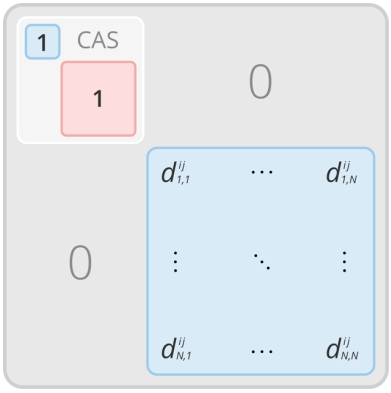

Figure 1. An illustration of the PAO/PNO transformation matrix for an active pair ij in DLPNO-TCC. The original transformation matrix $\mathbf{d}^{ij}$, with N being the number of PNOs, is enlarged by an identity matrix of size N_{CAS}, which is formally composed of two blocks corresponding to singly occupied (blue) and virtual orbitals (red) included in the active space.

$$\Delta E_{\mathrm{CutPNO}} = \sum_{ij}^{\mathrm{strong}} (\varepsilon_{ij}^{\mathrm{PAO}} - \varepsilon_{ij}^{\mathrm{PNO}}) + \sum_{ip}^{\mathrm{strong}} (\varepsilon_{ip}^{\mathrm{PAO}} - \varepsilon_{ip}^{\mathrm{PNO}}) + \sum_{pq}^{\mathrm{strong}} (\varepsilon_{pq}^{\mathrm{PAO}} - \varepsilon_{pq}^{\mathrm{PNO}}) \tag{13}$$

are stored as a correction to the final energy.

The resulting equations for singly excited amplitudes (eq 5) now become

$$\langle \Phi_i^{\bar{a}} | H \mathrm{e}^{\bar{T}_{\mathrm{ext}}^{(1)} + \bar{T}_{\mathrm{ext}}^{(2)}} \mathrm{e}^{T_{\mathrm{CAS}}} | \Phi_0 \rangle_c = 0 \qquad \{i, a\} \not\subseteq \mathrm{CAS} \tag{14}$$

where the barred index $\bar{a}$ indicates PNO basis. Similarly, the equations for doubly excited amplitudes (eq 6) become

$$\langle \Phi_{ij}^{\bar{a}\bar{b}} | H \mathrm{e}^{\bar{T}_{\mathrm{ext}}^{(1)} + \bar{T}_{\mathrm{ext}}^{(2)}} \mathrm{e}^{T_{\mathrm{CAS}}} | \Phi_0 \rangle_c = 0 \qquad \{i, j, a, b\} \not\subseteq \mathrm{CAS} \tag{15}$$

Once these equations are solved, the stored corrections (eqs 9 and 13) are added to the acquired energy. Except the fact that the active amplitudes are "frozen" during the CCSD iterations, these equations are identical to single-reference DLPNO-CCSD as implemented in ORCA.[89]

2.3. Perturbative Triples Correction to DLPNO-TCCSD.

To calculate the triples correction using the DLPNO approach,[120,121] it is first necessary to identify relevant compact parametrization of virtual space for every triple ijk. Domains for these triples are created as a union of i, j, and k domains, and the ij, jk, and ik pair densities are created within these triples domains.

Next, the triples densities are constructed by averaging over the respective pair densities

$$\mathbf{D}^{ijk} = \frac{1}{3}(\mathbf{D}^{ij} + \mathbf{D}^{jk} + \mathbf{D}^{ik}) \tag{16}$$

where the triple ijk is composed either of three strong pairs or of two strong and a weak pair, as it has been previously shown that using only the strong pairs is insufficient.[120] Since the amplitudes for weak pairs are not known prior to the triples calculation, the approximate MP2 amplitudes are used. The process then continues analogously to the construction of PNOs in CCSD.

Once the densities are constructed, they are diagonalized in order to obtain the triple natural orbitals (TNOs) and their corresponding natural occupation numbers. The TNO expansion is then truncated on the basis of the occupation numbers and the cutoff parameter T_{CutTNO}, and from the orbitals that passed the screening a transformation matrix is formed. This matrix is enlarged by a unit matrix of dimension N_{CAS}, and its final form is used to transform the integrals and amplitudes and subsequently to calculate the energy correction. As in the canonical version of the method, all active single and double amplitudes are set to zero during the calculation of the correction to prevent double-counting.

3. COMPUTATIONAL DETAILS

The DMRG calculations were performed by the Budapest QC-DMRG code.[122] The DLPNO-TCCSD and DLPNO-TCCSD-(T) methods were implemented in the ORCA program package,[116] which was also used to prepare the orbitals.

Prior to DMRG calculations, we split-localized the orbitals by the Pipek−Mezey method[58] in the following orbital subspaces: internal, active doubly occupied, active singly occupied, and active virtual. Orbital ordering was subsequently optimized using the Fiedler method[123,124] combined with minor manual adjustments. All DMRG runs were initialized by the CI-DEAS procedure[44,125] and employed the dynamical block state selection (DBSS) procedure[39,126] to control the accuracy of the calculation, with the truncation error criterion set to 10^{-6}. The convergence threshold was set to energy difference between two subsequent sweeps smaller than 10^{-6} a.u.

The core electrons were kept frozen throughout all coupled cluster calculations. The default set of DLPNO cutoff parameters $T_{\mathrm{CutPNO}} = 3.33 \times 10^{-7}$, $T_{\mathrm{CutPairs}} = 10^{-4}$, $T_{\mathrm{CutMKN}} = 10^{-3}$, and $T_{\mathrm{CutDO}} = 10^{-2}$ was employed unless otherwise stated. The other settings, referred to as TightPNO, were used for production runs: $T_{\mathrm{CutPNO}} = 10^{-7}$, $T_{\mathrm{CutPairs}} = 10^{-5}$, $T_{\mathrm{CutMKN}} = 10^{-3}$, and $T_{\mathrm{CutDO}} = 5.0 \times 10^{-3}$. For perturbative triples the default value of relevant cutoff parameter is $T_{\mathrm{CutTNO}} = 10^{-9}$ for both sets of settings. To estimate the dependence of DLPNO-TCCSD energies on these parameters, one parameter was varied with the remaining parameters fixed to the default value. We assess the amount of retrieved correlation energy by DLPNO approach with reference to the DMRG-TCCSD energy calculated with the canonical TCCSD implementation.

For TME, we used CASPT2(6,6)/cc-pVTZ geometries for seven values of the dihedral angle from our previous work.[54] The orbitals were prepared by CASSCF(6,6) calculation with the active space containing six $2p_z$ orbitals on carbon atoms. The cc-pV6Z/C auxiliary basis set was used for the resolution of the identity (RI) approximation.[127]

For oxo-Mn(Salen), we used the singlet CASSCF(10,10)/6-31G* optimized geometry by Ivanic et al.[128] The orbitals were optimized using the DMRG-CASSCF method[129−131] in Dunning's cc-pVXZ, X ∈ {D,T,Q}, basis sets.[132−134] The optimization was carried out with fixed bond dimension M = 1024 for the smaller CAS(28,22) and M = 2048 for CAS(28,27). The composition of these active spaces is discussed further in detail in the previous work.[111] The cc-pVQZ/C auxiliary basis set was used for RI.[135]

Finally, the calculations on FeP were performed at the triplet geometry from the previous study of Li Manni and Alavi,[136] with CASSCF/def2-SVP orbitals, for three distinct active spaces, which were selected on the basis of the entanglement analysis. For the largest CAS DMRG-CASSCF was applied, with the fixed

https://dx.doi.org/10.1021/acs.jctc.0c00065
J. Chem. Theory Comput. 2020, 16, 3028−3040

bond dimension $M = 1024$. The def2-SVP and def2-TZVP basis sets[137] were used with the def2-TZVPP/C auxiliary basis set[138] for RI.

4. RESULTS AND DISCUSSION

4.1. Tetramethyleneethane. Although small, the tetramethyleneethane molecule is a challenging system due to its complex electronic structure. To correctly describe the character of its singlet state, one needs to employ a theory with a balanced description of both static and dynamic correlation combined with a reasonably large basis set. This is the reason why it often serves as a benchmark system for multireference methods.[54,107,139−142] We previously studied the system with the canonical DMRG-TCCSD method,[54] as well as with its LPNO version.[111] In the latter, we encountered an issue with different accuracy for singlet and triplet states, which we attributed to the neglect of some terms in the LPNO-CCSD implementation in ORCA. For this reason, we revisit the system to investigate the improvement by the new DLPNO method, which should offer more robust approximation.

We performed calculations in seven different geometries corresponding to the rotation about the central C−C bond of the molecule (see Figure 2a) and different values of the cutoff parameters. These benchmarks were performed only for T_{CutPairs} and T_{CutPNO} parameters, since T_{CutDO} does not affect the results, unless an extremely small value is chosen. This behavior corresponds with the observations from previous studies.[89,109,110]

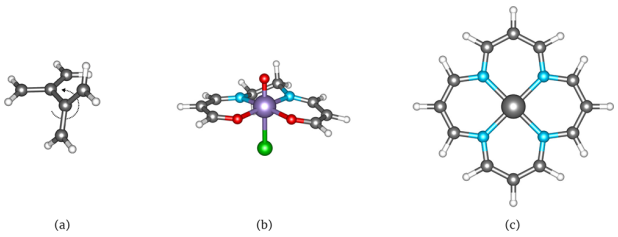

Figure 2. Dihedral rotation of tetramethyleneethane (a), a molecule of oxo-Mn(Salen) (b), and the model of iron(II)-porphyrin (c). Color key: iron (gray, large), manganese (violet), chlorine (green), oxygen (red), nitrogen (blue), carbon (gray, small), and hydrogen (white).

The left plot in Figure 3 shows the dependence of retrieved canonical correlation energy with respect to estimated pair correlation energies cutoff T_{CutPairs} averaged over the geometries. Both methods converge in a similar fashion, but DLPNO-TCCSD recovers 0.1−0.3% more correlation energy than LPNO-TCCSD. The right plot in the same figure shows the dependence on the second cutoff parameter, that is, PNO occupation number T_{CutPNO}, which is again averaged over the geometries. Here, DLPNO-TCCSD shows noticeably faster convergence to the canonical value compared to LPNO-TCCSD, with more accurate correlation energies even for higher values of the parameter. For instance, when the default values are used, DLPNO-TCCSD extracts over 99.91% of the canonical correlation energy.

One can notice the aforementioned discrepancy in accuracy for the LPNO-TCCSD method, which can be explained by the neglected terms in the UHF-LPNO formalism. DLPNO-TCCSD does not exhibit this behavior and describes both spin states equally well. This means that the difference of the recovered correlation energy is less than 0.01% compared to LPNO-TCCSD, for which this percentage is an order of magnitude worse.

Figure 4 shows the dependence of nonparallelity error (NPE) on T_{CutPNO} for both LPNO and DLPNO versions of TCCSD. It

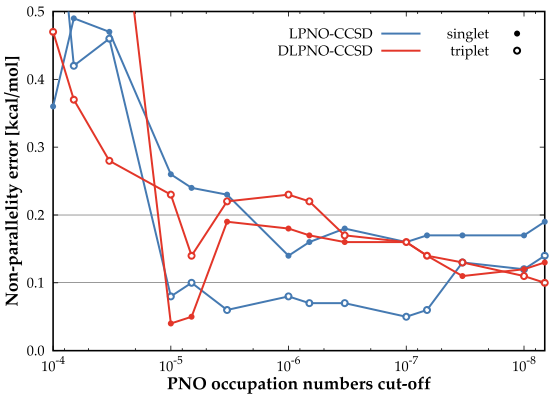

Figure 4. Nonparallelity error for TME in cc-pVTZ as a function of cutoff for PNO occupation numbers T_{CutPNO}.

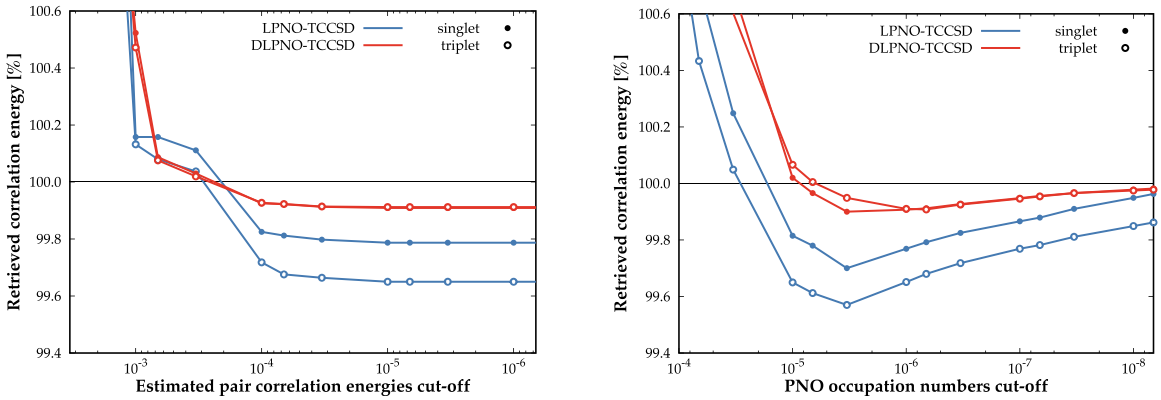

Figure 3. Percentage of correlation energy of TME in cc-pVTZ basis retrieved by LPNO-TCCSD and DLPNO-TCCSD with respect to canonical TCCSD calculations as a function of cutoff for estimated pair correlation energies T_{CutPairs} (left) and PNO occupation numbers T_{CutPNO} (right). The plotted values are averages over the set of all geometries.

https://dx.doi.org/10.1021/acs.jctc.0c00065
J. Chem. Theory Comput. 2020, 16, 3028−3040

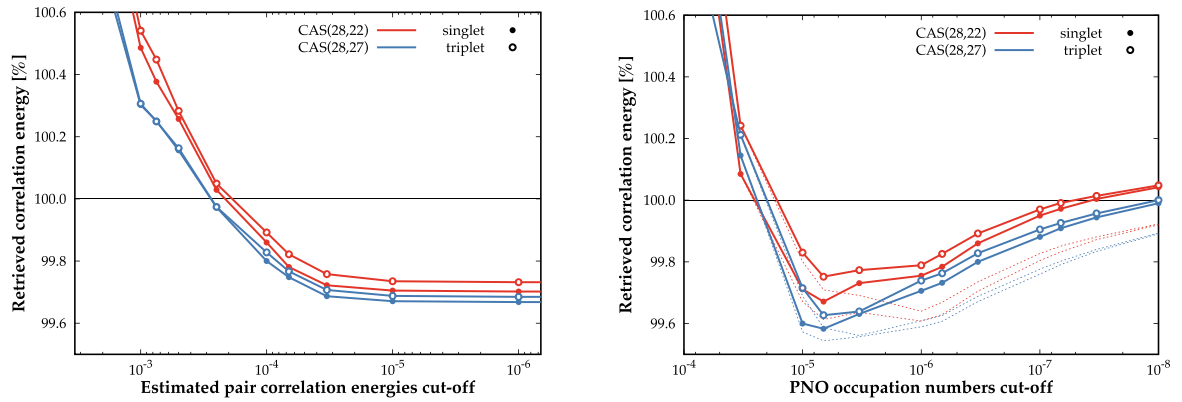

Figure 5. Percentage of correlation energy of oxo-Mn(Salen) in cc-pVDZ basis retrieved by DLPNO-TCCSD with respect to canonical TCCSD calculations as a function of cutoff for estimated pair correlation energies T_{CutPairs} (left) and cutoff for PNO occupation numbers T_{CutPNO} (right). The thin dashed lines in the right plot represent the values for $T_{\mathrm{CutPairs}} = 10^{-5}$.

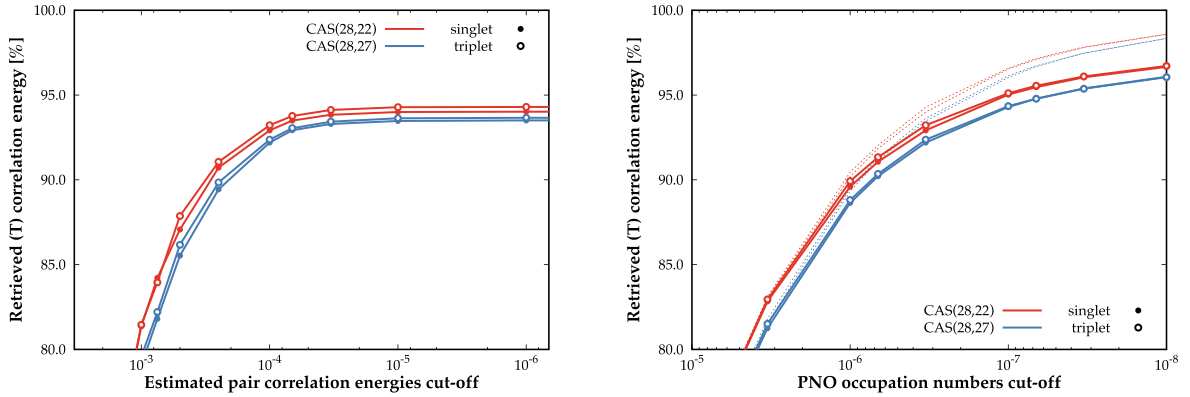

Figure 6. Percentage of perturbative triples correction correlation energy of oxo-Mn(Salen) in cc-pVDZ basis retrieved by DLPNO-TCCSD(T) with respect to canonical TCCSD(T) calculations as a function of cutoff for estimated pair correlation energies T_{CutPairs} (left) and cutoff for PNO occupation numbers T_{CutPNO} (right). The thin dashed lines in the right plot represent the values for $T_{\mathrm{CutPairs}} = 10^{-5}$.

can be seen that the NPE is no larger than 0.17 kcal/mol for either spin state, with very similar value for TightPNO settings, as well as for the LPNO version.

From the chemical point of view, the most interesting property is the behavior of the singlet−triplet gap with respect to the cutoff parameters. It can be observed from the presented data that this property is well described at the default and even looser settings, which means that it can be calculated by DLPNO-TCCSD with virtually no loss in accuracy.

4.2. oxo-Mn(Salen). The oxo-Mn(Salen) molecule (Figure 2b) has been a subject of numerous computational studies motivated mainly by its role in catalysis of the enantioselective epoxidation of unfunctional olefins.[143,144] Due to its closely lying singlet and triplet states it is also considered to be a challenging system even for multireference methods. Over the years, many multireference studies have been published,[128,145,146] some of which employed the DMRG method[117,147,148] and DMRG results with dynamic correlation treatment were presented as well.[30,111,149] This includes our previous studies, in which we used the system as a benchmark for the predecessors of the current method, namely, DMRG-TCCSD and its LPNO version.

Again, we first assessed the percentage of the recovered canonical TCCSD correlation energy with respect to the cutoff parameter T_{CutPairs}. The curve shown in the left plot of Figure 5 follows the same trend as that for TME and quickly converges. This means that the retrieved correlation energy is already converged by the value $T_{\mathrm{CutPairs}} = 10^{-5}$. Even though the correlation energy is not yet stable for the default value 10^{-4}, the difference in accuracy between two spin states is minimal. Since we are interested in the width of the singlet−triplet gap, it appears that even this setting provides quite reasonable accuracy.

The right plot of Figure 5 shows the dependence on the cutoff parameter T_{CutPNO}. These curves smoothly approach 100% as the parameter tightens, the behavior as observed for conventional DLPNO-CCSD. However, the energies overshoot for the very conservative values of the parameter, which is caused by overcompensation of the neglected pairs with the MP2 pair energy. For this reason, we calculated the same dependence also with the tighter setting of $T_{\mathrm{CutPairs}} = 10^{-5}$ (the thinner dotted lines in the plot). Since for this value the correlation energies are basically converged with respect to T_{CutPairs}, we can observe that the curves now smoothly converge toward 100%. The singlet−triplet gap seems reasonably accurate for the default value of T_{CutPNO} and for more conservative values the difference in accuracy completely disappears.

We also examined the effect of these cutoffs on the perturbative triples correction recovered by DLPNO-TCCSD-(T), which are shown in Figure 6. At the default value of T_{CutPairs}

https://dx.doi.org/10.1021/acs.jctc.0c00065
J. Chem. Theory Comput. 2020, 16, 3028−3040

the energies seem to be almost converged and are fully converged at the TightPNO setting; the actually relevant relative accuracy does not change. In the case of T_{CutPNO}, the curves seem to slowly converge toward 100%, which is even more apparent when tighter cutoff on pair energies is in place. Note that these values represent only the percentage of the canonical triples correction, not the total correlation energy, and for this particular system, the triples correction amounts to less than 3% of the total correlation energy. On top of that, we investigated the sensitivity of overall correlation energy on the T_{CutTNO} with the conclusion that the default value is more than adequate; see Figure 7.

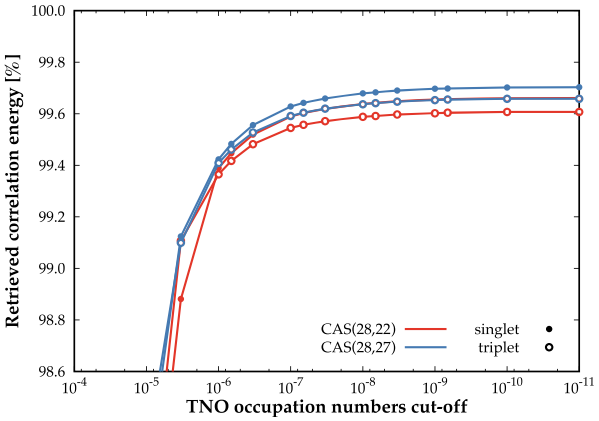

Figure 7. Percentage of correlation energy of oxo-Mn(Salen) in cc-pVDZ basis retrieved by DLPNO-TCCSD(T) with respect to canonical TCCSD(T) calculations as a function of cutoff for TNO occupation numbers T_{CutTNO}.

Table 1 contains the differences between DLPNO and canonical energies for the singlet−triplet gap. Although the errors in energies for singlet or triplet state alone are substantial (especially for the larger CAS), the errors for the gap are well within the chemical accuracy of 1 kcal/mol. When the perturbative triples correction is invoked, tighter cutoffs are preferable. The same can be observed in Figure 8, where the chemical accuracy is achieved even with looser than default settings. Also the behavior of the DLPNO approximation seems quite stable with respect to the size of the active space.

Table 1. Energy Differences (kcal/mol) between DLPNO-TCCSD and DLPNO−CCSD(T) Calculations with Different Settings of Cutoff Parameters and Equivalent Canonical Calculations on oxo-Mn(Salen) in cc-pVDZ

		CAS(28,22)		CAS(28,27)	
		default	TightPNO	default	TightPNO
SD	S	2.52	3.45	3.60	4.30
	T	1.92	3.01	3.06	3.97
	ΔE_{S-T}	0.60	0.44	0.54	0.33
SD(T)	S	6.38	5.30	7.33	6.19
	T	5.54	4.79	6.67	5.80
	ΔE_{S-T}	0.84	0.51	0.66	0.39

When we compare these results to the previous LPNO-CCSD calculations,[111] DLPNO-TCCSD has smaller error in absolute energies, but larger in gaps. This can be attributed to the rather fortunate cancellation of errors in the LPNO case, but otherwise the DLPNO implementation is more reliable due to smaller errors in absolute energies and smooth convergence toward the canonical correlation energies.

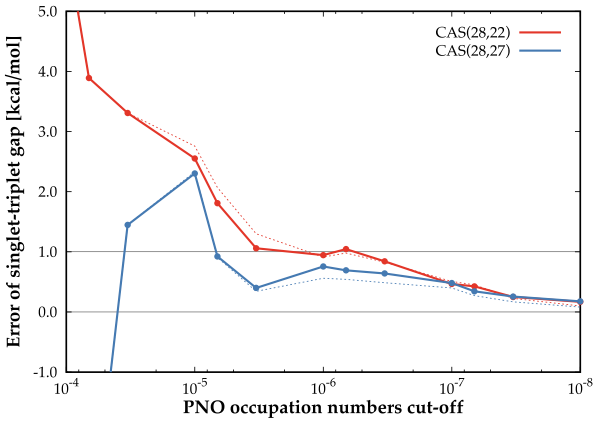

Figure 8. Error of DLPNO-TCCSD(T) in singlet−triplet gap of oxo-Mn(Salen) in cc-pVDZ basis with respect to canonical TCCSD(T) calculations as a function of cutoff for PNO occupation numbers T_{CutPNO}. The thin dashed lines represent the values for $T_{CutPairs} = 10^{-5}$.

Moreover, we performed calculations with up to cc-pVQZ basis set. We found the results to be consistent with the previous LPNO-TCCSD calculations and NEVPT2(28,22), with perturbative triples correction being responsible only for a minor shift in energy; see Table 2. Even though the calculation in cc-pVQZ, which amounts to 1178 basis functions, is perfectly within the possibilities of the LPNO approach, it took 60% longer to finish under the same conditions (8 cores, 30GB of memory per core) compared to the DLPNO calculation.

Table 2. Singlet and Triplet Energies of oxo-Mn(salen) in cc-pVXZ Basis Sets, Difference $E(^1A) - E(^3A)$ (kcal/mol), with Results for Different Active Spaces and in Various Basis Sets

	DZ	TZ	QZ
LPNO-TCCSD(28,22)[111]	6.2	6.3	6.3
DLPNO-TCCSD(28,22)	6.9	7.3	6.9
DLPNO-TCCSD(T)(28,22)	5.9	6.3	5.8
LPNO-TCCSD(28,27)[111]	3.7	3.1	2.9
DLPNO-TCCSD(28,27)	4.1	4.0	3.1
DLPNO-TCCSD(T)(28,27)	4.0	5.0	2.9
NEVPT2(28,22)[149]	− 7.4	1.6	2.4

4.3. Iron(II)−Porphyrin Model. Iron(II)−porphyrin derivatives play important roles in reactions related to material science and biological processes due to their closely lying spin states. The chosen model has previously been a subject of several large scale CASSCF studies,[136,150] and we therefore consider it to be an interesting system to test the efficiency of the method for several active spaces of different size.

The left plot in Figure 9 shows the dependence on the $T_{CutPairs}$ cutoff parameter. As for oxo-Mn(Salen), the curves converge smoothly and at 10^{-5} they are practically converged. The accuracy is consistent for triplet and quintet spin states, and it differs maximally by 0.05% of the retrieved canonical correlation energy. This is true regardless of the size of the active space,

https://dx.doi.org/10.1021/acs.jctc.0c00065
J. Chem. Theory Comput. 2020, 16, 3028−3040

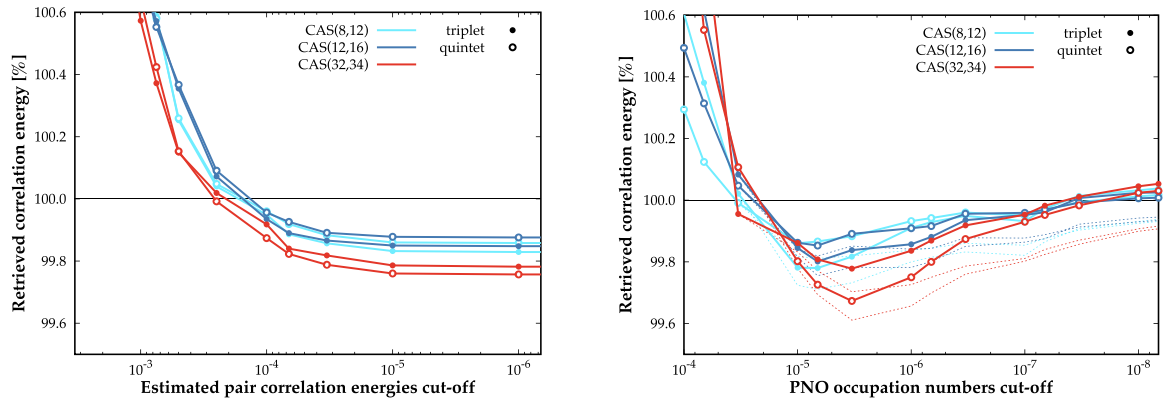

Figure 9. Percentage of correlation energy of FeP in def2-SVP basis retrieved by DLPNO-TCCSD with respect to canonical TCCSD calculations as a function of cutoff for estimated pair correlation energies T_{CutPairs} (left) and cutoff for PNO occupation numbers T_{CutPNO} (right). The thin dashed lines in the right plot represent the values for $T_{\mathrm{CutPairs}} = 10^{-5}$.

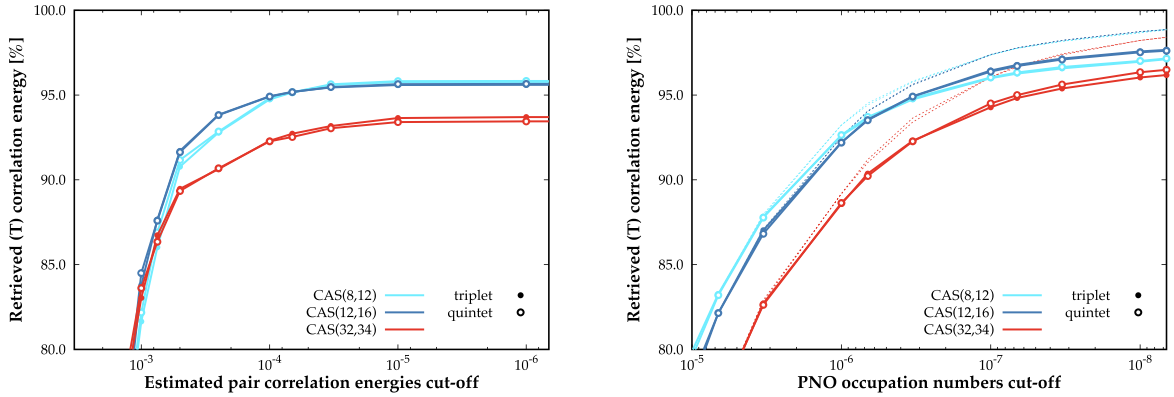

Figure 10. Percentage of perturbative triples correction correlation energy of FeP in def2-SVP basis retrieved by DLPNO-TCCSD(T) with respect to canonical TCCSD(T) calculations as a function of cutoff for estimated pair correlation energies T_{CutPairs} (left) and cutoff for PNO occupation numbers T_{CutPNO} (right). The thin dashed lines in the right plot represent the values for $T_{\mathrm{CutPairs}} = 10^{-5}$.

although the overall accuracy is slightly lower for the largest CAS.

The right plot in Figure 9 shows the dependence on the T_{CutPNO} cutoff parameter. For very loose values, the discrepancy in accuracy for different spin states is apparent, especially for the larger CAS. However, it disappears with default and TightPNO settings of the cutoff. The method once again overestimates the correlation energy for the default value of T_{CutPairs}, but for tighter value $T_{\mathrm{CutPairs}} = 10^{-5}$ it converges smoothly toward 100%.

Regarding the triples correction, the convergence behavior is similar to that for oxo-Mn(Salen). The percentages of retrieved triples energy with respect to both T_{CutPairs} and T_{CutPNO} are shown in Figure 10. The DLPNO approximation for this correction is again the most sensitive to changes in the T_{CutPNO} parameter but shows clear convergence toward 100%. Dependence of total DLPNO correlation energy on T_{CutTNO} is shown in Figure 11.

Finally, we assess the accuracy of the triplet−quintet gap, which is the actual value of interest. Table 3 lists the energy differences between TCCSD, TCCSD(T) and their DLPNO versions. At the CCSD level, the errors for absolute energies grow with growing CAS. These errors are larger for the TightPNO settings, which is understandable given the method overshoots for looser T_{CutPairs} thresholds. However, the tighter cutoffs significantly improve the accuracy in energy of the

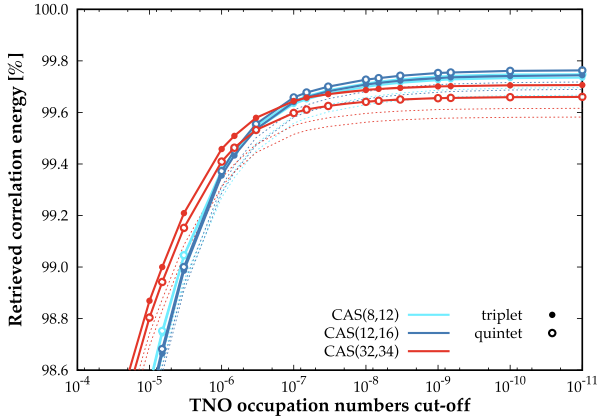

Figure 11. Percentage of correlation energy of FeP in cc-pVDZ basis retrieved by DLPNO-TCCSD(T) with respect to canonical TCCSD(T) calculations as a function of cutoff for TNO occupation numbers T_{CutTNO}. The thin dashed lines represent the values for $T_{\mathrm{CutPairs}} = 10^{-5}$.

triplet−quintet gap, with the exception of the smallest active space. Although the decrease in accuracy of the absolute energies is observed, once the perturbative triples correction is included, the errors in gaps are basically the same as in the CCSD case.

https://dx.doi.org/10.1021/acs.jctc.0c00065
J. Chem. Theory Comput. 2020, 16, 3028−3040

Table 3. Energy Differences (kcal/mol) between DLPNO-TCCSD and DLPNO-CCSD(T) Calculations with Different Settings of Cutoff Parameters and Equivalent Canonical Calculations on Iron(II)−Porphyrin Model in def2-SVP

		CAS(8,12)		CAS(12,16)		CAS(32,34)	
		default	TightPNO	default	TightPNO	default	TightPNO
SD	T	0.85	3.01	1.10	2.27	1.42	3.28
	Q	0.69	2.41	0.73	2.04	2.16	3.40
	ΔE_{T-Q}	0.16	0.60	0.37	0.23	−0.74	−0.12
SD(T)	T	4.87	5.03	4.77	4.20	5.49	5.43
	Q	4.58	4.38	4.34	3.90	6.19	5.52
	ΔE_{T-Q}	0.29	0.65	0.43	0.30	−0.70	−0.09

Moreover, the dependence of the DLPNO error on T_{CutPNO} is presented in Figure 12. Even for the default cutoffs, the error is well under 1 kcal/mol and is even smaller for the TightPNO settings, with the previously discussed exception of CAS(8,12). Interestingly, the accuracy of the quintet state is consistently lower than for the triplet state for the largest CAS, while it is the opposite for the smaller active spaces.

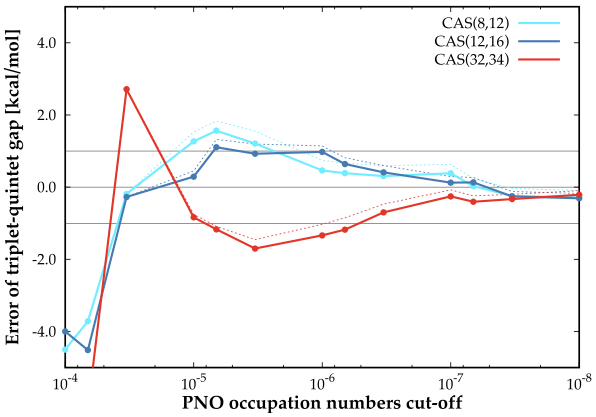

Figure 12. Error of DLPNO-TCCSD(T) in singlet−triplet gap of FeP in cc-pVDZ basis with respect to canonical TCCSD(T) calculations as a function of cutoff for PNO occupation numbers T_{CutPNO}.

5. CONCLUSIONS

We introduced a new version of the DMRG-TCCSD method, which employs the domain-based local pair natural orbital approach. The method was implemented in ORCA and should be available in the next release, while the Budapest DMRG code is used for the DMRG part.

We performed several accuracy assessments of the method employing three systems, two of which have been previously studied by the canonical and LPNO versions of the TCCSD method.

For tetramethyleneethane, we were able to retrieve over 99.9% of the canonical correlation energy, while using the default settings of cutoff parameters, with negligible non-parallelity error with respect to its dihedral rotation. Also, the drawbacks present in the LPNO version were eliminated.

For oxo-Mn(Salen), the amount of retrieved correlation was dependent on the size of the used active space, ranging from 99.8% for the larger CAS(28,27) to 99.9% for smaller CAS(28,22), which is an improvement about 0.2% with respect to LPNO-TCCSD. Using the default settings resulted in the singlet−triplet gap being off by 0.5−0.6 kcal/mol and with tighter cutoffs only 0.3−0.4 kcal/mol compared to canonical calculation. These results are slightly worse than those of LPNO-TCCSD, which we believe is a consequence of a fortunate cancellation of errors in LPNO-TCCSD, since DLPNO-TCCSD are consistently better for the remaining two systems. Moreover, new implementation offers significantly better timing than the LPNO one.

For iron(II)−porphyrin, the dependence on cutoff parameters was very similar to that for oxo-Mn(Salen). With the default settings, we were able to retrieve more than 99.9% canonical correlation energy. Irrespective of the active space size, the method determined the triplet−quintet gap with error safely within the chemical accuracy of 1 kcal/mol even with the default settings.

To summarize, we believe that DLPNO−DMRG-TCCSD(T) is a possible approach to treat systems with a moderate multireference character. In the near future, we plan to implement the DLPNO version of multireference TCCSD, which we hope to further enhance the capabilities of this method.

AUTHOR INFORMATION

Corresponding Author

Jiří Pittner − *J. Heyrovský Institute of Physical Chemistry, Academy of Sciences of the Czech Republic, 18223 Prague 8, Czech Republic*; Email: jiri.pittner@jh-inst.cas.cz

Authors

Jakub Lang − *J. Heyrovský Institute of Physical Chemistry, Academy of Sciences of the Czech Republic, 18223 Prague 8, Czech Republic; Faculty of Sciences, Charles University, 128 00 Prague 2, Czech Republic*

Andrej Antalík − *J. Heyrovský Institute of Physical Chemistry, Academy of Sciences of the Czech Republic, 18223 Prague 8, Czech Republic; Faculty of Mathematics and Physics, Charles University, 12116 Prague 2, Czech Republic*; orcid.org/0000-0002-8422-8410

Libor Veis − *J. Heyrovský Institute of Physical Chemistry, Academy of Sciences of the Czech Republic, 18223 Prague 8, Czech Republic*; orcid.org/0000-0002-4229-6335

Jan Brandejs − *J. Heyrovský Institute of Physical Chemistry, Academy of Sciences of the Czech Republic, 18223 Prague 8, Czech Republic; Faculty of Mathematics and Physics, Charles University, 12116 Prague 2, Czech Republic*

Jiří Brabec − *J. Heyrovský Institute of Physical Chemistry, Academy of Sciences of the Czech Republic, 18223 Prague 8, Czech Republic*; orcid.org/0000-0002-7764-9890

Örs Legeza − *Strongly Correlated Systems "Lendület" Research group, Wigner Research Centre for Physics, H-1525 Budapest, Hungary*

Complete contact information is available at: https://pubs.acs.org/10.1021/acs.jctc.0c00065

https://dx.doi.org/10.1021/acs.jctc.0c00065
J. Chem. Theory Comput. 2020, 16, 3028−3040

Notes

The authors declare no competing financial interest.

■ ACKNOWLEDGMENTS

We thank Prof. Frank Neese for providing us with access to ORCA source code, as well as for helpful discussions; Dr. Frank Wennmohs for technical assistance with the ORCA code; and Dr. Ondřej Demel for helpful discussions.This work has been supported by the Czech Science Foundation (Grant Nos. 18-24563S, 16-12052S, and 18-18940Y), the Hungarian National Research, Development and Innovation Office (NKFIH; through Grant No. K120569), the Hungarian Quantum Technology National Excellence Program (Project No. 2017-1.2.1-NKP-2017-00001), the Pacific Northwest National Laboratory (Contract No. 462268), and the Czech Ministry of Education, Youth and Sports (Project No. LTAUSA17033) and the Large Infrastructures for Research, Experimental Development and Innovations project "IT4Innovations National Supercomputing Center—LM2015070". Ö.L. acknowledges financial support from the Alexander von Humboldt Foundation. Mutual visits with members of the Hungarian group have been partly supported by the Hungarian-Czech Joint Research Project MTA/19/04.

■ REFERENCES

(1) Čížek, J. On the Correlation Problem in Atomic and Molecular Systems. Calculation of Wavefunction Components in Ursell-Type Expansion Using Quantum-Field Theoretical Methods. *J. Chem. Phys.* **1966**, *45*, 4256−4266.

(2) Gauss, J. In *The Encyclopedia of Computational Chemistry*; Schleyer, P. v. R., Allinger, N. L., Clark, T., Gasteiger, J., Kollman, P. A., Schaefer, H. F., III, Scheiner, P. R., Eds.; Wiley: Chichester, U.K., 1998; pp 615−636.

(3) Raghavachari, K.; Trucks, G. W.; Pople, J. A.; Head-Gordon, M. A fifth-order perturbation comparison of electron correlation theories. *Chem. Phys. Lett.* **1989**, *157*, 479−483.

(4) Bartlett, R. J.; Musiał, M. Coupled-cluster theory in quantum chemistry. *Rev. Mod. Phys.* **2007**, *79*, 291−352.

(5) Tew, D. P.; Hättig, C.; Bachorz, R. A.; Klopper, W. In *Recent Progress in Coupled Cluster Methods*; Čársky, P., Paldus, J., Pittner, J., Eds.; Springer Science: New York, 2010; p 535.

(6) Lyakh, D. I.; Musiał, M.; Lotrich, V. F.; Bartlett, R. J. Multireference Nature of Chemistry: The Coupled-Cluster View. *Chem. Rev.* **2012**, *112*, 182−243.

(7) Li, X.; Paldus, J. Reduced multireference CCSD method: An effective approach to quasidegenerate states. *J. Chem. Phys.* **1997**, *107*, 6257−6269.

(8) Li, X. Benchmark study of potential energies and vibrational levels using the reduced multireference coupled cluster method. The HF molecule. *J. Mol. Struct.: THEOCHEM* **2001**, *547*, 69−81.

(9) Li, X.; Paldus, J. Energy versus amplitude corrected coupled-cluster approaches. II. Breaking the triple bond. *J. Chem. Phys.* **2001**, *115*, 5774−5783.

(10) Li, X.; Paldus, J. Energy versus amplitude corrected coupled-cluster approaches. I. *J. Chem. Phys.* **2001**, *115*, 5759−5773.

(11) Paldus, J.; Planelles, J. Valence bond corrected single reference coupled cluster approach. *Theor. Chim. Acta* **1994**, *89*, 13−31.

(12) Piecuch, P.; Toboła, R.; Paldus, J. Approximate account of connected quadruply excited clusters in single-reference coupled-cluster theory via cluster analysis of the projected unrestricted Hartree-Fock wave function. *Phys. Rev. A: At., Mol., Opt. Phys.* **1996**, *54*, 1210−1241.

(13) Li, X.; Peris, G.; Planelles, J.; Rajadall, F.; Paldus, J. Externally corrected singles and doubles coupled cluster methods for open-shell systems. *J. Chem. Phys.* **1997**, *107*, 90−98.

(14) Kinoshita, T.; Hino, O.; Bartlett, R. J. Coupled-cluster method tailored by configuration interaction. *J. Chem. Phys.* **2005**, *123*, 074106.

(15) Lyakh, D. I.; Lotrich, V. F.; Bartlett, R. J. The 'tailored' CCSD(T) description of the automerization of cyclobutadiene. *Chem. Phys. Lett.* **2011**, *501*, 166−171.

(16) Melnichuk, A.; Bartlett, R. J. Relaxed active space: Fixing tailored-CC with high order coupled cluster. I. *J. Chem. Phys.* **2012**, *137*, 214103.

(17) Melnichuk, A.; Bartlett, R. J. Relaxed active space: Fixing tailored-CC with high order coupled cluster. II. *J. Chem. Phys.* **2014**, *140*, 064113.

(18) Piecuch, P.; Oliphant, N.; Adamowicz, L. A state-selective multireference coupled-cluster theory employing the single-reference formalism. *J. Chem. Phys.* **1993**, *99*, 1875−1900.

(19) Piecuch, P.; Adamowicz, L. State-selective multireference coupled-cluster theory employing the single-reference formalism: Implementation and application to the H8 model system. *J. Chem. Phys.* **1994**, *100*, 5792−5809.

(20) Adamowicz, L.; Piecuch, P.; Ghose, K. B. The state-selective coupled cluster method for quasi-degenerate electronic states. *Mol. Phys.* **1998**, *94*, 225−234.

(21) Piecuch, P. Active-space coupled-cluster methods. *Mol. Phys.* **2010**, *108*, 2987−3015.

(22) Piecuch, P.; Kowalski, K.; Pimienta, I. S. O.; Mcguire, M. J. Recent advances in electronic structure theory: Method of moments of coupled-cluster equations and renormalized coupled-cluster approaches. *Int. Rev. Phys. Chem.* **2002**, *21*, 527−655.

(23) Piecuch, P.; Kowalski, K.; Pimienta, I. Method of Moments of Coupled-Cluster Equations: Externally Corrected Approaches Employing Configuration Interaction Wave Functions. *Int. J. Mol. Sci.* **2002**, *3*, 475−497.

(24) Kowalski, K.; Piecuch, P. Extension of the method of moments of coupled-cluster equations to excited states: The triples and quadruples corrections to the equation-of-motion coupled-cluster singles and doubles energies. *J. Chem. Phys.* **2002**, *116*, 7411−7423.

(25) Łoch, M. W.; Lodriguito, M. D.; Piecuch, P.; Gour, J. R. Two new classes of non-iterative coupled-cluster methods derived from the method of moments of coupled-cluster equations. *Mol. Phys.* **2006**, *104*, 2149−2172.

(26) Lodriguito, M. D.; Kowalski, K.; Włoch, M.; Piecuch, P. Non-iterative coupled-cluster methods employing multi-reference perturbation theory wave functions. *J. Mol. Struct.: THEOCHEM* **2006**, *771*, 89−104.

(27) Piecuch, P.; Kowalski, K.; Pimienta, I. S. O.; Fan, P.-D.; Lodriguito, M.; McGuire, M. J.; Kucharski, S. A.; Kuś, T.; Musiał, M. Method of moments of coupled-cluster equations: a new formalism for designing accurate electronic structure methods for ground and excited states. *Theor. Chem. Acc.* **2004**, *112*, 349−393.

(28) Kowalski, K.; Piecuch, P. New type of noniterative energy corrections for excited electronic states: Extension of the method of moments of coupled-cluster equations to the equation-of-motion coupled-cluster formalism. *J. Chem. Phys.* **2001**, *115*, 2966−2978.

(29) Kowalski, K.; Piecuch, P. The method of moments of coupled-cluster equations and the renormalized CCSD[T], CCSD(T), CCSD(TQ), and CCSDT(Q) approaches. *J. Chem. Phys.* **2000**, *113*, 18−35.

(30) Veis, L.; Antalík, A.; Brabec, J.; Neese, F.; Legeza, Ö.; Pittner, J. Coupled Cluster Method with Single and Double Excitations Tailored by Matrix Product State Wave Functions. *J. Phys. Chem. Lett.* **2016**, *7*, 4072−4078.

(31) Veis, L.; Antalík, A.; Brabec, J.; Neese, F.; Legeza, Ö.; Pittner, J. Correction to Coupled Cluster Method with Single and Double Excitations Tailored by Matrix Product State Wave Functions. *J. Phys. Chem. Lett.* **2017**, *8*, 291.

(32) Li, X.; Paldus, J. Reduced multireference CCSD method: An effective approach to quasidegenerate states. *J. Chem. Phys.* **1997**, *107*, 6257.

(33) Deustua, J. E.; Magoulas, I.; Shen, J.; Piecuch, P. Communication: Approaching exact quantum chemistry by cluster

https://dx.doi.org/10.1021/acs.jctc.0c00065
J. Chem. Theory Comput. 2020, 16, 3028−3040

analysis of full configuration interaction quantum Monte Carlo wave functions. *J. Chem. Phys.* **2018**, *149*, 151101.
(34) White, S. R.; Noack, R. M. Real-space quantum renormalization groups. *Phys. Rev. Lett.* **1992**, *68*, 3487−3490.
(35) White, S. R. Density matrix formulation for quantum renormalization groups. *Phys. Rev. Lett.* **1992**, *69*, 2863−2866.
(36) White, S. R. Density-matrix algorithms for quantum renormalization groups. *Phys. Rev. B: Condens. Matter Mater. Phys.* **1993**, *48*, 10345−10356.
(37) White, S. R.; Martin, R. L. Ab initio quantum chemistry using the density matrix renormalization group. *J. Chem. Phys.* **1999**, *110*, 4127−4130.
(38) Chan, G. K.-L.; Head-Gordon, M. Highly correlated calculations with a polynomial cost algorithm: A study of the density matrix renormalization group. *J. Chem. Phys.* **2002**, *116*, 4462−4476.
(39) Legeza, O.; Röder, J.; Hess, B. A. Controlling the accuracy of the density-matrix renormalization-group method: The dynamical block state selection approach. *Phys. Rev. B: Condens. Matter Mater. Phys.* **2003**, *67*, 125114.
(40) Legeza, Ö.; Noack, R.; Sólyom, J.; Tincani, L. Applications of Quantum Information in the Density-Matrix Renormalization Group. *Computational Many-Particle Physics*; Springer: Berlin, Heidelberg, 2008; Vol. *739*, pp653−664,.
(41) Marti, K. H.; Reiher, M. The Density Matrix Renormalization Group Algorithm in Quantum Chemistry. *Z. Phys. Chem.* **2010**, *224*, 583−599.
(42) Chan, G. K.-L.; Sharma, S. The Density Matrix Renormalization Group in Quantum Chemistry. *Annu. Rev. Phys. Chem.* **2011**, *62*, 465−481.
(43) Wouters, S.; Van Neck, D. The density matrix renormalization group for ab initio quantum chemistry. *Eur. Phys. J. D* **2014**, *68*, 272.
(44) Szalay, S.; Pfeffer, M.; Murg, V.; Barcza, G.; Verstraete, F.; Schneider, R.; Legeza, Ö. Tensor product methods and entanglement optimization for ab initio quantum chemistry. *Int. J. Quantum Chem.* **2015**, *115*, 1342−1391.
(45) Yanai, T.; Kurashige, Y.; Mizukami, W.; Chalupský, J.; Lan, T. N.; Saitow, M. Density matrix renormalization group forab initioCalculations and associated dynamic correlation methods: A review of theory and applications. *Int. J. Quantum Chem.* **2015**, *115*, 283−299.
(46) Kurashige, Y.; Yanai, T. Second-order perturbation theory with a density matrix renormalization group self-consistent field reference function: Theory and application to the study of chromium dimer. *J. Chem. Phys.* **2011**, *135*, 094104.
(47) Freitag, L.; Knecht, S.; Angeli, C.; Reiher, M. Multireference Perturbation Theory with Cholesky Decomposition for the Density Matrix Renormalization Group. *J. Chem. Theory Comput.* **2017**, *13*, 451−459.
(48) Saitow, M.; Kurashige, Y.; Yanai, T. Multireference configuration interaction theory using cumulant reconstruction with internal contraction of density matrix renormalization group wave function. *J. Chem. Phys.* **2013**, *139*, 044118.
(49) Neuscamman, E.; Yanai, T.; Chan, G. K.-L. A review of canonical transformation theory. *Int. Rev. Phys. Chem.* **2010**, *29*, 231−271.
(50) Sharma, S.; Chan, G. K.-L. Communication: A flexible multi-reference perturbation theory by minimizing the Hylleraas functional with matrix product states. *J. Chem. Phys.* **2014**, *141*, 111101.
(51) Sharma, P.; Bernales, V.; Knecht, S.; Truhlar, D. G.; Gagliardi, L. Density matrix renormalization group pair-density functional theory (DMRG-PDFT): singlet−triplet gaps in polyacenes and polyacetylenes. *Chem. Sci.* **2019**, *10*, 1716−1723.
(52) Faulstich, F. M.; Laestadius, A.; Legeza, Ö.; Schneider, R.; Kvaal, S. Analysis of the Tailored Coupled-Cluster Method in Quantum Chemistry. *SIAM J. Numer. Anal.* **2019**, *57*, 2579−2607.
(53) Faulstich, F. M.; Máté, M.; Laestadius, A.; Csirik, M. A.; Veis, L.; Antalik, A.; Brabec, J.; Schneider, R.; Pittner, J.; Kvaal, S.; Legeza, Ö. Numerical and Theoretical Aspects of the DMRG-TCC Method Exemplified by the Nitrogen Dimer. *J. Chem. Theory Comput.* **2019**, *15*, 2206−2220.
(54) Veis, L.; Antalík, A.; Legeza, Ö.; Alavi, A.; Pittner, J. The Intricate Case of Tetramethyleneethane: A Full Configuration Interaction Quantum Monte Carlo Benchmark and Multireference Coupled Cluster Studies. *J. Chem. Theory Comput.* **2018**, *14*, 2439−2445.
(55) Pulay, P. Localizability of dynamic electron correlation. *Chem. Phys. Lett.* **1983**, *100*, 151−154.
(56) Sæbø, S.; Pulay, P. Local configuration interaction: An efficient approach for larger molecules. *Chem. Phys. Lett.* **1985**, *113*, 13−18.
(57) Foster, J. M.; Boys, S. F. Canonical Configurational Interaction Procedure. *Rev. Mod. Phys.* **1960**, *32*, 300−302.
(58) Pipek, J.; Mezey, P. G. A fast intrinsic localization procedure applicable for ab initio and semiempirical linear combination of atomic orbital wave functions. *J. Chem. Phys.* **1989**, *90*, 4916−4926.
(59) Knizia, G. Intrinsic Atomic Orbitals: An Unbiased Bridge between Quantum Theory and Chemical Concepts. *J. Chem. Theory Comput.* **2013**, *9*, 4834−4843.
(60) Sæbø, S.; Pulay, P. Fourth-order Møller−Plessett perturbation theory in the local correlation treatment. I. Method. *J. Chem. Phys.* **1987**, *86*, 914−922.
(61) Sæbø, S.; Pulay, P. The local correlation treatment. II. Implementation and tests. *J. Chem. Phys.* **1988**, *88*, 1884−1890.
(62) Hampel, C.; Werner, H.-J. Local treatment of electron correlation in coupled cluster theory. *J. Chem. Phys.* **1996**, *104*, 6286−6297.
(63) Schütz, M.; Werner, H.-J. Low-order scaling local electron correlation methods. IV. Linear scaling local coupled-cluster (LCCSD). *J. Chem. Phys.* **2001**, *114*, 661.
(64) Schütz, M. A new, fast, semi-direct implementation of linear scaling local coupled cluster theory. *Phys. Chem. Chem. Phys.* **2002**, *4*, 3941−3947.
(65) Werner, H.-J.; Schütz, M. An efficient local coupled cluster method for accurate thermochemistry of large systems. *J. Chem. Phys.* **2011**, *135*, 144116.
(66) Schütz, M. Low-order scaling local electron correlation methods. V. Connected triples beyond (T): Linear scaling local CCSDT-1b. *J. Chem. Phys.* **2002**, *116*, 8772−8785.
(67) Kristensen, K.; Ziółkowski, M.; Jansík, B.; Kjærgaard, T.; Jørgensen, P. A Locality Analysis of the Divide−Expand−Consolidate Coupled Cluster Amplitude Equations. *J. Chem. Theory Comput.* **2011**, *7*, 1677−1694.
(68) Høyvik, I.-M.; Kristensen, K.; Jansik, B.; Jørgensen, P. The divide-expand-consolidate family of coupled cluster methods: Numerical illustrations using second order Møller-Plesset perturbation theory. *J. Chem. Phys.* **2012**, *136*, 014105.
(69) Kobayashi, M.; Nakai, H. Extension of linear-scaling divide-and-conquer-based correlation method to coupled cluster theory with singles and doubles excitations. *J. Chem. Phys.* **2008**, *129*, 044103.
(70) Stoll, H. The correlation energy of crystalline silicon. *Chem. Phys. Lett.* **1992**, *191*, 548−552.
(71) Rolik, Z.; Kállay, M. A general-order local coupled-cluster method based on the cluster-in-molecule approach. *J. Chem. Phys.* **2011**, *135*, 104111.
(72) Fedorov, D. G.; Kitaura, K. Coupled-cluster theory based upon the fragment molecular-orbital method. *J. Chem. Phys.* **2005**, *123*, 134103.
(73) Li, S.; Ma, J.; Jiang, Y. Linear scaling local correlation approach for solving the coupled cluster equations of large systems. *J. Comput. Chem.* **2002**, *23*, 237−244.
(74) Edmiston, C.; Krauss, M. Configuration-Interaction Calculation of H3 and H2. *J. Chem. Phys.* **1965**, *42*, 1119−1120.
(75) Meyer, W. Ionization energies of water from PNO-CI calculations. *Int. J. Quantum Chem.* **1971**, *5*, 341−348.
(76) Meyer, W. PNO-CI and CEPA studies of electron correlation effects. *Theor. Chim. Acta* **1974**, *35*, 277−292.
(77) Werner, H.-J.; Meyer, W. PNO-CI and PNO-CEPA studies of electron correlation effects. *Mol. Phys.* **1976**, *31*, 855−872.
(78) Botschwina, P.; Meyer, W. PNO-CEPA calculation of collinear potential energy barriers for thermoneutral exchange reactions. *Chem. Phys.* **1977**, *20*, 43−52.

https://dx.doi.org/10.1021/acs.jctc.0c00065
J. Chem. Theory Comput. 2020, 16, 3028−3040

(79) Rosmus, P.; Meyer, W. PNO-CI and CEPA studies of electron correlation effects. VI. Electron affinities of the first-row and second-row diatomic hydrides and the spectroscopic constants of their negative ions. *J. Chem. Phys.* **1978**, *69*, 2745.
(80) Ahlrichs, R.; Kutzelnigg, W. Ab initio calculations on small hydrides including electron correlation. *Theor. Chim. Acta* **1968**, *10*, 377−387.
(81) Ahlrichs, R.; Driessler, F.; Lischka, H.; Staemmler, V.; Kutzelnigg, W. PNO-CI (pair natural orbital configuration interaction) and CEPA-PNO (coupled electron pair approximation with pair natural orbitals) calculations of molecular systems. II. The molecules BeH_2, BH, BH_3, CH_4, CH_3^-, NH_3 (planar and pyramidal), H_2O, OH_3^+, HF and the Ne atom. *J. Chem. Phys.* **1975**, *62*, 1235−1247.
(82) Neese, F.; Wennmohs, F.; Hansen, A. Efficient and accurate local approximations to coupled-electron pair approaches: An attempt to revive the pair natural orbital method. *J. Chem. Phys.* **2009**, *130*, 114108.
(83) Neese, F.; Hansen, A.; Liakos, D. G. Efficient and accurate approximations to the local coupled cluster singles doubles method using a truncated pair natural orbital basis. *J. Chem. Phys.* **2009**, *131*, 064103.
(84) Hansen, A.; Liakos, D. G.; Neese, F. Efficient and accurate local single reference correlation methods for high-spin open-shell molecules using pair natural orbitals. *J. Chem. Phys.* **2011**, *135*, 214102.
(85) Huntington, L. M. J.; Hansen, A.; Neese, F.; Nooijen, M. Accurate thermochemistry from a parameterized coupled-cluster singles and doubles model and a local pair natural orbital based implementation for applications to larger systems. *J. Chem. Phys.* **2012**, *136*, 064101.
(86) Riplinger, C.; Neese, F. An efficient and near linear scaling pair natural orbital based local coupled cluster method. *J. Chem. Phys.* **2013**, *138*, 034106.
(87) Pinski, P.; Riplinger, C.; Valeev, E. F.; Neese, F. Sparse maps—A systematic infrastructure for reduced-scaling electronic structure methods. I. An efficient and simple linear scaling local MP2 method that uses an intermediate basis of pair natural orbitals. *J. Chem. Phys.* **2015**, *143*, 034108.
(88) Riplinger, C.; Pinski, P.; Becker, U.; Valeev, E. F.; Neese, F. Sparse maps—A systematic infrastructure for reduced-scaling electronic structure methods. II. Linear scaling domain based pair natural orbital coupled cluster theory. *J. Chem. Phys.* **2016**, *144*, 024109.
(89) Saitow, M.; Becker, U.; Riplinger, C.; Valeev, E. F.; Neese, F. A new near-linear scaling, efficient and accurate, open-shell domain-based local pair natural orbital coupled cluster singles and doubles theory. *J. Chem. Phys.* **2017**, *146*, 164105.
(90) Werner, H.-J.; Knizia, G.; Krause, C.; Schwilk, M.; Dornbach, M. Scalable Electron Correlation Methods I.: PNO-LMP2 with Linear Scaling in the Molecular Size and Near-Inverse-Linear Scaling in the Number of Processors. *J. Chem. Theory Comput.* **2015**, *11*, 484−507.
(91) Menezes, F.; Kats, D.; Werner, H.-J. Local complete active space second-order perturbation theory using pair natural orbitals (PNO-CASPT2). *J. Chem. Phys.* **2016**, *145*, 124115.
(92) Schwilk, M.; Ma, Q.; Köppl, C.; Werner, H.-J. Scalable Electron Correlation Methods. 3. Efficient and Accurate Parallel Local Coupled Cluster with Pair Natural Orbitals (PNO-LCCSD). *J. Chem. Theory Comput.* **2017**, *13*, 3650−3675.
(93) Tew, D. P.; Helmich, B.; Hättig, C. Local explicitly correlated second-order Møller−Plesset perturbation theory with pair natural orbitals. *J. Chem. Phys.* **2011**, *135*, 074107.
(94) Helmich, B.; Hättig, C. A pair natural orbital implementation of the coupled cluster model CC2 for excitation energies. *J. Chem. Phys.* **2013**, *139*, 084114.
(95) Schmitz, G.; Helmich, B.; Hättig, C. A scaling PNO−MP2 method using a hybrid OSV−PNO approach with an iterative direct generation of OSVs†. *Mol. Phys.* **2013**, *111*, 2463−2476.
(96) Guo, Y.; Sivalingam, K.; Valeev, E. F.; Neese, F. SparseMaps—A systematic infrastructure for reduced-scaling electronic structure methods. III. Linear-scaling multireference domain-based pair natural orbital N-electron valence perturbation theory. *J. Chem. Phys.* **2016**, *144*, 094111.
(97) Antony, J.; Grimme, S.; Liakos, D. G.; Neese, F. Protein−Ligand Interaction Energies with Dispersion Corrected Density Functional Theory and High-Level Wave Function Based Methods. *J. Phys. Chem. A* **2011**, *115*, 11210−11220.
(98) Anoop, A.; Thiel, W.; Neese, F. A Local Pair Natural Orbital Coupled Cluster Study of Rh Catalyzed Asymmetric Olefin Hydrogenation. *J. Chem. Theory Comput.* **2010**, *6*, 3137−3144.
(99) Liakos, D. G.; Neese, F. Interplay of Correlation and Relativistic Effects in Correlated Calculations on Transition-Metal Complexes: The $(Cu_2O_2)^{2+}$ Core Revisited. *J. Chem. Theory Comput.* **2011**, *7*, 1511−1523.
(100) Zade, S. S.; Zamoshchik, N.; Reddy, A. R.; Fridman-Marueli, G.; Sheberla, D.; Bendikov, M. Products and Mechanism of Acene Dimerization. A Computational Study. *J. Am. Chem. Soc.* **2011**, *133*, 10803−10816.
(101) Kubas, A.; Bräse, S.; Fink, K. Theoretical Approach Towards the Understanding of Asymmetric Additions of Dialkylzinc to Enals and Iminals Catalysed by [2.2] Paracyclophane-Based N, O-Ligands. *Chem. - Eur. J.* **2012**, *18*, 8377−8385.
(102) Ashtari, M.; Cann, N. Proline-based chiral stationary phases: A molecular dynamics study of the interfacial structure. *J. Chromatogr. A* **2011**, *1218*, 6331−6347.
(103) Zhang, J.; Dolg, M. Dispersion Interaction Stabilizes Sterically Hindered Double Fullerenes. *Chem. - Eur. J.* **2014**, *20*, 13909−13912.
(104) Minenkov, Y.; Chermak, E.; Cavallo, L. Accuracy of DLPNO−CCSD(T) Method for Noncovalent Bond Dissociation Enthalpies from Coinage Metal Cation Complexes. *J. Chem. Theory Comput.* **2015**, *11*, 4664−4676.
(105) Sparta, M.; Neese, F. Chemical applications carried out by local pair natural orbital based coupled-cluster methods. *Chem. Soc. Rev.* **2014**, *43*, 5032−5041.
(106) Liakos, D. G.; Sparta, M.; Kesharwani, M. K.; Martin, J. M. L.; Neese, F. Exploring the Accuracy Limits of Local Pair Natural Orbital Coupled-Cluster Theory. *J. Chem. Theory Comput.* **2015**, *11*, 1525−1539.
(107) Demel, O.; Pittner, J.; Neese, F. A Local Pair Natural Orbital-Based Multireference Mukherjee's Coupled Cluster Method. *J. Chem. Theory Comput.* **2015**, *11*, 3104−3114.
(108) Lang, J.; Švaňa, M.; Demel, O.; Brabec, J.; Kedžuch, S.; Noga, J.; Kowalski, K.; Pittner, J. A MRCC study of the isomerisation of cyclopropane. *Mol. Phys.* **2017**, *115*, 2743−2754.
(109) Brabec, J.; Lang, J.; Saitow, M.; Pittner, J.; Neese, F.; Demel, O. Domain-Based Local Pair Natural Orbital Version of Mukherjee's State-Specific Coupled Cluster Method. *J. Chem. Theory Comput.* **2018**, *14*, 1370−1382.
(110) Lang, J.; Brabec, J.; Saitow, M.; Pittner, J.; Neese, F.; Demel, O. Perturbative triples correction to domain-based local pair natural orbital variants of Mukherjee's state specific coupled cluster method. *Phys. Chem. Chem. Phys.* **2019**, *21*, 5022−5038.
(111) Antalík, A.; Veis, L.; Brabec, J.; Demel, O.; Legeza, Ö.; Pittner, J. Toward the efficient local tailored coupled cluster approximation and the peculiar case of oxo-Mn(Salen). *J. Chem. Phys.* **2019**, *151*, 084112.
(112) Kowalski, K. Properties of coupled-cluster equations originating in excitation sub-algebras. *J. Chem. Phys.* **2018**, *148*, 094104.
(113) Bauman, N. P.; Bylaska, E. J.; Krishnamoorthy, S.; Low, G. H.; Wiebe, N.; Granade, C. E.; Roetteler, M.; Troyer, M.; Kowalski, K. Downfolding of many-body Hamiltonians using active-space models: Extension of the sub-system embedding sub-algebras approach to unitary coupled cluster formalisms. *J. Chem. Phys.* **2019**, *151*, 014107.
(114) Moritz, G.; Reiher, M. Decomposition of density matrix renormalization group states into a Slater determinant basis. *J. Chem. Phys.* **2007**, *126*, 244109.
(115) Boguslawski, K.; Marti, K. H.; Reiher, M. Construction of CASCI-type wave functions for very large active spaces. *J. Chem. Phys.* **2011**, *134*, 224101.
(116) Neese, F. The ORCA program system. *Wiley Interdiscip. Rev.: Comput. Mol. Sci.* **2012**, *2*, 73−78.

https://dx.doi.org/10.1021/acs.jctc.0c00065
J. Chem. Theory Comput. 2020, 16, 3028−3040

(117) Olivares-Amaya, R.; Hu, W.; Nakatani, N.; Sharma, S.; Yang, J.; Chan, G. K.-L. The ab-initio density matrix renormalization group in practice. *J. Chem. Phys.* **2015**, *142*, 034102.
(118) Adler, T. B.; Werner, H.-J. An explicitly correlated local coupled cluster method for calculations of large molecules close to the basis set limit. *J. Chem. Phys.* **2011**, *135*, 144117.
(119) Adler, T. B.; Werner, H.-J. Local explicitly correlated coupled-cluster methods: Efficient removal of the basis set incompleteness and domain errors. *J. Chem. Phys.* **2009**, *130*, 241101.
(120) Riplinger, C.; Sandhoefer, B.; Hansen, A.; Neese, F. Natural triple excitations in local coupled cluster calculations with pair natural orbitals. *J. Chem. Phys.* **2013**, *139*, 134101.
(121) Guo, Y.; Riplinger, C.; Becker, U.; Liakos, D. G.; Minenkov, Y.; Cavallo, L.; Neese, F. Communication: An improved linear scaling perturbative triples correction for the domain based local pair-natural orbital based singles and doubles coupled cluster method [DLPNO-CCSD(T)]. *J. Chem. Phys.* **2018**, *148*, 011101.
(122) Legeza, Ö.; Veis, L.; Mosoni, T. *QC-DMRG-Budapest, a program for quantum chemical DMRG calculations*; Wigner Research Center: Budapest, 2000−2020.
(123) Barcza, G.; Legeza, Ö.; Marti, K. H.; Reiher, M. Quantum-information analysis of electronic states of different molecular structures. *Phys. Rev. A: At., Mol., Opt. Phys.* **2011**, *83*, 012508.
(124) Fertitta, E.; Paulus, B.; Barcza, G.; Legeza, O. Investigation of metal−insulator-like transition through theab initiodensity matrix renormalization group approach. *Phys. Rev. B: Condens. Matter Mater. Phys.* **2014**, *90*, 245129.
(125) Legeza, O.; Sólyom, J. Optimizing the density-matrix renormalization group method using quantum information entropy. *Phys. Rev. B: Condens. Matter Mater. Phys.* **2003**, *68*, 195116.
(126) Legeza, O.; Sólyom, J. Quantum data compression, quantum information generation, and the density-matrix renormalization-group method. *Phys. Rev. B: Condens. Matter Mater. Phys.* **2004**, *70*, 205118.
(127) Bross, D. H.; Hill, J. G.; Werner, H.-J.; Peterson, K. A. Explicitly correlated composite thermochemistry of transition metal species. *J. Chem. Phys.* **2013**, *139*, 094302.
(128) Ivanic, J.; Collins, J. R.; Burt, S. K. Theoretical Study of the Low Lying Electronic States of oxoX(salen) (X = Mn, Mn-, Fe, and Cr-) Complexes. *J. Phys. Chem. A* **2004**, *108*, 2314−2323.
(129) Ghosh, D.; Hachmann, J.; Yanai, T.; Chan, G. K.-L. Orbital optimization in the density matrix renormalization group, with applications to polyenes and β-carotene. *J. Chem. Phys.* **2008**, *128*, 144117.
(130) Zgid, D.; Nooijen, M. The density matrix renormalization group self-consistent field method: Orbital optimization with the density matrix renormalization group method in the active space. *J. Chem. Phys.* **2008**, *128*, 144116.
(131) Yanai, T.; Kurashige, Y.; Ghosh, D.; Chan, G. K.-L. Accelerating convergence in iterative solution for large-scale complete active space self-consistent-field calculations. *Int. J. Quantum Chem.* **2009**, *109*, 2178−2190.
(132) Dunning, T. H. Gaussian basis sets for use in correlated molecular calculations. I. The atoms boron through neon and hydrogen. *J. Chem. Phys.* **1989**, *90*, 1007−1023.
(133) Woon, D. E.; Dunning, T. H. Gaussian basis sets for use in correlated molecular calculations. III. The atoms aluminum through argon. *J. Chem. Phys.* **1993**, *98*, 1358−1371.
(134) Balabanov, N. B.; Peterson, K. A. Systematically convergent basis sets for transition metals. I. All-electron correlation consistent basis sets for the 3d elements Sc−Zn. *J. Chem. Phys.* **2005**, *123*, 064107.
(135) Weigend, F.; Köhn, A.; Hättig, C. Efficient use of the correlation consistent basis sets in resolution of the identity MP2 calculations. *J. Chem. Phys.* **2002**, *116*, 3175−3183.
(136) Li Manni, G.; Alavi, A. Understanding the Mechanism Stabilizing Intermediate Spin States in Fe(II)-Porphyrin. *J. Phys. Chem. A* **2018**, *122*, 4935−4947.
(137) Weigend, F.; Ahlrichs, R. Balanced basis sets of split valence, triple zeta valence and quadruple zeta valence quality for H to Rn: Design and assessment of accuracy. *Phys. Chem. Chem. Phys.* **2005**, *7*, 3297.
(138) Hellweg, A.; Hättig, C.; Höfener, S.; Klopper, W. Optimized accurate auxiliary basis sets for RI-MP2 and RI-CC2 calculations for the atoms Rb to Rn. *Theor. Chem. Acc.* **2007**, *117*, 587−597.
(139) Pittner, J.; Nachtigall, P.; Čársky, P.; Hubač, I. State-Specific Brillouin-Wigner Multireference Coupled Cluster Study of the Singlet-Triplet Separation in the Tetramethyleneethane Diradical. *J. Phys. Chem. A* **2001**, *105*, 1354−1356.
(140) Bhaskaran-Nair, K.; Demel, O.; Šmydke, J.; Pittner, J. Multireference state-specific Mukherjee's coupled cluster method with noniterative triexcitations using uncoupled approximation. *J. Chem. Phys.* **2011**, *134*, 154106.
(141) Chattopadhyay, S.; Chaudhuri, R. K.; Sinha Mahapatra, U. Ab Initio Multireference Investigation of Disjoint Diradicals: Singlet versus Triplet Ground States. *ChemPhysChem* **2011**, *12*, 2791−2797.
(142) Pozun, Z. D.; Su, X.; Jordan, K. D. Establishing the Ground State of the Disjoint Diradical Tetramethyleneethane with Quantum Monte Carlo. *J. Am. Chem. Soc.* **2013**, *135*, 13862−13869.
(143) Zhang, W.; Loebach, J. L.; Wilson, S. R.; Jacobsen, E. N. Enantioselective epoxidation of unfunctionalized olefins catalyzed by salen manganese complexes. *J. Am. Chem. Soc.* **1990**, *112*, 2801−2803.
(144) Irie, R.; Noda, K.; Ito, Y.; Matsumoto, N.; Katsuki, T. Catalytic asymmetric epoxidation of unfunctionalized olefins. *Tetrahedron Lett.* **1990**, *31*, 7345−7348.
(145) Sears, J. S.; Sherrill, C. D. The electronic structure of oxo-Mn(salen): Single-reference and multireference approaches. *J. Chem. Phys.* **2006**, *124*, 144314.
(146) Ma, D.; Li Manni, G.; Gagliardi, L. The generalized active space concept in multiconfigurational self-consistent field methods. *J. Chem. Phys.* **2011**, *135*, 044128.
(147) Wouters, S.; Bogaerts, T.; Van Der Voort, P.; Van Speybroeck, V.; Van Neck, D. Communication: DMRG-SCF study of the singlet, triplet, and quintet states of oxo-Mn(Salen). *J. Chem. Phys.* **2014**, *140*, 241103.
(148) Stein, C. J.; Reiher, M. Automated Selection of Active Orbital Spaces. *J. Chem. Theory Comput.* **2016**, *12*, 1760−1771.
(149) Sharma, S.; Knizia, G.; Guo, S.; Alavi, A. Combining Internally Contracted States and Matrix Product States To Perform Multi-reference Perturbation Theory. *J. Chem. Theory Comput.* **2017**, *13*, 488−498.
(150) Li Manni, G.; Kats, D.; Tew, D. P.; Alavi, A. Role of Valence and Semicore Electron Correlation on Spin Gaps in Fe(II)-Porphyrins. *J. Chem. Theory Comput.* **2019**, *15*, 1492−1497.

https://dx.doi.org/10.1021/acs.jctc.0c00065
J. Chem. Theory Comput. 2020, 16, 3028−3040

PCCP

ROYAL SOCIETY OF CHEMISTRY

COMMUNICATION

View Article Online
View Journal | View Issue

Cite this: *Phys. Chem. Chem. Phys.*, 2020, **22**, 17033

Received 8th June 2020,
Accepted 20th July 2020

DOI: 10.1039/d0cp03086d

rsc.li/pccp

Ground state of the Fe(II)-porphyrin model system corresponds to quintet: a DFT and DMRG-based tailored CC study†

Andrej Antalík, [ab] Dana Nachtigallová, *[cd] Rabindranath Lo,[cd] Mikuláš Matoušek,[ab] Jakub Lang, [a] Örs Legeza,[e] Jiří Pittner,[a] Pavel Hobza *[cd] and Libor Veis *[a]

Fe(II)-porphyrins play an important role in many reactions relevant to material science and biological processes, due to their closely lying spin states. Although the prevalent opinion is that these systems posses the triplet ground state, the recent experiment on Fe(II)-phthalocyanine under conditions matching those of an isolated molecule points toward the quintet ground state. We present a thorough DFT and DMRG-based tailored CC study of Fe(II)-porphyrin model, in which we address all previously discussed correlation effects. We examine the importance of geometrical parameters, the Fe–N distances in particular, and conclude that the system possesses the quintet ground state.

Porphyrins are conjugated aromatic systems composed of four pyrrole rings connected at their C_α atoms by CH groups (see Fig. 1). Their metal-derivates, in particular Fe(II)-porphyrins based on Fe(II)-porphyrin (FeP, Fig. 1a) (Fe(II)-phthalocyanine (FePc, Fig. 1b) and Fe(II)-porphyrazine (FePz, Fig. 1c)), play an important role in reactions related to material science and biological processes due to the near degeneracy of their high-spin (quintet), intermediate-spin (triplet) and low-spin (singlet) states. A well-known example is the triplet to singlet spin crossover upon binding of molecular oxygen to the Fe(II) active site of hemoglobin.[1]

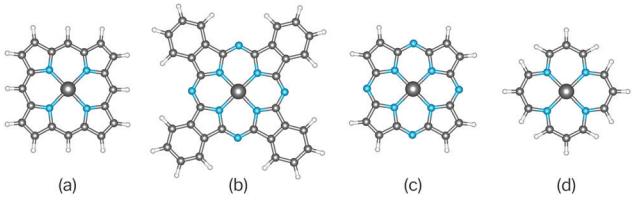

Fig. 1 Structures of Fe(II)-porphyrin (a), Fe(II)-phtalocyanine (b), Fe(II)-porphyrazine (c), and a model system of Fe(II)-porphyrin (d) studied in this work and in the text denoted as **1**, or depending on the geometry, the Fe–N distance in particular, employed **1a**, **1b**, and **1c** (see Table 1).

Since neither FeP, nor FePz exists in an unsubstituted state, the direct comparison of theoretical and experimental results is not possible. Although the existing experimental studies on four-coordinated Fe(II) embedded in substituted porphyrin systems[2–10] mostly predict the triplet ground state, they have been performed either in the crystal phase or polar solvent, which are far from the gas phase conditions of computational studies.

We have recently investigated the effect of different environments on the FePc ground state by means of the Mössbauer spectroscopy and various computational methods.[11] Our experiments have unambiguously indicated the triplet ground state of FePc in the crystalline form and dissolved in dimethylformamide, and the quintet when dissolved in monochlorobenzene (resemblance to gas phase conditions of computational studies). The quintet ground state was also confirmed by the multireference density matrix renormalization group (DMRG) calculations. These findings clearly contradict the prevalent opinion in the literature.

The experimental observations of Fe(II)-porphyrins guided several follow-up computational studies on FeP and FePz with the density functional theory (DFT)[5,11–23] and multireference methods.[24–32] Nevertheless, due to the complexity of the problem, an unambiguous answer to the state ordering has not been found even with the multireference methods that are able to correlate a relatively large number of electrons.[28,29,33,34]

[a] *J. Heyrovský Institute of Physical Chemistry, Academy of Sciences of the Czech Republic, v.v.i., Dolejškova 3, 18223 Prague 8, Czech Republic. E-mail: libor.veis@jh-inst.cas.cz*
[b] *Faculty of Mathematics and Physics, Charles University, Ke Karlovu 3, 12116, Prague 2, Czech Republic*
[c] *Institute of Organic Chemistry and Biochemistry, Academy of Sciences of the Czech Republic, v.v.i., Flemingovo nám. 2, 16610 Prague 6, Czech Republic. E-mail: dana.nachtigallova@uochb.cas.cz, pavel.hobza@uochb.cas.cz*
[d] *Regional Centre of Advanced Technologies and Materials, Palacký University, 77146 Olomouc, Czech Republic*
[e] *Strongly Correlated Systems "Lendület" Research group, Wigner Research Centre for Physics, H-1525, Budapest, Hungary*

† Electronic supplementary information (ESI) available: Computational details, CAS(32,34) natural orbitals, all geometries, one-orbital entropies, complete DMRG and DLPNO-TCC results. See DOI: 10.1039/d0cp03086d

The effects of different contributions to electron correlation,[25,26,30] have recently been investigated by calculations on model system of Fe(II)-porphyrin in which the bridging CH groups are replaced by hydrogen atoms (model **1**, Fig. 1d). In the recent work of Li Manni *et al.*,[31] the complete active space (CAS) was constructed from 32 electrons in 34 orbitals, in particular, the Fe(3d), Fe(4d), σ lone pairs, and all π orbitals of the porphyrin model ring to cover the valence correlation. The active space was then augmented by the semi-core Fe(3s,3p) orbitals resulting in CAS(40,38) and a minor increase in the quintet-triplet gap. The inclusion of beyond-CAS correlation by employing the single reference coupled cluster correction further stabilized the triplet ground state and provided the final estimate of the triplet-quintet energy gap as 5.7 kcal mol^{-1}. Comparing these results to the FePc experimental data[11] and our preliminary DFT calculations on the spin state ordering in FeP and FePc (see ESI†), we reopen the debate over the character of the Fe(II)-porphyrins and their modelling. Besides discussing the extent of electron correlation in the multireference approach, we explore the role of other parameters which may influence the ground state predictions.

Among such parameters, particular attention should be paid to the geometry of FeP systems. The Fe–N bond distance (R_{FeN}) has been discussed by several authors,[35–37] with some proposing that the increase in R_{FeN} stabilizes quintet states *via* the relaxation of $d_{x^2-y^2}$ orbital.[38] The calculated Fe–N bond distances obtained for the quintet states typically range from 2.0 to 2.1 Å.[35,39,40] In comparison, the value of 1.972 Å taken from the X-ray diffraction of Fe(II)-tetraphenylporphyrin (FeTPP)[8] is closer to the value of 1.989 Å obtained for the FeP triplet state by employing the PBE0 functional in DFT optimization.[40] This result confirms the suggestion discussed in ref. 11 for Fe(II)-Pc, according to which the ground spin state observed in the crystalline form of Fe(II)-porphyrins very likely differs from the ground state of an isolated molecule in the gas phase.

This discussion on various effects influencing the spin state ordering raises the following question: Does the improved electron correlation treatment result in the same changes in the triplet-quintet state ordering of the FeP model regardless of whether the triplet optimized or quintet optimized distance is used?

To resolve this issue, apart from the DFT calculations with the B97-D3 functional, we investigated the electronic structure of **1** by means of DMRG-based methods. DMRG is a well-established and very powerful approach suitable for treatment of strongly correlated problems that require large active spaces.[41,42] However, despite its favorable scaling, it is still computationally prohibitive to treat the dynamic correlation solely with DMRG. As a possible solution, we have introduced the TCCSD method, in which the CC wave function is externally corrected using the information extracted from the DMRG calculation.[43] We showed that it is able to describe both non-dynamic and dynamic correlation in a balanced way,[44,45] but due to the scaling of the CCSD part, the TCCSD methodology quickly becomes unfeasible for larger systems. To remove this bottleneck, we have recently developed its domain-based local pair natural orbital (DLPNO) version,[46] which employs the pair natural orbitals to exploit the locality of electron correlation.[47–49]

Table 1 The Fe–N distance (R_{FeN}, in Å) optimized for each state at the B97-D3/TZVPP level for FeP-based systems with the exception of **1a** which is from ref. 31

	Triplet	Quintet
FeP model (**1**)	1.989 (**1a**)	
	2.048 (**1b**)	2.180 (**1c**)
FeP	1.997	2.064
FeTPP	1.995, 1.998	2.063–2.065

The R_{FeN} values resulting from spin separate triplet and quintet optimizations of model **1**, performed at the B97-D3/TZVPP level, are given in Table 1. For comparison, we also report the distances for FeP and FeTPP, which are in very good agreement with the PBE0 values of 1.989 Å and 2.053 Å optimized for the FeP triplet and quintet states, respectively.[40] Additionally, the R_{FeN} values obtained from the triplet optimizations agree reasonably well with the distance of 1.972 Å found in the X-ray diffraction experiment[8] (where FeTPP is predicted to possess the triplet state), thus confirming the reliability of B97-D3 functional. In agreement with the discussion above, the quintet-optimized R_{FeN} values of FeP, FeTPP and **1** are larger compared to the triplet state, with the differences 0.060 Å, 0.067 Å and 0.132 Å, respectively. The significant increase in elongation for **1** compared to FeP and FeTPP stems from the larger flexibility of the surrounding ring because of the missing bridging CH groups.

Table 2 lists the relative spin state energies from DFT obtained by employing the B97-D3 functional for various geometries of **1** and their comparison with the previously reported results on **1a** obtained with the Stochastic-CASSCF.[30,31] The B97-D3 adiabatic energy gap is determined as 11.0 kcal mol^{-1} with the quintet ground state by using the Fe–N distances from the fully optimized triplet **1b** and quintet **1c** geometries (the difference in R_{FeN} is 0.132 Å). This gap then reduces to 2.8 kcal mol^{-1} when R_{FeN} values from the optimized FeP are used (the difference in R_{FeN} is 0.067 Å). The vertical gap at the triplet geometry **1b** results in reversed ordering with the triplet state more stable than quintet by 2.9 kcal mol^{-1} and it increases to 8.0 kcal mol^{-1} when R_{FeN} optimized for FeP triplet is used. At the similar Fe–N distance **1a**, the Stochastic-CASSCF

Table 2 Relative energies in kcal mol^{-1} of the triplet and quintet states of 1 based on the DFT calculations and Stochastic-CASSCF calculations from ref. 31. Geometry denotes the source of geometry parameters

Method	Excitation	Geometry	Triplet	Quintet
B97-D3/TZVPP	Adiab.	**1b**, **1c**	11.0	0.0
	Vert.	**1b**	0.0	2.9
	Adiab.	FeP (T,Q)	2.8	0.0
	Vert.	FeP (T)	0.0	8.0
Stoch.-CASSCF(32,34)	Vert.	**1a**	0.0	3.1
(40,38)	Vert.	**1a**	0.0	4.4[a]

[a] Involving CCSD(T) correlation treatment increases the gap to 5.7 kcal mol^{-1}.

calculations[30,31] predict the triplet ground state as well, but with the smaller energy gap of 3.1 and 4.4 kcal mol^{-1} using the CAS(32,34) and CAS(40,38), respectively.

These results indicate that the Fe–N bond distances play a significant role in the spin state ordering of FeP systems, but the extent of its influence has not yet been evaluated in detail. In fact, it seems that the value of this structure parameter can dominate the energy balance and thus relative ordering of the spin states. We evaluate this effect together with another significant influence which is the level of electron correlation treatment. In the following, we present the main results of (DMRG-)CASSCF and TCC calculations, while the complete set of energies together with Computational Details is provided in the ESI.†

Based on the previous discussions on the ground state of FeP systems in literature, only the lowest quintet ($^5A_{1g}$) and triplet states are considered. Unlike in the study of Li Manni *et al.*,[31] the lowest triplet state in all our (DMRG-)CASSCF and TCC calculations corresponds to $^3A_{2g}$ with the occupation $(d_{x^2-y^2})^2(d_{z^2})^2(d_{xz})^1(d_{yz})^1(d_{xy})^0$. Considering a very small energy gap of only about 0.5 kcal mol^{-1} between the two lowest triplets ($^3A_{2g}$ and ^3E_g) in the aforementioned study, this discrepancy might be attributed to the difference in basis sets. Nevertheless, we believe that such a small energy gap is below the resolution of the employed methods. Also, the $^3A_{2g}$ state was found to be the lowest triplet state of FeP in ref. 40.

In order to assess the accuracy of the DLPNO approximation, we first performed a series of benchmark calculations. In these, we calculated the energy differences of the studied quintet to triplet energy gaps $\Delta E^{Q\rightarrow T} = E^T - E^Q$ between the canonical TCC methods and its DLPNO counterparts in the smaller SVP basis set. The resulting errors coming from the DLPNO approximation are well below 0.5 kcal mol^{-1}, except those obtained for **1a** with CAS(8,12), where the errors are about 0.6 kcal mol^{-1}.

We first discuss the results for vertical $\Delta E^{Q\rightarrow T}$ in the **1a** geometry which are presented in Fig. 2a. This system has already been a subject of previous studies by Li Manni *et al.*[30,31] and it therefore offers an opportunity to compare our approach with a different method. Starting with the smaller CAS(8,12) and CAS(12,16), CASSCF results show an initial stabilization of the quintet state. Similarly to ref. 31, the additional dynamic correlation on top of the CASSCF reference wave functions by means of the DLPNO-TCCSD stabilizes the triplet, *i.e.*, decreases $\Delta E^{Q\rightarrow T}$. Its further, yet less prominent stabilization is observed when perturbative triples are employed. At this point, it is obvious that the inclusion of four Gouterman's π-orbitals[50] in CAS does not change the relative energies of the lowest quintet and triplet states and virtually no difference in enegy gap between CAS(8,12) and CAS(12,16) at all levels of correlation treatment is observed. However, the situation is different when the largest active space is used.

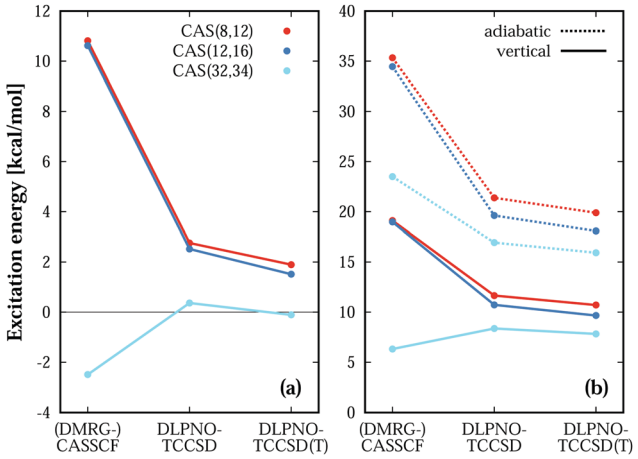

Fig. 2 The (DMRG-)CASSCF, DLPNO-TCCSD, and DLPNO-TCCSD(T) (a) vertical $\Delta E^{Q\rightarrow T}$ energy gaps of **1a**,[31] (b) vertical $\Delta E^{Q\rightarrow T}$ energy gaps of **1b** and adiabatic energy gaps of fully optimized **1** in kcal mol^{-1} in def2-TZVP basis. The keys are shared by both plots.

While for the smaller active spaces each method assigns the quintet ground state, the addition of all π-orbitals stabilizes the triplet state with respect to quintet at the DMRG-CASSCF(32,34) level. Thus, the triplet becomes the ground state with $\Delta E^{Q\rightarrow T}$ gap corresponding to −2.49 kcal mol^{-1}, which agrees well with the energy gap of −3.1 kcal mol^{-1} of the said study.[30] The difference between these two values might originate in the use of different basis sets and/or slightly differently optimized CASSCF orbitals, since the bond dimension in DMRG-CASSCF is not in full accordance with the given number of walkers in Stochastic-CASSCF. When the dynamic correlation is added on top of DMRG-CASSCF, the change in $\Delta E^{Q\rightarrow T}$ is less prominent compared to the smaller active spaces. This means that the majority of important correlations is already captured by the active space containing 34 orbitals as previously discussed.[30] Interestingly, the dynamic correlation stabilizes the quintet state, resulting in $\Delta E^{Q\rightarrow T}$ of −0.11 kcal mol^{-1} at our highest level of theory DLPNO-TCCSD(T)(32,34), which contrasts with the previous observations −5.7 kcal mol^{-1}.[31] The effect of active space on the energetic ordering of parent FeP was recently studied by means of another post-DMRG method, namely DMRG-based pair density functional theory.[34] In this work, the ground state was identified as triplet, but the impact of geometry was not discussed.

This inconsistency between our and the previously published results deserves a few comments. In the study,[31] the authors investigated the effect of Fe(3s,3p) orbitals, as well as the virtual orbitals not included in CAS(32,34). Both groups of orbitals have a different stabilization effect: semi-core orbitals stabilize the triplet state, whereas the dynamic correlation of the full virtual space stabilizes the quintet state. In our opinion, the observed discrepancy stems from the fact that in the article by Li Manni *et al.*[31] the correlation effects have been studied at a different level of theory. The semi-core orbitals have been eventually included into the active space, and thus described at the multireference level, while the effect of full virtual space has been studied by means of single-reference CC. Taking into account that in our TCC calculations the HF determinants contribute to the total wave function with the weight of about 0.6, the single-reference level of theory might be inadequate. Even though we employ the single-reference CC formalism (using one-determinant Fermi vacuum), our TCC approach

systematically accounts for the strong-correlation effects *via* the CC amplitudes extracted from the DMRG wave function. The semi-core correlation is included directly at the CCSD level and the effect of triplet stabilization is even more prominent than in Li Manni *et al.*[31] (with respect to calculations with frozen Fe(3s,3p) orbitals, see ESI†). Nevertheless, further studies which would employ alternative computational methods of calculation of dynamic correlation on top of CASSCF(32,34) (*e.g.*, adiabatic connection[51]) are necessary to confirm our hypothesis. We additionally carried out single reference DLPNO-CCSD(T) calculations of the FeP model with DMRG-CASSCF(32,34) and B3LYP orbitals, since Radoń showed that CCSD(T) method itself can perform well on FeP.[52] The resulting vertical gaps presented in ESI† are in qualitative agreement with the DLPNO-TCCSD(T) results, in case of DMRG-CASSCF(32,34) reference orbitals differing by 2.8 and 3.6 kcal mol^{-1} for **1a** and **1b** geometry respectively. The difference between DLPNO-CCSD(T) energy gaps with DMRG-CASSCF(32,34) and B3LYP orbitals is negligible.

Next, the results are analyzed in terms of R_{FeN} distance for spin state specific optimized structures of FeP model **1** and presented in Fig. 2b. The solid lines show the values of vertical $\Delta E^{\mathrm{Q}\rightarrow\mathrm{T}}$ calculated for the **1b** geometry, which with improving treatment of electronic correlation exhibit very similar trends as for **1a**, but shifted by about 8 kcal mol^{-1} towards the more stable quintet. The dashed lines show the values of adiabatic $\Delta E^{\mathrm{Q}\rightarrow\mathrm{T}}$ calculated for fully optimized **1** *i.e.*, with the triplet and quintet states in **1b** and **1c** geometries, respectively. Compared to the vertical $\Delta E^{\mathrm{Q}\rightarrow\mathrm{T}}$, these stabilize the quintet even more.

Now, considering the most important geometrical parameter R_{FeN} of the models used in this study, our best estimate of the vertical $\Delta E^{\mathrm{Q}\rightarrow\mathrm{T}}$ of **1a** (R_{FeN} = 1.989 Å) obtained at the DLPNO-TCCSD(T)(32,34)/def2-TZVP level of theory puts the triplet state below quintet with the negligible gap of −0.11 kcal mol^{-1}. On the other hand, the same calculations of **1b** (R_{FeN} = 2.048 Å), which is optimized for the triplet state, result in quintet being more stable by 7.83 kcal mol^{-1}. Note that although the **1b** model comes from the triplet optimized geometry, its Fe–N distance closely reflects the quintet state geometry of FeP and its derivatives and the conclusions made on these systems will thus be slightly biased towards quintet (just as **1a** reflects their triplet geometry and is biased towards triplet, see Table 1). As can be seen from the comparison of the spin state ordering of **1** with FeP and FePc (see Table 2 and ESI†), the former is not a sufficient model to describe the correlation of electrons in Fe(3d,4d) orbitals and pyrrolic π-electron system in Fe(II)-porphyrins. In addition, the changes in triplet and quintet geometries of **1** are overestimated due to the increased flexibility caused by removing the CH groups. Despite this, our results highlight the crucial role of Fe–N distance in the spin-state ordering and shed new light on the experimental data interpretation of Fe(II)-porphyrins.

In this communication, we presented a thorough study of Fe(II)-porphyrin model, which explored various effects influencing the spin state ordering of FeP systems. We included all previously discussed correlation effects[28,30,31,34] – non-dynamic valence correlation *via* DMRG-CASSCF(32,34), and beyond-active-space and semi-core dynamic correlation *via* DMRG-based DLPNO-TCCSD(T). The use of the latter method allowed us to employ basis sets flexible enough to capture subtle changes in the spin state ordering. On top of that, we stress the crucial importance of geometrical parameters, the Fe–N distances in particular, which is an aspect that has not been previously addressed and has a substantial impact on the ground state character. By exploring different geometries, we conclude that by using the model structure with Fe–N distances close to the quintet optimized geometry of FeP and its derivatives, the ground state is found to be a quintet (vertical $\Delta E^{\mathrm{Q}\rightarrow\mathrm{T}}$ = 7.8 kcal mol^{-1}), which is consistent with the previous measurements on an isolated molecule of Fe(II)-phthalocyanine.[11]

Conflicts of interest

There are no conflicts to declare.

Acknowledgements

This work has been supported by the Czech Science Foundation (18-18940Y; PH, DN and RL acknowledge grant no. 19-27454X), Charles University (GAUK 376217), Czech Ministry of Education (LTAUSA17033), the Hungarian National Research, Development and Innovation Office (K120569) and the Hungarian Quantum Technology National Excellence Program (2017-1.2.1-NKP-2017-00001). We acknowledge the IT4 Innovations National Supercomputing Center. ÖL acknowledges financial support from the Alexander von Humboldt foundation. The development of the MOLMPS library was supported by the Center for Scalable and Predictive methods for Excitation and Correlated phenomena (SPEC), which is funded by the U.S. Department of Energy (DOE), Office of Science, Office of Basic Energy Sciences, the Division of Chemical Sciences, Geosciences, and Biosciences.

Notes and references

1 K. P. Kepp, *Coord. Chem. Rev.*, 2017, **344**, 363–374.
2 K. Spartalian, G. Lang and C. A. Reed, *J. Chem. Phys.*, 1979, **71**, 1832–1837.
3 M. Evangelisti, J. Bartolomé, L. J. de Jongh and G. Filoti, *Phys. Rev. B: Condens. Matter Mater. Phys.*, 2002, **66**, 144410.
4 G. Filoti, M. D. Kuz'min and J. Bartolomé, *Phys. Rev. B: Condens. Matter Mater. Phys.*, 2006, **74**, 134420.
5 J. Bartolomé, F. Bartolomé, L. M. García, G. Filoti, T. Gredig, C. N. Colesniuc, I. K. Schuller and J. C. Cezar, *Phys. Rev. B: Condens. Matter Mater. Phys.*, 2010, **81**, 195405.
6 M. Gruyters, T. Pingel, T. G. Gopakumar, N. Néel, C. Schütt, F. Köhler, R. Herges and R. Berndt, *J. Phys. Chem. C*, 2012, **116**, 20882–20886.
7 T. Kitagawa and J. Teraoka, *Chem. Phys. Lett.*, 1979, **63**, 443–446.
8 J. P. Collman, J. L. Hoard, N. Kim, G. Lang and C. A. Reed, *J. Am. Chem. Soc.*, 1975, **97**, 2676–2681.

9 J. Mispelter, M. Momenteau and J. M. Lhoste, *J. Chem. Phys.*, 1980, **72**, 1003–1012.
10 J. R. Sams and T. B. Tsin, *Chem. Phys. Lett.*, 1974, **25**, 599–601.
11 D. Nachtigallová, A. Antalík, R. Lo, R. Sedlák, D. Manna, J. Tuček, J. Ugolotti, L. Veis, Ö. Legeza, J. Pittner, R. Zbořil and P. Hobza, *Chem. – Eur. J.*, 2018, **24**, 13413–13417.
12 T. Kroll, R. Kraus, R. Schönfelder, V. Y. Aristov, O. V. Molodtsova, P. Hoffmann and M. Knupfer, *J. Chem. Phys.*, 2012, **137**, 054306.
13 M. D. Kuz'min, A. Savoyant and R. Hayn, *J. Chem. Phys.*, 2013, **138**, 244308.
14 V. E. J. Berryman, R. J. Boyd and E. R. Johnson, *J. Chem. Theory Comput.*, 2015, **11**, 3022–3028.
15 M.-S. Liao, J. D. Watts and M.-J. Huang, *J. Comput. Chem.*, 2006, **27**, 1577–1592.
16 A. R. Groenhof, M. Swart, A. W. Ehlers and K. Lammertsma, *J. Phys. Chem. A*, 2005, **109**, 3411–3417.
17 V. E. J. Walker, N. Castillo, C. F. Matta and R. J. Boyd, *J. Phys. Chem. A*, 2010, **114**, 10315–10319.
18 B. Brena, C. Puglia, M. de Simone, M. Coreno, K. Tarafder, V. Feyer, R. Banerjee, E. Göthelid, B. Sanyal, P. M. Oppeneer and O. Eriksson, *J. Chem. Phys.*, 2011, **134**, 074312.
19 N. Marom and L. Kronik, *Appl. Phys. A: Mater. Sci. Process.*, 2008, **95**, 165–172.
20 S. Obara and H. Kashiwagi, *J. Chem. Phys.*, 1982, **77**, 3155–3165.
21 M. D. Kuz'min, R. Hayn and V. Oison, *Phys. Rev. B: Condens. Matter Mater. Phys.*, 2009, **79**, 024413.
22 P. A. Reynolds and B. N. Figgis, *Inorg. Chem.*, 1991, **30**, 2294–2300.
23 M.-S. Liao and S. Scheiner, *J. Chem. Phys.*, 2001, **114**, 9780–9791.
24 T. Ichibha, Z. Hou, K. Hongo and R. Maezono, *Sci. Rep.*, 2017, **7**, 2011.
25 K. Pierloot, Q. M. Phung and A. Domingo, *J. Chem. Theory Comput.*, 2017, **13**, 537–553.
26 Q. M. Phung, M. Feldt, J. N. Harvey and K. Pierloot, *J. Chem. Theory Comput.*, 2018, **14**, 2446–2455.
27 Q. Sun, J. Yang and G. K.-L. Chan, *Chem. Phys. Lett.*, 2017, **683**, 291–299.
28 G. L. Manni, S. D. Smart and A. Alavi, *J. Chem. Theory Comput.*, 2016, **12**, 1245–1258.
29 J. E. T. Smith, B. Mussard, A. A. Holmes and S. Sharma, *J. Chem. Theory Comput.*, 2017, **13**, 5468–5478.
30 G. L. Manni and A. Alavi, *J. Phys. Chem. A*, 2018, **122**, 4935–4947.
31 G. L. Manni, D. Kats, D. P. Tew and A. Alavi, *J. Chem. Theory Comput.*, 2019, **15**, 1492–1497.
32 M. Radoń and K. Pierloot, *J. Phys. Chem. A*, 2008, **112**, 11824–11832.
33 R. Olivares-Amaya, W. Hu, N. Nakatani, S. Sharma, J. Yang and G. K.-L. Chan, *J. Chem. Phys.*, 2015, **142**, 034102.
34 C. Zhou, L. Gagliardi and D. G. Truhlar, *J. Phys. Chem. A*, 2019, **123**, 3389–3394.
35 Y.-K. Choe, T. Nakajima, K. Hirao and R. Lindh, *J. Chem. Phys.*, 1999, **111**, 3837–3845.
36 S. F. Sontum, D. A. Case and M. Karplus, *J. Chem. Phys.*, 1983, **79**, 2881–2892.
37 U. Nagashima, T. Takada and K. Ohno, *J. Chem. Phys.*, 1986, **85**, 4524–4529.
38 Y.-K. Choe, T. Hashimoto, H. Nakano and K. Hirao, *Chem. Phys. Lett.*, 1998, **295**, 380–388.
39 C. Rovira, P. Ballone and M. Parrinello, *Chem. Phys. Lett.*, 1997, **271**, 247–250.
40 S. Vancoillie, H. Zhao, V. T. Tran, M. F. A. Hendrickx and K. Pierloot, *J. Chem. Theory Comput.*, 2011, **7**, 3961–3977.
41 S. R. White, *Phys. Rev. Lett.*, 1992, **69**, 2863–2866.
42 G. K.-L. Chan and S. Sharma, *Annu. Rev. Phys. Chem.*, 2011, **62**, 465–481.
43 L. Veis, A. Antalík, J. Brabec, F. Neese, Ö. Legeza and J. Pittner, *J. Phys. Chem. Lett.*, 2016, **7**, 4072–4078.
44 L. Veis, A. Antalík, Ö. Legeza, A. Alavi and J. Pittner, *J. Chem. Theory Comput.*, 2018, **14**, 2439–2445.
45 F. M. Faulstich, M. Máté, A. Laestadius, M. A. Csirik, L. Veis, A. Antalik, J. Brabec, R. Schneider, J. Pittner, S. Kvaal and Ö. Legeza, *J. Chem. Theory Comput.*, 2019, **15**, 2206–2220.
46 J. Lang, A. Antalík, L. Veis, J. Brandejs, J. Brabec, O. Legeza and J. Pittner, *J. Chem. Theory Comput.*, 2020, **16**, 3028–3040.
47 F. Neese, A. Hansen and D. G. Liakos, *J. Chem. Phys.*, 2009, **131**, 064103.
48 F. Neese, F. Wennmohs and A. Hansen, *J. Chem. Phys.*, 2009, **130**, 114108.
49 C. Riplinger and F. Neese, *J. Chem. Phys.*, 2013, **138**, 034106.
50 M. Gouterman, *J. Mol. Spectrosc.*, 1961, **6**, 138–163.
51 E. Pastorczak and K. Pernal, *J. Phys. Chem. Lett.*, 2018, **9**, 5534–5538.
52 M. Radoń, *J. Chem. Theory Comput.*, 2014, **10**, 2306–2321.